

# University of Cape Town

Division of Biomedical Engineering, Department of Human Biology



Dissertation submitted in partial fulfilment of the requirements for the  
degree of MSc (Med) Biomedical Engineering

## **Towards the Development of a Dynamic Device for the Evaluation of Hypertonia of the Upper Extremity**

Author: Matthew Proxenos (PRXMAT001)

Supervisor: Dr Lester R. John

February 2014

The copyright of this thesis vests in the author. No quotation from it or information derived from it is to be published without full acknowledgement of the source. The thesis is to be used for private study or non-commercial research purposes only.

Published by the University of Cape Town (UCT) in terms of the non-exclusive license granted to UCT by the author.

## Abstract

**Background:** Traditional evaluation techniques for spastic hypertonia, such as the Modified Ashworth Scale (MAS), are prone to subjectivity and have been shown to have poor inter- and intra-rater reliability. Automated objective electromechanical devices for upper-limb evaluation do exist, such as the commercially available NeuroFlexor device. These assess combined wrist and finger flexor tone by monitoring wrist joint torque during passive wrist extension. Wrist flexor tone evaluations made by manipulation of the wrist joint alone, however, could be affected by possible hypertonia of the finger flexors due to the moment arm that these muscles' tendons have at the wrist joint. As such, robotic wrist flexor evaluation devices that measure only the wrist joint torque cannot distinguish between wrist and finger flexor hypertonia. **Hypothesis:** A robotic device measuring involuntary resistance at the wrist and finger joints separately during wrist manipulation can be used to provide wrist flexor tone assessments that compensate for the influence of hypertonia of the finger flexor muscles, and therefore provide more accurate tone assessments of the wrist flexor muscles. **Objectives:** To design, construct and evaluate a patient-safe device for the independent measurement of wrist and finger joint torque during wrist extension, and to use the device to accurately evaluate wrist flexor tone, in isolation from possible effects of finger flexor tone. **Methods:** Evaluations were made using the device in a clinical setting with volunteers (n=6) with varying levels of hypertonia in the hands and wrists. Volunteers' wrist flexor tone was also assessed by three clinicians using the MAS score. **Results:** The averages of therapist assessments were compared to the force applied at the wrist joint as measured by the device, as well as to an estimate of the wrist flexor tendon tension made using the device assessments with a biomechanical model. Both of the force evaluations made using the device (peak wrist force and estimated wrist flexor tendon tension) correlated identically with the MAS scores ( $\rho=0.81$ ,  $p<0.05$ ). Various factors could have influenced the correlations, however, such as the unreliability of the MAS as a gold standard. **Conclusion:** Results suggest that the estimate of the wrist flexor tendon tension offers no benefit over peak wrist force alone for wrist flexor tone assessments. This could indicate that the influence of finger flexor hypertonia at the wrist joint is small compared to that due to wrist flexor hypertonia, although further investigation is required to improve experimental robustness. The opportunity exists to make device design modifications which would allow for further testing.

## **Declaration**

I, Matthew Ryece Proxenos, hereby declare that the work on which this dissertation is based is my original work (except where acknowledgments indicate otherwise) and that neither the whole work nor any part has been, is being, or is to be submitted for another degree in this or any other university. I empower the university to reproduce for the purposes of research the whole or any portion of the contents in any manner whatsoever.

The Harvard referencing style was used for citation and referencing. Each contribution to, and quotation from the work(s) of other people has been cited and referenced.

---

Matthew Ryece Proxenos

---

Date

## **Acknowledgements**

I would like to thank all who collaborated on this project, providing guidance and advice. Most noteworthy is Dr Lester John, without whom this project wouldn't have been possible. Many others were also involved: Prof Alan Bryer, Carolyn Davids, Elmarie Du Preez, and all other clinical staff provided invaluable advice. Henri Carrara helped with statistics and Charles Harris with construction. The other postgraduate students in the lab helped immensely too. My sincerest thanks go out to all of these people.

I would like to acknowledge and thank the University of Cape Town and the National Research Foundation for financial assistance.

Lastly, I would like to make special mention of all of the people who provided support on a personal level. My friends and family, especially my parents, deserve my most heartfelt thanks. I do not know where I might be without them.

# Contents

Abstract.....	i
Declaration.....	ii
Acknowledgements.....	iii
Contents .....	iv
List of Acronyms and Abbreviations.....	viii
List of Figures.....	ix
List of Tables .....	xii
1. Introduction.....	1
1.1. Physiology Background.....	2
1.1.1. Neuroanatomy of the Healthy Motor System .....	2
1.1.2. Upper Motor Neuron Syndrome, Spasticity and Hypertonia.....	4
1.1.3. Prevalence of UMNS and Spasticity.....	7
1.1.4. Clinical Observations in UMNS .....	8
1.1.5. Assessment and Treatment.....	10
1.2. Robot-aided Neuro-rehabilitation and Objective Evaluation of Hypertonia .....	12
1.2.1. Examples of Electromechanical Devices for Rehabilitation.....	13
1.2.2. Devices for Objective Evaluation of Hypertonia .....	19
1.2.3. Opportunity for Further Development .....	22
1.3. Objectives .....	23
2. Apparatus.....	25
2.1. Device Design Specifications .....	25
2.1.1. Coordinate system.....	26

2.2 Device Construction.....	27
2.2.1. Overview of System Components.....	27
2.2.2. Torque and Speed Specifications.....	31
2.2.3. Safety Features.....	32
2.3. EMG Signal Acquisition and Processing.....	33
2.3.1. EMG Safety Features.....	36
2.4. Force Transducers and Associated Electronics.....	37
2.5. Data Logging and PC Software.....	38
2.6. Modes of Operation.....	41
3. Methodology.....	43
3.1. Methodology Overview.....	43
3.1.1. Participants Inclusion/Exclusion Criteria.....	46
3.1.2. Muscles for EMG acquisition.....	47
3.1.3. Design Modifications Following the Preliminary Safety Test.....	47
3.2. Detailed Testing Protocols.....	48
3.2.1. Preliminary Safety Test.....	48
3.2.2. Pilot Clinical Trial.....	49
3.3. Data Processing.....	55
3.3.1. Preliminary Safety Tests.....	55
3.3.2. Pilot Clinical Trial.....	55
3.4. Biomechanical Model.....	59
3.5. Precautions.....	62
3.5.1. Preliminary Safety Test.....	62
3.5.2. Pilot Clinical Trial.....	63
4. Results.....	65
4.1. Preliminary Safety Tests.....	65

4.2. Pilot Clinical Trial.....	67
4.2.1. Processed Data.....	67
4.2.2. Statistical Analysis.....	76
5. Discussion.....	80
5.1. Preliminary Safety Tests.....	80
5.2. Pilot Clinical Trial.....	81
5.2.1. Discussion of Statistical Results:.....	81
5.2.2. Force Recordings.....	83
5.2.3. Biomechanical Model.....	85
5.2.4. EMG and Neural vs. Non-neural Hypertonia.....	85
5.2.5. MAS Scores.....	86
5.3.6. Ergonomics.....	87
5.3. Recommendations for Future Work.....	88
5.3.1. Device Design Modifications.....	88
5.3.2. Experimental Protocol.....	89
5.3.3. Other Recommendations.....	90
5.3.4. Opportunities for Further Research and Development:.....	90
6. Conclusions.....	92
References.....	94
Appendix A – Device Design and Manufacture.....	98
A.1. Device Structure.....	98
A.2. Ergonomic Elements.....	98
A.3. Design of the Force Transducer Elements.....	100
A.3.1. Calculation of Force Sensing Element Material Thickness.....	101
A.3.2. Force Transducer Calibration.....	104

A.4. Finite Element Analysis of Selected Components .....	108
A.4.1. Finite Element Analysis of the Distal Force Sensing Element .....	108
A.4.2. Finite Element Analysis of Structural Elements .....	116
Appendix B – Electronics and Actuator Information .....	124
B.1. Electric Motor and Motor Driver Specifications.....	124
B.2. EMG Signal Acquisition .....	124
B.3. EMG Signal Processing Circuit .....	128
B.3.1. Filtering .....	128
B.3.2. Rectification .....	129
B.3.3. Enveloping .....	129
B.4. Strain Gauge Signal Processing Circuit .....	130
B.5. Microprocessor and System Integration.....	131
B.6. User Interface Electronics .....	133
Appendix C – Modifications to the OpenEEG System.....	135
Appendix D – Calibration of the EMG Amplification System.....	137
D.1. Generation and Amplification of the Input Signal.....	137
D.2. Inference of the Transfer Function.....	138
D.3. Inference of Unamplified EMG signals .....	141
Appendix E – Microcontroller Code.....	147
Appendix F – Matlab Code.....	162
Appendix G – UCT Human Research Ethics Committee Approval Documentation and Participant Consent Forms .....	169

## List of Acronyms and Abbreviations

<b>CAD</b>	Computer-aided Design
<b>CNS</b>	Central Nervous System
<b>DRL</b>	Driven Right Leg (can refer to the active common mode noise cancelling ground electrode in EMG and cardiology)
<b>EMG</b>	Electromyography (or electromyogram)
<b>EMI</b>	Electromagnetic Interference
<b>FEA</b>	Finite Element Analysis
<b>GUI</b>	Graphical User Interface
<b>MCP joint</b>	Metacarpophalangeal Joint
<b>Op-amp</b>	Operational Amplifier
<b>PROM</b>	Passive Range of Motion
<b>UMNS</b>	Upper Motor Neuron Syndrome

## List of Figures

<b>Figure 1.1</b>	Nervous pathways involved in the monosynaptic stretch reflex .....	3
<b>Figure 1.2</b>	The flexor (or “withdrawal”) reflex.....	4
<b>Figure 1.3</b>	Commonly adopted posture in spastic patients.....	9
<b>Figure 1.4</b>	Relationship between spasticity and PROM .....	12
<b>Figure 1.5</b>	A subject demonstrating the use of the MIT-Manus.....	14
<b>Figure 1.6</b>	Position and speed plots of a patient using the MIT-Manus.....	15
<b>Figure 1.7</b>	The HWARD hand rehabilitation robot.....	16
<b>Figure 1.8</b>	fMRI activation volumes before and after treatment .....	17
<b>Figure 1.9</b>	A subject demonstrating the REHAROB robot.....	18
<b>Figure 1.10</b>	Unilateral and bilateral movements with the MIME device.....	18
<b>Figure 1.11</b>	Bi-Manu-Trak device bilateral training .....	19
<b>Figure 1.12</b>	Photograph of the NeuroFlexor device.....	20
<b>Figure 1.13</b>	Illustration of raw force data collected with the NeuroFlexor.....	21
<b>Figure 2.1</b>	Convention for specifying joint rotational position and velocity.....	27
<b>Figure 2.2</b>	Overview of all components making up the system.....	28
<b>Figure 2.3</b>	The neutral position of the device .....	29
<b>Figure 2.4</b>	Back view of device .....	29
<b>Figure 2.5</b>	Functional overview of the components of the system .....	30
<b>Figure 2.6</b>	Exploded view .....	31
<b>Figure 2.7</b>	Handheld safety buttons motor power .....	33
<b>Figure 2.8</b>	Top view of selected structural components .....	34
<b>Figure 2.9</b>	Limit switches for wrist flexion and extension .....	35
<b>Figure 2.10</b>	Analogue EMG signal processing .....	35
<b>Figure 2.11</b>	Schematic diagram of a strain gauge amplifier circuit .....	38
<b>Figure 2.12</b>	Force amplifier calibration curves .....	39
<b>Figure 2.13</b>	Screenshot of the GUI.....	40
<b>Figure 3.1</b>	Overview of the various phases of development .....	43
<b>Figure 3.2</b>	The experimental setup for the preliminary safety tests.....	44
<b>Figure 3.3</b>	Image illustrating the experimental setup for the pilot clinical trial.....	45

<b>Figure 3.4</b>	Bipolar EMG electrodes on the extensor compartment of the forearm.....	52
<b>Figure 3.5</b>	Bipolar EMG electrodes on the flexor compartment of the forearm.....	52
<b>Figure 3.6</b>	Prescribed movements for wrist and finger manipulation.....	53
<b>Figure 3.7</b>	Prescribed movements for wrist only manipulation.....	54
<b>Figure 3.8</b>	Repeatability of the drift in force readings with device joint movement ....	56
<b>Figure 3.9</b>	Effectiveness of digital subtraction to correct for artificial force drift .....	57
<b>Figure 3.10</b>	The participant's hand and force diagram for the biomechanical model.....	59
<b>Figure 3.11</b>	Various moment arms that tendons possess at the various joints.....	60
<b>Figure 4.1</b>	Times to complete repetitions during the first test.....	65
<b>Figure 4.2</b>	Times to complete repetitions during the second test.....	65
<b>Figure 4.3</b>	Times to complete repetitions during the third.....	66
<b>Figure 4.4</b>	Force recordings for Participant A .....	67
<b>Figure 4.5</b>	Force recordings for Participant B .....	68
<b>Figure 4.6</b>	EMG and force recordings for Participant C .....	69
<b>Figure 4.7</b>	EMG and force recordings for Participant D .....	70
<b>Figure 4.8</b>	EMG and force recordings for Participant E .....	71
<b>Figure 4.9</b>	EMG and force recordings for Participant F .....	72
<b>Figure 4.10</b>	Graphical representation of MAS scores.....	73
<b>Figure 5.1</b>	Hypothetical variables which vary linearly and exponentially.....	82
<b>Figure A.1</b>	Partially exploded view of a CAD model of the device.....	97
<b>Figure A.2</b>	The device with a participant's hand secured.....	98
<b>Figure A.3</b>	CAD model of a force sensing element .....	99
<b>Figure A.5</b>	Sketch of calibration apparatus .....	101
<b>Figure A.6</b>	Plots of raw data collected during calibration.....	104
<b>Figure A.8</b>	Plots of processed calibration data .....	105
<b>Figure A.9</b>	CAD model of a partially exploded assembly.....	106
<b>Figure A.10</b>	CAD model of a force sensing element.....	106
<b>Figure A.11</b>	CAD models of the force sensing element.....	109
<b>Figure A.12</b>	FEA model of the element (negative forces, 2mm mesh elements).....	110
<b>Figure A.13</b>	FEA model of the element (negative forces, 1mm mesh elements).....	111
<b>Figure A.14</b>	FEA model of the element (negative forces, 3mm mesh elements).....	112

<b>Figure A.15</b>	FEA model of the element (positive forces, 2mm mesh elements).....	113
<b>Figure A.16</b>	FEA model of the element (positive forces, 1mm mesh elements).....	113
<b>Figure A.17</b>	FEA model of the element (positive forces, 3mm mesh elements).....	114
<b>Figure A.18</b>	CAD models of the proximal and distal structural elements.....	116
<b>Figure A.19</b>	CAD models of the proximal and distal structural elements.....	117
<b>Figure A.20</b>	FEA models of the distal structural element (2mm mesh element).....	117
<b>Figure A.21</b>	FEA models of the distal structural element (1mm mesh element).....	118
<b>Figure A.22</b>	FEA models of the distal structural element (3mm mesh element).....	118
<b>Figure A.23</b>	FEA models of proximal structural element (2mm mesh element).....	119
<b>Figure A.24</b>	FEA models of proximal structural element (1mm mesh element).....	119
<b>Figure A.25</b>	FEA models of proximal structural element (3mm mesh element).....	120
<b>Figure B.1</b>	Geared brushed DC electric motor .....	124
<b>Figure B.2</b>	The OpenEEG digital and amplifier boards.....	124
<b>Figure B.3</b>	Schematic of the unmodified OpenEEG amplifier board.....	125
<b>Figure B.4</b>	Schematic of the unmodified OpenEEG digital board.....	126
<b>Figure B.5</b>	Functional requirements of the EMG signal processing circuit.....	127
<b>Figure B.6</b>	EMG signal processing circuit for one channel.....	127
<b>Figure B.7</b>	Precision rectifier in the EMG signal processing board.....	128
<b>Figure B.8</b>	Peak detector circuit used in the EMG signal processing board.....	129
<b>Figure B.9</b>	Schematic diagram of a strain gauge amplifier circuit .....	130
<b>Figure B.10</b>	Functional overview of the components of the system.....	131
<b>Figure D.1</b>	Schematic representation of the calibration setup for a single channel.....	136
<b>Figure D.2</b>	The attenuated input signal to the amplifier for calibration.....	139
<b>Figure D.3</b>	The recording of the amplified output signal from the amplifier .....	139
<b>Figure D.4</b>	Estimates of the transfer functions and phase shifts.....	141
<b>Figure D.5</b>	Example of an amplified EMG waveform.....	142
<b>Figure D.6</b>	Original spectral density, the transfer function and final spectral density.....	143
<b>Figure D.7</b>	Original (amplified) and final (unamplified) EMG data.....	144

## List of Tables

<b>Table 1.1</b>	Features of Upper Motor Neuron Syndrome.....	5
<b>Table 1.2</b>	The Modified Ashworth Scale for evaluation of muscle tone.....	10
<b>Table 2.1</b>	Truth table for sensed EMG and joint activity.....	37
<b>Table 3.1</b>	Summary of muscles monitored the study.....	47
<b>Table 3.2</b>	Summary of the testing protocols in the pilot trial.....	51
<b>Table 4.1</b>	Summary of data collected during the pilot trial.....	74
<b>Table 4.2</b>	Summary of the results of the statistical analysis.....	77
<b>Table 5.1</b>	Hypothetical variables which vary linearly and exponentially.....	81
<b>Table A.1</b>	Results from FEA model of force sensing element with positive forces.....	110
<b>Table A.2</b>	Results from FEA model of force sensing element with negative forces.....	111
<b>Table A.3</b>	Results from the FEA model of the proximal structural element.....	120
<b>Table A.4</b>	Results from the FEA model of the distal structural element.....	120
<b>Table C.1</b>	Summary of modification of the OpenEEG system.....	134
<b>Table D.1</b>	Bandwidths of amplifiers as calculated from transfer functions.....	138

# 1. Introduction

Neurological disorders often result in motor dysfunction which causes substantial disability in patients. The healthy motor system relies upon reflexes to maintain innate tone in muscles as well as for rapid responses to potential threats. Upper motor neuron lesions, however, can result in a variety of observable signs and features of motor dysfunction collectively termed Upper Motor Neuron Syndrome (UMNS). These can be broadly categorized into negative or positive features which result in losses of function (e.g. paralysis) or excesses and hyperactivity respectively (e.g. spasticity). Negative features often result from the disruption of direct commands issued from the brain. The positive features are often a result of disruption of the brain's ability to modulate healthy reflex action. UMNS is commonly associated with disorders affecting the central nervous system. The most commonly observed cases occur with disorders such as cerebrovascular accident (i.e. stroke), multiple sclerosis, cerebral palsy, traumatic brain injuries and spinal cord injuries.

While the features of UMNS are often easily observed, seeking consensus on formal definitions has proven less facile. For example, the term „spasticity“, which refers to a velocity-dependent increase in tonic stretch reflexes, is often used incorrectly in the field as a catch-all term encompassing all observations of increased muscle tone. A more correct term would be „hypertonia“, which doesn't imply velocity dependence.

In clinical practice, the evaluation of muscle tone is often performed by making use of ordinal scales - most commonly the Modified Ashworth Scale (MAS). The convenience offered by such techniques is enough to outweigh the inherent flaws, specifically rater subjectivity and unreliability. The use of robotic devices for the evaluation (and also for treatment) of motor disorders is not a new trend, although it has largely been confined to the research environment. The results of such research have indicated clear benefits over traditional techniques.

The research presented in this thesis sought to improve upon some of the work that has been done in the field of objective hypertonia evaluation. An electromechanical device for this purpose was sought, with special focus on attempting to isolate the effects of wrist flexor spasticity from those of finger flexor spasticity.

## 1.1. Physiology Background

### 1.1.1. Neuroanatomy of the Healthy Motor System

Within the Central Nervous System (CNS), the ultimate planner and controller of the body and its functions, motor control can be divided into hierarchical levels. Marieb and Hoehn (2006) name these as, in descending hierarchical order, the pre-command level (the most complex, comprised of the basal ganglia and cerebellum), the projection level (the upper motor neurons of the motor cortices and brainstem) and the segmental level (spinal cord circuits). The segmental level, being of interest here, will be discussed further.

The segmental level is responsible for, among other things, the elements of the neuromuscular system which need not be under direct voluntary control. Stretch reflexes are an example: The intrafusal muscle spindles sense the stretch and transmit signals along the large type Ia fibres (the sensory endings of which are stimulated by rate and degree of stretch) and type II (stimulated by degree of stretch only). These afferent fibres enter the spinal cord as an input to spinal circuitry as well as to relay proprioceptive information to the brain. In the case of the aptly named monosynaptic stretch reflex, the spinal circuitry is as simple as a single synapse with an efferent  $\alpha$ -motor neuron that exits the spinal cord to stimulate the same muscle in which the original stretch stimulus occurred. As such, when a muscle is sharply stretched it also experiences an involuntary contraction (see Figure 1.1).

As the required response to stimulus grows in complexity, so too does the complexity of the spinal circuitry controlling it. The flexor or “withdrawal” reflex exhibits more complex movement as well as reciprocal inhibition whereby muscles which act antagonistically to the reflex are actively inhibited, requiring the presence of so called interneurons. More complex still are reflexes that require activation or inhibition of contralateral muscles to maintain balance and posture upset by the intended reflexive movement (see figure 1.2). Healthy stretch reflexes are under the influence of supraspinal modulation. That is to say, the brain can exert a level of control over the gain (the amplitude of the response) or threshold (the level stimulus required to elicit a response) of the reflexes” spinal circuitry. This is achieved via the pyramidal tracts (from the cortices) and parapyramidal tracts (from the brainstem – vestibular nucleus, superior colliculus and reticular formations) (Stevenson and Thompson, 2006).

*“By sending commands to the motor neurons, the brain essentially sets a muscle’s length. The stretch reflex makes sure that the muscle stays at that length” (Marieb and Hoehn, 2006)*

As will be discussed in section 1.1.2., it is the interruption of this modulation that is thought to be the cause of hypertonia and other symptoms of UMNS.

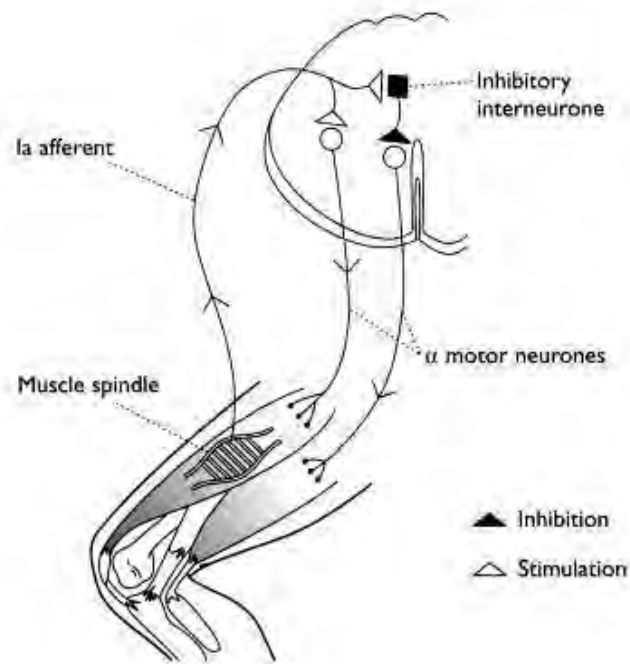


**Figure 1.1** Illustration of the nervous pathways involved in the monosynaptic stretch reflex (Stevenson and Thompson, 2006)

According to Stevenson and Thompson (2006), muscle tone refers to “the ongoing tension in a muscle, apparent as a resistance experienced to passive movement and stretch”, however the resistance itself can be attributed to two prime sources. These are chiefly the neural component due to the stretch reflex and the non-neural component due to the viscoelastic (biomechanical) properties of the connective tissue and muscles crossing the joint. The term “muscle tone” can be somewhat confusing, since resistance is not only due to muscle contraction in an intuitive sense. As Barnes and Johnson (2001) state, it is worthwhile to note that while both factors (neural and non-neural) can contribute to pathologically increased muscle tone, normal muscle tone (i.e. passive resistance to manipulation) is comprised entirely from soft tissue biomechanics and there is no contribution from neurological components at normal passive movement velocities. In a pathological state, both neural and non-neural hypertonia (increased tone) can be exhibited (this is discussed in Section 1.1.2). Indeed, it is important to distinguish between neural and non-neural hypertonia because the treatments paradigms for these are affected – such as stretching and/or splinting, pharmacology or even surgery. Methods suggested for making such a distinction include careful examination of the affected body segments with fast and slow passive joint manipulation, as well as less subjective methods such as electromyography (EMG) analysis and the use of techniques such as local anaesthetic or ischemic nerve blocks to temporarily negate the effects of any neural hypertonia and observe if resistance is still exhibited (Barnes and Johnson, 2001; Stevenson and Thompson, 2006). Studies, such as the one

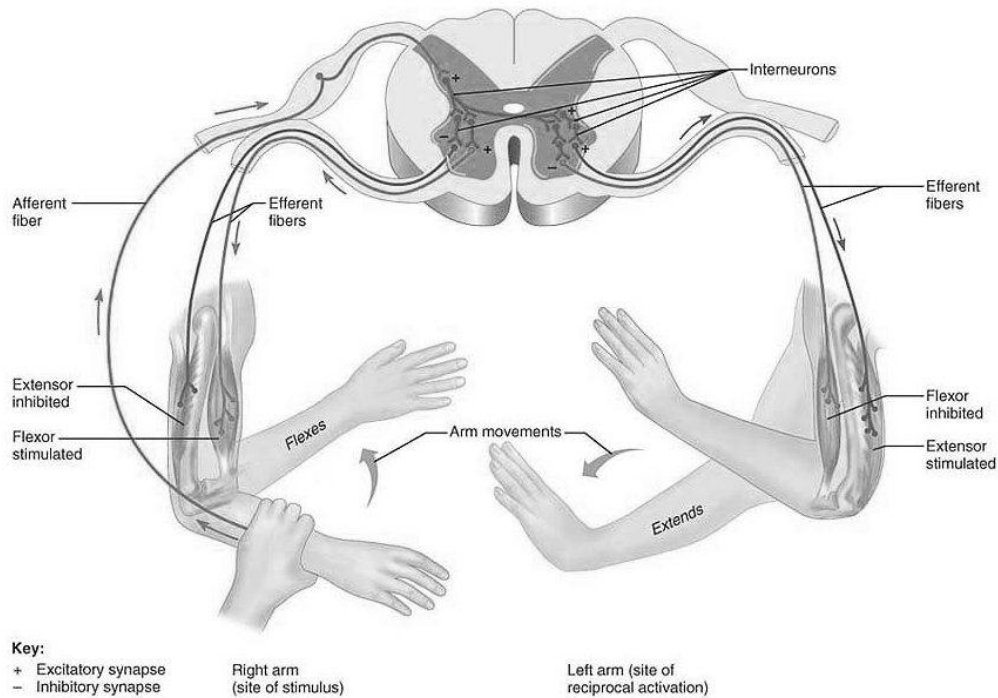


**Figure 1.2** The flexor (or “withdrawal”) reflex, illustrating how more complex reflexes can cause muscle activity in contralateral segments to the original stimulus. (Marieb and Hoehn, 2006)

by Albani et al. (2010) have used EMG to quantify an increase in muscle tone, and as such would only detect the neural components thereof. Lindberg et al. (2011) have used torque measurement and biomechanical models to distinguish between neural and non-neural hypertonia.

### 1.1.2. Upper Motor Neuron Syndrome, Spasticity and Hypertonia

Upper Motor Neuron Syndrome (UMNS) is the collective term for a set of observable neurological features, any of which can develop after an upper motor neuron lesion. The common features of UMNS are shown Table 1.1. As can be seen, such features of UMNS can be divided into negative (losses) and positive (excesses).

It is thought that the positive features of UMNS are due, at least in part, to the interruption of the genesis or transmission of modulating signals from the central nervous system which interact with the segmental level spinal circuitry. With these impaired, there is reduced inhibition of reflex activity.

**Table 1.1** Features of Upper Motor Neuron Syndrome (Barnes and Johnson, 2001)

Positive Features	Negative Features
<ul style="list-style-type: none"> <li>• Increased tendon reflexes</li> <li>• Clonus</li> <li>• Positive Babinski sign</li> <li>• Spasticity</li> <li>• Extensor spasms</li> <li>• Flexor spasms</li> <li>• Mass reflex</li> <li>• Dyssynergistic patterns of co-contraction during movement</li> <li>• Associated reactions and other dyssynergistic and stereotypical spastic dystonias</li> </ul>	<ul style="list-style-type: none"> <li>• Muscle weakness</li> <li>• Loss of dexterity</li> <li>• Reduced postural response</li> </ul>

Among the medical community, consensus for a precise and all-encompassing definition for “spasticity” has proven elusive - with good reason. The most widely quoted definition among scholarly publications was put forward by Lance (1980):

*“[Spasticity is] a motor disorder, characterized by a velocity-dependent increase in tonic stretch reflexes (muscle tone) with exaggerated tendon jerks, resulting from hyper-excitability of the stretch reflex as one component of the upper motor neurone syndrome.”*

While this definition seems simple and clear, the phenomenon is still poorly understood in clinical practice. Most physicians and clinicians will agree that they can identify spasticity when they encounter it in their patients, however their observations do not strictly conform to how they perceive Lance’s definition. The use of the term and the definition thereof has been the subject of criticism (e.g. Malhotra et al., 2009, showed that a large proportion of studies do not confirm to a single definition or even explicitly state a definition). Barnes and Johnson (2001) explain further:

*“It may be difficult for a clinician to correlate this definition with a typical patient pictured in his or her mind.... The clinician tends to picture the whole UMN syndrome and regard all the „positive“ features of the syndrome as „spasticity“.”*

The research by Ibrahim et al. (1993) show that spastic response is not as simple as Lance's definition implies, with early and late responses to passive stretch (observable both with torque and EMG measurement).

Often, clinicians will apply the term „spasticity“ to any increase in muscle tone (although „hypertonia“ would be a better term). True spasticity is velocity-dependent and as such often exhibits a specific presentation, such as the clasp knife phenomenon (upon passive stretch, a muscle will briefly contract or “catch” followed by a release). In the case of increased tone over the whole range of motion (without the initial catch), a more correct name would be neural hypertonia, but soft tissue changes should be investigated since tone can have non-neural origins.

Over the years since Lance's initial description, new definitions for spasticity have been proposed such as the following by the EU-SPASM group in 2005 (Pandyan et al., 2005):

*“Spasticity – disordered sensorimotor control, resulting from an upper motor neuron lesion, presenting as intermittent or sustained involuntary contraction.”*

This definition is broader and consequently it becomes less useful in the evaluation and treatment of spasticity. Despite this, it is the definition that will be adopted for the remainder of this thesis due to having the advantage of being an „umbrella“ term. This was motivated by the fact that, in interviews, clinicians appear to use the terms “spasticity” and “hypertonia” interchangeably.

UMNS and Spasticity are associated with a number of diseases and causes. Some affect the spinal cord while others affect the brain directly. For a disease to result in exhibition of some or all of the features of UMNS, it must inhibit the transmission of communication between the brain and the spinal circuitry and stretch reflexes (or inhibit the genesis of such communications). The most commonly associated causes of spasticity are listed below, but this list is by no means exhaustive:

- Cerebrovascular accident (i.e. a stroke) is the most common cause (see the discussion of prevalence in Section 1.1.3).
- Diseases such as Amyotrophic Lateral Sclerosis, Multiple Sclerosis, brain or spinal cord neoplasms, certain forms of cerebral palsy such as spastic diplegia (also known as Little's disease), etc.
- Traumatic brain or spinal cord injury

### 1.1.3. Prevalence of UMNS and Spasticity

Little reliable data exists on the incidence of spasticity, and even less on UMNS in general. For instance, in a study by Sommerfeld et al. (2004), it was concluded that 19% of stroke patients (n=95) experienced spasticity in the first 3 months following a stroke, and 20% after 18 months. Watkins et al. (2002) concluded that 29% of their cohort (n=106) showed increased muscle tone after 12 months. Indeed, the latter study also showed up to 38% of their cohort exhibited spasticity if a different kind of assessment scale was used (The Tone Assessment scale, as opposed to the MAS, discussed in Section 1.1.5). A study of multiple sclerosis by Barnes et al. (2003) reports that 47% of participants developed spasticity (n=65). This is somewhat inconsistent with the results presented by Rizzo et al., (2004) from a much wider study (n=513) which stated that up to 70% of multiple sclerosis patients will experience “some degree of spasticity”.

Symptoms may be experienced in lesser or greater degrees by different people – indeed even the same person at different times - the difference in study conclusions may be attributed to, among other things, what degree the authors deem symptoms to be clinically significant or the evaluation methods currently employed. Another source of inconsistency could arise in the working definition of spasticity being used in each study. While all of the three studies cited here assessed multiple parameters in their participants (motor performance, dexterity, etc.), “spasticity” was assessed in two of the three by means of the MAS score (see Section 1.1.5). The trial by Rizzo et al. (2004) investigated participant-reported spasticity using their own definition and ordinal scale. This ad hoc definition was „unusual tightening of muscles that feels like leg stiffness, jumping of legs, a repetitive bouncing of the foot, muscle cramping in legs or arms, legs going out tight and straight or drawing up“ and the ordinal scale, like the MAS, ranged from 0 to 5. It was worded to test the frequency with which „spasticity“ interfered with daily activities. None of the studies used any non-subjective measures to test for spasticity or UMNS, and none truly measured spasticity in terms of Lance’s definition (see Section 1.1.2). Nonetheless, despite the insufficiency and inconsistency of the literature, what it does illustrate is that spasticity is a common effect of such neurological disorders as stroke and multiple sclerosis.

In the South African context, when one compares the results of recent censuses conducted in 1996 (Lehohla, 1998) and 2001 (Lehohla, 2003), the population group aged 60 or older increased from 2.8 million to 3.3 million over the five year period. This increase of 16.1% is disproportionate to the total population increase of only 10.4% over the same period. This disproportionate increase is again observed (and drastically increased) in the 2011 census (Lehohla, 2012) – the population aged 60 or older grew by 26.6% (to 4.2 million) from 2001, while the total population only grew 15.5%. This indicates that the population is aging. The increase in the proportion of elderly will affect the

occurrence of strokes (since age is a significant risk factor for stroke) and as thus the prevalence of resultant UMNS.

A similar contribution to patient numbers is imposed, ironically, by advances in the stroke treatment: While a trend towards more effective emergency stroke treatment methods is yielding an increase in the number of stroke survivors, it is also increasing the number of patients requiring rehabilitation. The problem of increasing patient numbers is compounded by the limited usefulness of effective evaluation techniques, and financial constraints (which preclude most of the expensive technological evaluation or rehabilitation aids currently available on the market). A result of this is that there is a trend towards disability compensation in rehabilitation due to facility constraints regarding patient volumes. It comes at the expense of impairment reduction which is clearly the better solution. That is to say, instead of rehabilitating patients such that they can perform tasks as they used to (impairment reduction), care facilities are teaching patients to “work around” their disabilities (disability compensation).

#### **1.1.4. Clinical Observations in UMNS**

Precise clinical consequences and observations of UMNS are difficult to predict, as the possible manifestations from any neurological disorder are often numerous. The specific manifestations will depend on the neurological structures involved. In terms of positive features, severity in a patient can sometimes fluctuate and can often be affected by many factors such as cutaneous stimulation (i.e. from clothing), the patient’s level of fatigue, and even their emotional state or alertness. Often, but not always, spasms are stronger either during passive flexion of a joint rather than extension, known as flexion dominance, or vice versa, known as extensor dominance. Severe hypertonia could manifest as rigidity of the joint in both directions. Flexion dominance, more commonly observed in the upper limbs, often leads to the commonly observed posture in those presenting with abnormal tone in the upper limb adopts: adducted and internally rotated shoulders, flexion of the wrist, elbow and fingers ((Thibaut et al., 2013). This flexion dominance, which is not always observed, is can be observed in the results of a study done by Sherwood et al. (2000), in which the EMG during passive movement of spastic subjects’ hip joints were recorded and analysed.

UMNS, especially severe cases, demands specific considerations from care givers:

- Impairment of movement in the fingers and wrist can affect the ability to perform activities of daily living (ADL’s). The disability here is largely caused by the negative features of UMNS.



**Figure 1.3** Commonly adopted posture in spastic patients – adduction and internal rotation of the shoulder, and flexion of the elbow, wrist, and fingers (Thibaut et al., 2013)

- Indeed, depression and frustration brought on by dependence on caregivers or failure to perform simple tasks can warrant special psychological care considerations.
- If the lower limbs are affected, then patient mobility becomes impaired. In mild cases, the subject may require a crutch, cane or walker. More severe cases will confine a patient to bed or a wheelchair. Subjects are frequently elderly (age is the primary risk factor for stroke, a common cause of spasticity), and a fall due to impaired mobility can result in significant trauma.
- In these severe cases, where patients require wheelchairs, spasticity in the lower limbs can result in pressure sores arising from abnormal seating postures.
- Hygiene concerns are also paramount. If a patient’s spasticity causes a permanently rigid and clenched fist, then cleaning inside the palm or trimming of the patients fingernails may prove difficult.
- If left untreated, or if improperly treated, the rigidly contracted muscles will undergo contractures – permanent and often painful conversion of muscle to connective tissue. Once developed, contractures cannot be “stretched out”, but can only be alleviated surgically, so their prevention is critical.
- Personal communications with care givers have confirmed that the time consuming physical therapy required is not always possible in overburdened care facilities.

### 1.1.5. Assessment and Treatment

There exist varying techniques to evaluate hypertonia. Both qualitative and quantitative techniques exist, with varying levels of reliability and practicality. Quantitative assessment relies on the use of specialized instrumentation. This is discussed further in Section 1.2. Qualitative systems, largely in the form of ordinal scales, have been more accepted in clinical practice, since they are fast, simple and do not require expensive or specialized equipment. Their disadvantage is that they are less reliable - the subjectivity and lack of resolution of these scales limits their practical use (reliability will be discussed shortly). A widely accepted measure of increased muscle tone is the Modified Ashworth Scale - an ordinal scale in which the tester assigns the subject a score from zero to four, where zero represents a normal level of functionality, observed in a healthy subject. It is so named because it is a revision of the similar Ashworth scale, modified to improve discrimination between mild and moderate increases in tone – see the addition of the „1+“ option in Table 1.2. Other ordinal scales include the Fugl-Meyer score which assesses levels of functional impairment including balance, joint range of motion, and a number of other measures (Duncan et al., 1983). Alternatives such as the Tardieu Scale are also sometimes used to measure spasticity, but require some training to perform. The Tardieu Scale involves manipulating a joint at three specific velocities and noting the joint angle at which an involuntary resistance is felt. While there are numerous available methods for measurement, the MAS score is by far the most widely practiced.

**Table 1.2** The Modified Ashworth Scale for evaluation of muscle tone

Score	Description
0	No increase in muscle tone.
1	Slight increase in tone with a catch and release or minimal resistance at end of range.
1+	As for 1 but with minimal resistance through range following catch.
2	More marked increase tone through range of motion.
3	Considerable increase in tone, passive movement difficult.
4	Affected part rigid in flexion or extension.

The MAS assessment was first applied by Bohannon and Smith (1987). It was used to assess elbow flexor spasticity. The procedure was as follows:

1. The patient is to be in a supine position on a padded mat or table
2. The arm was stabilized proximal to the elbow, and the forearm was grasped distally (just proximal to the wrist). The forearm was in neutral supination.
3. The patient's elbow was extended from a position of maximal flexion to maximal extension over a period of 1 second
4. Five to eight sequential extensions were performed
5. The patient was graded using the MAS score (Table 1.2)

Opinion on the reliability of the MAS score especially remains equivocal. While some studies claim that the method is acceptable (Bohannon and Smith, 1987; Brashear et al., 2002) others suggest that one or more aspects of the test are not reliable enough (Blackburn et al., 2002; Ansari et al., 2006; Alibiglou et al., 2008; Mutlu et al., 2008; Fleuren et al., 2009) or that further work was needed to determine the scope and limitations of the technique (Pandyan et al., 1999). Common criticisms are that the scales have poor intra- and inter-rater reliability due to the lack of objective quantification and thus a reliance on the physiotherapist's interpretation of the wording. For example, the point at which a "slight increase" in muscle tone becomes a "more marked increase" is subjective. Furthermore, the scale cannot distinguish between neural and non-neural hypertonia (see Section 1.1.1). Despite these shortcomings, the MAS score is commonly used as a measure of hypertonia in research, and is often treated as an acceptable proxy for hypertonia severity. It is, however, often used in research in conjunction with other related outcome measures, or quantifications of muscle activity (e.g. electromyography).

Examples of such evaluation measures include the passive range of motion (PROM), and measurement of torque or the resistance to passive motion (Bovendeerd et al., 2008). These are usually used in conjunction with other measures. Also noteworthy is that a relationship between the passive ROM and the severity of hypertonia has been shown (Pizzi et al., 2005). See Figure 1.4.

Treatment regimens may consist of various elements, depending on the severity of symptoms. Almost all neuromuscular rehabilitation programs will include a stretching routine (Bovendeerd et al., 2008; Smedes et al., 2014), and more severe cases will include prescription medication indicated for spasticity such as Baclofen, or botulinum toxin type A (Botox). Therapy is usually conducted by trained clinicians, as is the evaluation of the level of severity of hypertonia. Since there is no one "cause" for UMNS, and because the exact pathophysiology and mechanisms behind components like spasticity are unknown, there are many varying viewpoints regarding the proper courses of action to take. Berta and Karel Bobath pioneered the concept of "neuro-developmental treatment" (also known as NDT or the „Bobath“ concept), which is one of the major approaches to CNS pathology. It is non-standardized, broad and evolving concept, largely involving employment of techniques to guide

patients towards completion of tasks. It has been the subject of scientific study (Paci, 2003; Kollen et al., 2009). A good review of rehabilitation techniques for the positive signs of UMNS was published by Logan (2011). In this review, it is remarked that therapists need multiple modalities, and that evidence shows that no one modality is sufficient for improvement. They conclude that therapies need to be “high intensity, repetitive, and task specific, and they need to provide feedback on performance to produce functional changes”.

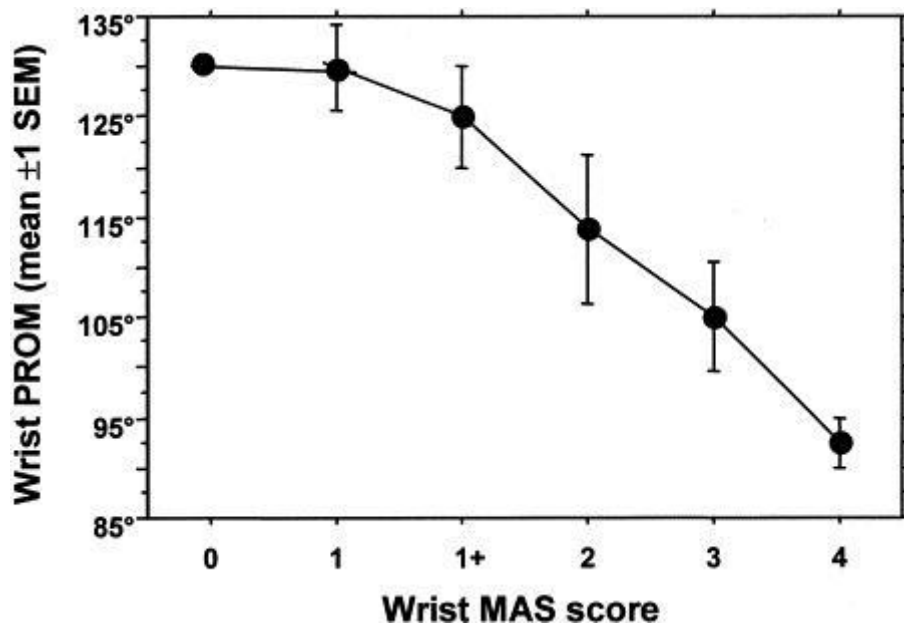


**Figure 1.4** Relationship between severity of spasticity (MAS score), and passive range of motion (PROM) at the wrist. Values are mean  $\pm$ 1 standard error of the mean (SEM). (Pizzi et al., 2005)

## 1.2. Robot-aided Neuro-rehabilitation and Objective Evaluation of Hypertonia

The challenges for therapists are mounting, and advancements in robot-aided therapy are intended to alleviate this burden. Electromechanical devices have been shown to assisting in neuro-rehabilitation, although this is still a relatively new trend. Similarly, devices have been used in clinical environments for the purpose of objective evaluation of the various features of UMNS, as well as to aide therapy while having evaluation as a secondary feature: technological therapy aides often have their own outcome measures, such as quantification of the ability of participants to perform tasks.

Technological devices are slowly finding their way into clinical practice. Simple torque-measurement devices have been applied to the purpose of hypertonia evaluation, and in some cases these devices have been developed into commercially available products (see Section 1.2.2). Similarly, robotically

aided rehabilitation has largely been a practice confined to the research environment, although recently research devices are being commercialized (see Section 1.2.1).

Commonly cited (although somewhat dated) reviews of robotically aided rehabilitation devices were presented by Riener et al. (2005) and Prange et al. (2006). Furthermore, in a research setting, the effectiveness of robotic rehabilitation devices is usually assessed against one or more traditional evaluation methods. A recent review of the outcome measures used in assessment of robot-assisted exercise trials (RAET) was presented by Sivan et al. (2011).

Volpe et al. (2001) raised the question of robot aided therapy as a realistic option - and indeed, the same concerns could be raised about technological solutions for objective evaluation as opposed to traditional, subjective assessments. They conclude their review with the following statement:

*“A final determination regarding whether the use of robotic devices in stroke rehabilitation is realistic needs to be postponed, because more work is required. However, arguments have been advanced that the proper question might be whether neglecting to arm the therapist with new tools, among them robotic devices, can continue to be a realistic option.”*

### **1.2.1. Examples of Electromechanical Devices for Rehabilitation**

The following section gives examples of robotic rehabilitation aides. These largely appear to be designed to assist with paresis (i.e. muscle weakness associated with negative features of UMNS) as opposed to hypertonia. Furthermore, the majority of attention has been devoted to rehabilitation aides for the shoulder and elbow (proximal arm rehabilitation), rather than the hand/wrist. Despite not having direct clinical relevance to this research, some examples of these are discussed here, because their design provided insight into the design challenges presented by upper limb exoskeleton devices, and also because some examples have evaluation features built in. It should be noted that this discussion only includes a selection of prominent devices in the field, and is not exhaustive.

Some devices act as assistive movement aides, providing the subject with assistance in their rehabilitation exercises when needed. The most prominent examples that come up in the field are the MIT-Manus robotic rehabilitation aide (see Figure 1.5). This class of devices was patented in 1995 (Hogan et al., 1995) and has been extensively studied, developed and reviewed since then (Krebs et al., 1998, 2004, 2007; Volpe et al., 1999). Recently, the MIT-Manus device has been commercialized by Interactive Motion Technologies, Inc. as part of the InMotion range of rehabilitative robots.

The MIT-Manus and InMotion devices attempt to assist in rehabilitation by encouraging neural plasticity after central nervous system impairment. The subject is prompted to perform certain goal-directed movements, and is mechanically assisted by the device if he or she lacks the ability to complete it. If the subject has an extremely weak arm then the robot will provide a larger assistance, but if the patient has more strength, then little or no assistance will be supplied. This principle is sometimes referred to as the „assist when needed“ approach. Similarly, the device will help to correct involuntary movement such as spasms. In mechanical terms, to allow this the robot must be back-drivable - that is to say that it must have low intrinsic endpoint mechanical impedance. This advantage of reinforcing neural links to stimulate plasticity is not offered by passive stretching techniques. In other words, if the limb is only passively stretched then the brain will not “re-learn” how to control the affected limb.

The original versions of the MIT-Manus did not originally extend rehabilitation to the hand or wrist for grasping tasks, and movements were almost entirely restricted to the horizontal plane (a small amount of passive vertical motion was allowed by means of springs). Since its original incarnations, extensions to the MIT-Manus have been developed to allow movement in the vertical direction (Krebs et al., 2004) and also to allow hand and wrist training (Krebs et al., 2007).



**Figure 1.5** A subject demonstrating the use of the MIT-Manus for shoulder and elbow rehabilitation in the horizontal plane with two degrees of freedom (Krebs et al., 2004). See Figure 1.6.

It is generally accepted that while passive stretching should be a part of the therapy regimen, there should also be a large component of task-oriented “learning”. The MIT-Manus achieves interactive task-orientated therapy with a display prompting the user to perform tasks. The device includes data logging elements which record patient performance (force, velocity, position, EMG, etc.) and can provide feedback in the form of various metrics (see Figure 1.6).

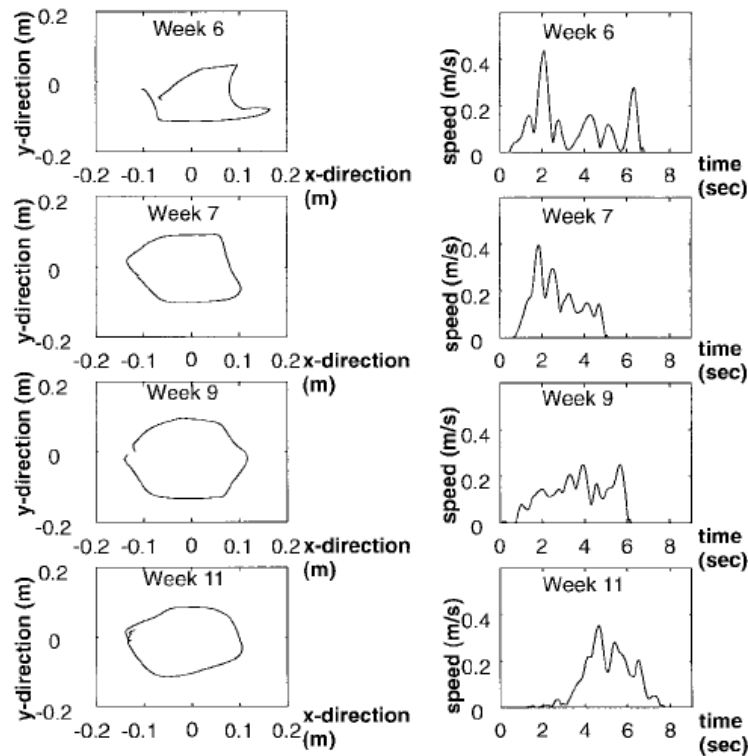


**Figure 1.6** Position and speed plots of a patient using the MIT-Manus device to draw clockwise circles starting at the 9 o'clock position, showing improving ability to smoothly and accurately perform the task through various stages of rehabilitation. The hand was within view, but no explicit feedback was provided. Note that no robotic assistance was provided for motion in this exercise, since the intention was to test patient performance. (Krebs et al., 1998). See Figure 1.5.

(Takahashi et al., 2005) developed the Hand Wrist Rehabilitation Assistive Device or HWARD as a sensorimotor rehabilitation aide (see Figure 1.7). The device has three degrees of freedom (flexion/extension of wrist, fingers as a whole and thumb), and is intended for the rehabilitation of hand weakness. It is pneumatically actuated and back-drivable, and employs separate monitors and software for interaction with the participant and the examiner (each has their own monitor). The device design minimally obstructs the palmar surfaces of the hand, so that grasping tasks can be exercised. Similarly to the MIT Manus, therapy with the device is not passive, but rather requires movement to be initiated by the participant, and the device would assist in completion of the task if

necessary. While the 2005 paper only describes the design of the device, in more recent work researchers assessed the effectiveness of the device as a rehabilitation aide (Takahashi et al., 2008). Over the course of 3 weeks, patient's motor abilities using a number of tests were monitored (including the MAS score). EMG in three muscles, and functional magnetic resonance imaging (fMRI) studies were also conducted before and after treatment to assess the benefits of therapy with the device. The behavioural and motor ability scores mostly showed improvements. The fMRI findings showed significant and interesting cortical reorganization (see Figure 1.8), but the EMG study failed to show significant muscle activation improvement post-therapy. This indicated a cortical reorganization, but not task performance improvement. Behavioural gains were observed, however, in other outcome measures (such as the Fugl-Meyer score).

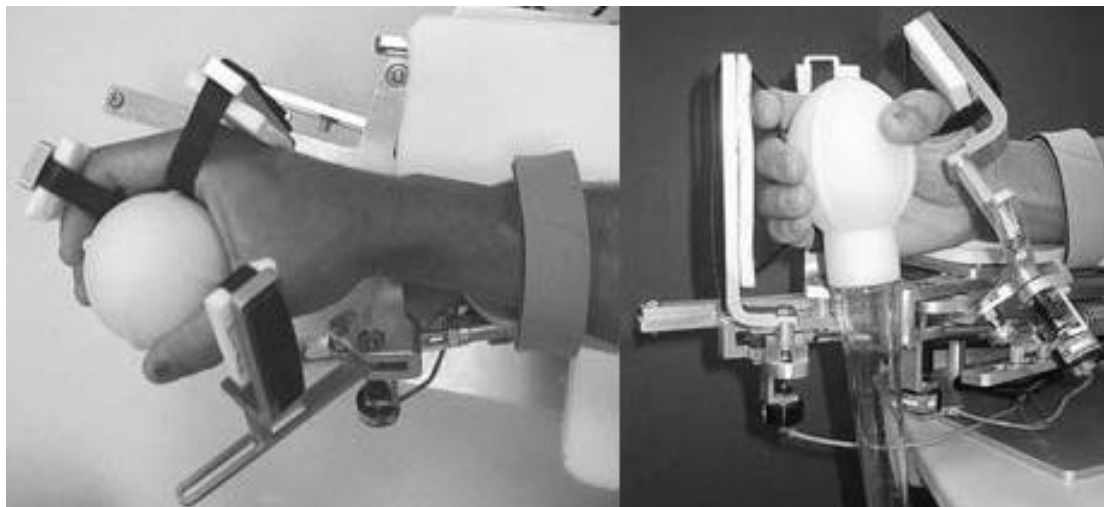


**Figure 1.7** Subject demonstrating the use of the HWARD hand rehabilitation robot. Note the unobstructed palmar surface of the hand, allowing grasping of objects (Takahashi et al., 2005)

The REHAROB system (specifically designed for treatment of spastic hemiparesis) attempted the use of standard, unmodified industrial robots for rehabilitation (see Figure 1.9). The results of clinical trials were presented by Toth et al. (2005), showing that the device is safe and performs as intended. With the REHAROB system, exercises can be three-dimensional, complex, anti-spastic passive movements, however the device is completely passive and movements are completely prescribed. The operation of the device involves strapping the patient into the device, following which the therapist “teaches” the device the motions that are required by manipulating the patients arm and the device together. At this point, the therapy program can be edited (such as decreasing the velocity of movements), and then “played back” – the device recreates the learned movements to the desired number of repetitions and with the desired alterations.

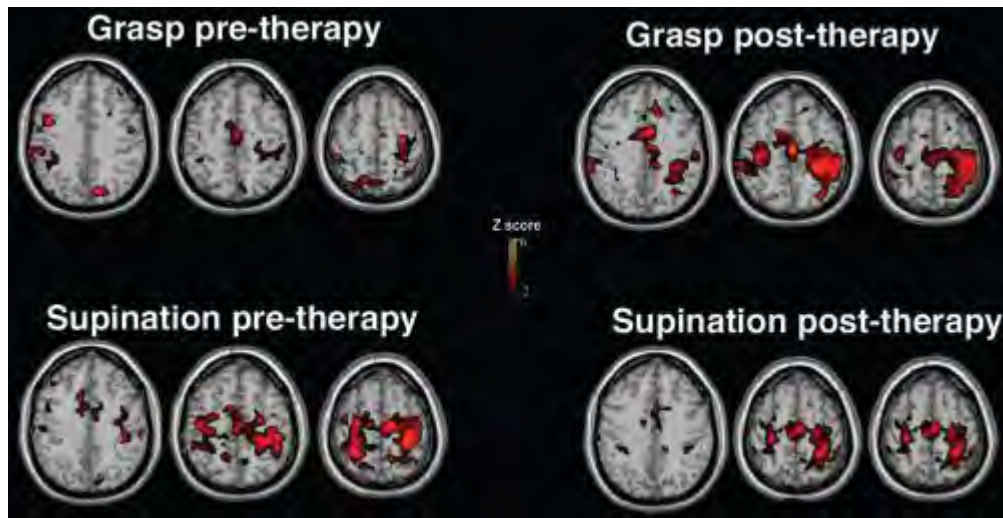


**Figure 1.8** fMRI activation volumes before and after treatment with the HWARD hand device, illustrating clear increases of activation volume in the practised task (grasping) but not for the unpractised task (supination). (Takahashi et al., 2005)

Devices such as the Mirror Image Movement Enabler or MIME (Burgar et al., 2000) and the Bi-Manu-Trak (Hesse et al., 2005) (see Figure 1.10 and Figure 1.11 respectively) use a technique to enhance rehabilitation whereby the affected hand's movement is guided by the movement of the unaffected hand. The patient is asked to perform the same action in both hands, such as pronation of both forearms, but will have impaired control over one hand due to their pathology. The machine will exert appropriate forces onto the more affected limb to mirror the movements of the less affected limb. In addition, the MIME machine has a setting which allows for passive (predefined) movement, which is not initiated by the patient. It was deemed that while task-oriented movement is effective at encouraging cortical plasticity, passive movement was also beneficial in treatment.

The devices discussed in this section are designed to be used as rehabilitation aides, but often will incorporate some form of outcome measure. For example, in-depth information was recorded by the MIT-Manus device, such as joint torques and velocities as well as EMG. It should be noted, however, that while devices such as the ones discussed in this section often include internal evaluation systems, these remain secondary to rehabilitation features of the device. As will be discussed in Section 1.2.2, other devices, for which the evaluation of hypertonia evaluation is the primary feature, also exist.



**Figure 1.9** A subject demonstrating the REHAROB robot, an adapted industrial robot for passive movement of the upper extremity (Toth et al., 2005)

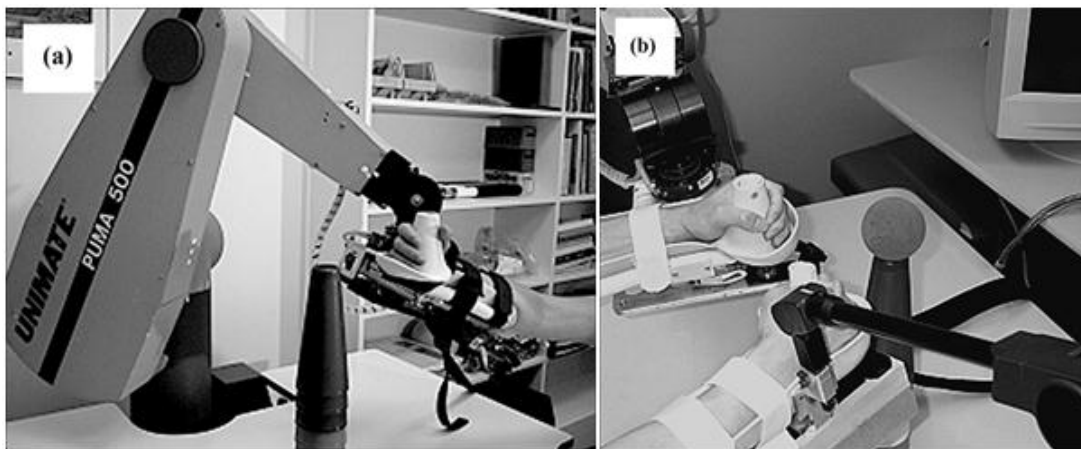


**Figure 1.10** Unilateral (a), and bilateral (b) movements with the MIME device (Burgar et al., 2000)

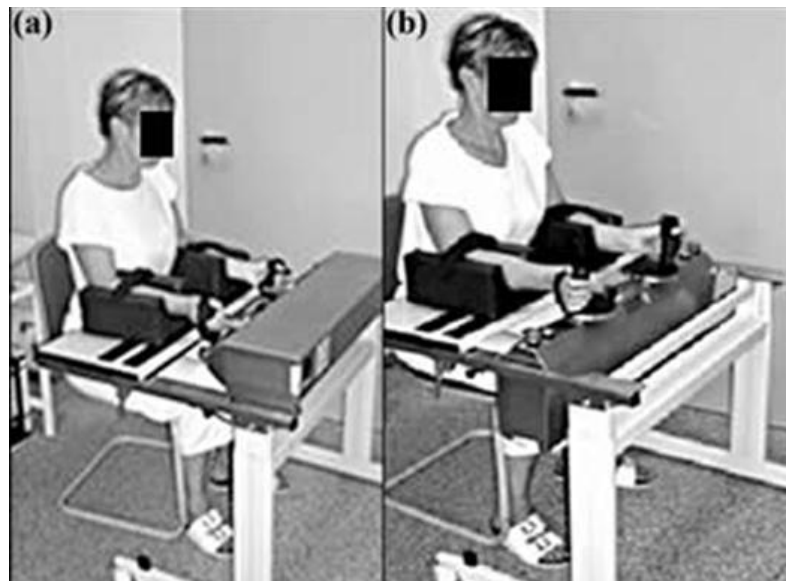


**Figure 1.11** Bi-Manu-Trak device bilateral forearm pronation/supination (a), and wrist flexion/extension (b) (Hesse et al., 2005)

### 1.2.2. Devices for Objective Evaluation of Hypertonia

In this section the use of electromechanical devices to quantify muscle performance (including increases in muscle tone), will be discussed.

As was discussed in Section 1.1.5, the most commonly used evaluation techniques for hypertonia are ordinal scales, such as the MAS score. The clinical popularity of such methods has been largely due to the convenience benefit. The reliability and resolution of these scales, however, have driven research into technological alternatives. EMG has also been used to provide an indication of muscle activity for research involving muscle tone (e.g. Levin and Feldman, 1994; Jobin and Levin, 2000).

The complexity of such devices varies from simple hand held instruments to large non-portable systems. Smaller devices offer convenience, but are limited in their functionality to that for which they were designed (for example, only being useful for assessment of one joint). Larger systems, such as the Biodex (“Biodex Dynamometers,” 2014), allow measurement of many parameters with many settings, and have been used to analyse muscle tone. For example, computational techniques have been used with similar such devices and to separate the effects of muscle, passive stretch and reflexive action (Mirbagheri et al., 1998, 2000; Alibiglou et al., 2008) Furthermore, such systems allow features as computer-numerically controlled isokinetic evaluation. However, while intuition dictates that isokinetic systems would provide better results than simple hand-held systems due to the velocity-

dependent nature of spasticity, this may not necessarily be the case, as is suggested by the results when different systems are compared (Boiteau et al., 1995).

The Myoton device (see Figure 1.XX) is a small, hand-held device for quantifying muscle tone. Reliability of the device has been demonstrated, but it has yet to be used outside of a research environment. The device uses the myotonometric measure (Bizzini and Mannion, 2003) for estimating muscle tone: the device is pressed gently against the skin above the belly of the tested muscle and applies a short mechanical impulse. This causes a brief deformation in that muscle, followed by damped oscillations which are recorded by an accelerometer in the device. Muscle tone estimates are inferred based on the properties of the recorded oscillations.

While electromechanical devices are common in the research environment, some devices are finding their way to commercial availability. A prominent example is the NeuroFlexor device (Lindberg et al., 2011).

The NeuroFlexor device, visible in Figure 1.12, is specifically designed to measure the resistive force during wrist extension. The designers presented a validation of a biomechanical model for use with the device that can help to isolate the neural component of this resistive force (Lindberg et al., 2011).

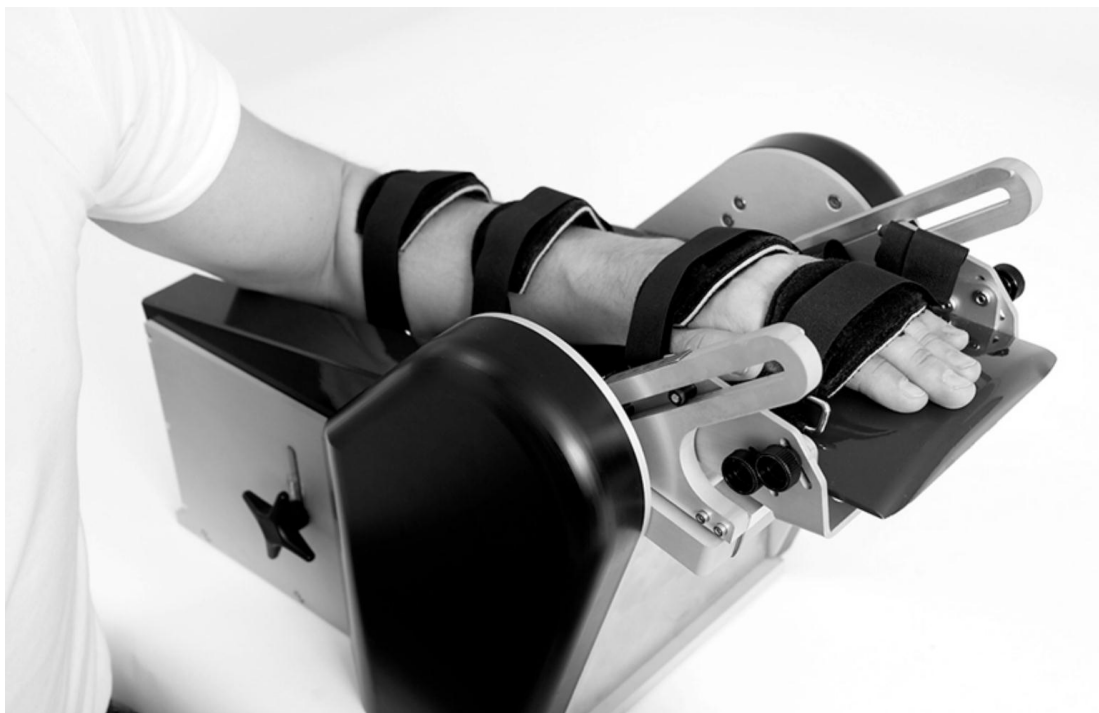


**Figure 1.12** Photograph of the NeuroFlexor device, a commercially available device for the evaluation of spasticity of the finger and wrist joint (“NeuroFlexor Online Brochure,” 2012). See Figure 1.13.

According to their biomechanical model, the total resistive force can be subdivided into the passive and active components. The passive component can be further subdivided into the passive elastic force, viscous force and inertial force. The model is as follows:

$$F_m(\theta) = F_{Passive}(\theta) + F_{Active}(\theta)$$

(Equation 1.1)

Where  $\theta$  is the joint angle of interest,  $F_m$  is the total resistive force,  $F_{Passive}$  is the passive component and  $F_{Active}$  is the active (i.e. neural) component of this force.  $F_{Passive}$  is comprised of elastic, viscous, and inertial components.

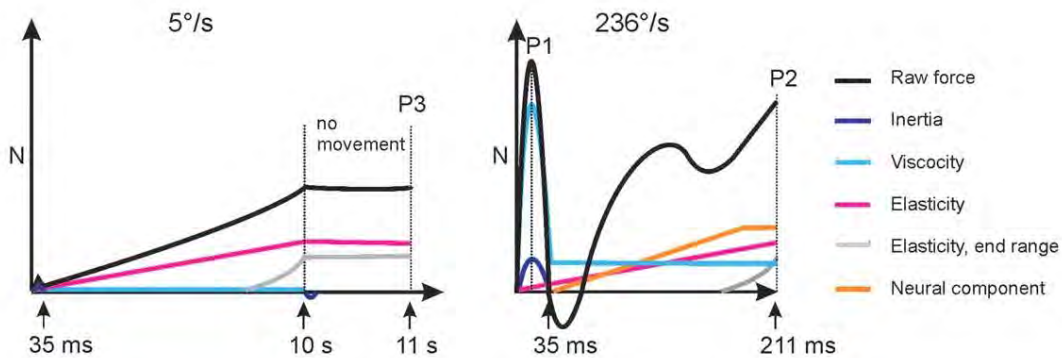


**Figure 1.13** Illustration of raw force data collected with the NeuroFlexor device for the slow (left) and fast (right) repetitions, indicating where the forces at the three points of interest (P1, P2 and P3) were noted (Lindberg et al., 2011). See figure F1.12.

The values of the passive components of the total resistive force are estimated based on points of interest in the force data recorded during passive wrist extension across the range of motion at various velocities (see Figure 1.13). The neural component of the force recorded at the end of the range of motion is what remains when these passive components have been subtracted.

This neural component corresponds to the late stretch-evoked responses as observed by Ibrahim et al., (1993), and not the initial spinal stretch reflex (which has a latency of 40ms).

The validation of this biomechanical model included the assessments of chronic stroke patients (n=31), while simultaneous EMG in addition to traditional assessments obtained with the MAS score and other performance measures.

The primary method of validation of the model was to repeat the test with an ischemic nerve block in the affected limbs of some participants (n=7) to negate the effect of the neural component. Other analyses included correlating EMG power with the measured neural component, confirmation of velocity dependence of the neural component, and correlation between resistive forces and the MAS score.

The results indicate that the model can be used to accurately separate the active and passive components of the resistive force. The authors reported that both the resistive forces and the neural components “correlated strongly” with the MAS score ( $r>0.6$ ,  $P<0.001$ ). In a thesis (an evaluation of the performance of the NeuroFlexor system), presented by Gäverth (2013) on the same work, it is reported that there is a stronger correlation between the MAS score and the total force than with the neural component alone. This finding suggests that the MAS score is a more accurate measure of passive resistance, rather than true spasticity.

### **1.2.3. Opportunity for Further Development**

In short, the literature revealed that there is currently a trend towards robotics in rehabilitation (both for treatment and evaluation), and that there is a definite advantage to be offered by such methods. The art is, however, in its infancy. Many challenges exist, but these challenges are not insurmountable. While there are multiple devices that may assist in motor-rehabilitation and assessment of various features of UMNS, attention is seemingly diverted from hand/wrist therapy. Reaching tasks are important for day-to-day activities, but fine motor control is also important. As such, neither aspect of therapy should be neglected. They should be developed in parallel.

While some devices exist, even commercially, for the evaluation of hypertonia in the hand and wrist, there is still opportunity for development. The NeuroFlexor device, as discussed in Section 1.2.2, measures the hypertonia in the fingers and wrist flexors, and even goes so far as to use a biomechanical model to distinguish between the neural and non-neural components of the increased tone. The device cannot, however, determine the relative contributions from each. This is because the

finger flexor muscles have a moment arm at the wrist joint (see Figure 1.12) and as a result, extension of the wrist joint acts to extend the finger flexor muscles as well. Hypertonia in the finger flexor muscles would result in a torque about the wrist joint which, using the NeuroFlexor in its current incarnation, would be indistinguishable from torque due to wrist flexor hypertonia. These two components (finger and wrist flexor hypertonia) are reported as a combined value.

The opportunity exists to investigate the potential benefit of measuring the finger and wrist joint torques, either separately during finger and wrist manipulation respectively or possibly simultaneously during only wrist extension by measuring the force applied by the finger and wrist separately. Using the results from these separate analyses, and using a biomechanical model, it would be possible to develop a robotic device for the evaluation of wrist flexor hypertonia that compensates for the effects of finger flexor hypertonia thereby providing more accurate assessments.

Following an investigation into the effects of isolating the finger and wrist flexor contribution to wrist joint torque has been established, future analyses on repeating the protocol of using the NeuroFlexor's approach (for isolation of the neural component of torque) can be considered.

### **1.3. Objectives**

The work presented in this thesis had two main objectives:

#### **Objective 1**

To design and construct a patient-safe device for the manipulation and torque measurement of the wrist and finger joints, which can be used with a simple biomechanical model for wrist flexor muscle tone evaluation.

#### **Objective 2:**

To assess the evaluations obtained from the device in Objective 1 in a clinical setting, by comparing the device evaluation results to those from commonly used assessment methods:

Compare the device evaluation using wrist-only force data to the average of three assessments from three clinicians:

- 1- Compare the torque measured at the wrist joint to evaluations using the Modified Ashworth Scale
- 2- Compare the device evaluations using a biomechanical model which considers wrist and finger torques to evaluations using the Modified Ashworth Scale

[This page is intentionally left blank]

## 2. Apparatus

A robotic exoskeleton for the manipulation of the hand and wrist joints was specifically designed and built to achieve the objectives of this research project (see Section 1.3). This device differs from the NeuroFlexor (see Section 1.2.2), in that it specifically measures the torque contributions from finger and wrist flexors separately, as opposed to only wrist torque. The design also features vertical joint axes to mitigate the possible effects of gravity on the outcomes (compare Figure 1.12 with Figure 2.3).

In this thesis, the mechanical components are referred to as “the device” for simplicity. All components as a whole – including the device, control electronics, cables and all other components - are referred to as “the system”. The device and its components are a subset of the system (see Figure 2.2). This chapter provides an overview of system specifications, and more information about the design and manufacturing of the system is presented in Appendix A and Appendix B.

The system used in this project was developed following consultations with neurologist Professor Alan Bryer and physiotherapist Carolyn Davids of the Department of Neurology and Physiotherapy at Groote Schuur Hospital, Cape Town, South Africa. These discussions yielded the initial clinical requirements for the system and, from these the starting point for the design was derived.

### 2.1. Device Design Specifications

The system functioned to emulate and automate the standard procedure for performing a MAS assessment. The device functioned as follows:

- The system was designed for use with participants with mildly to moderately increased muscle tone of the wrist and finger joints (i.e. a MAS score of below 3). Participants with severe spasticity were excluded from testing. It was estimated that the resistance applied to each force transducer (wrist and finger joint) due to increased tone would be below 30 N.
- The participant was secured into the device and asked to relax. Only involuntary resistance was of interest.
- The system firmly but gently moved the participant’s metacarpophalangeal joint (MCP or „knuckle” joint) and the wrist joint between the flexed and extended positions:
  - The finger joint was manipulated over a 90° range (from straight to 90° flexion).
  - The wrist joint was allowed a range of 105° (from 70° in flexion to 35° in extension).

These wrist ranges was selected based on the expected comfortable range of motion of participants with mildly to moderately increased tone (see Figure 1.4).

- During the movement, force transducers measured the resistance to the passive motion (see Section 2.4).
- A four channel EMG signal acquisition system was also included (see Section 2.3).

The EMG signal acquisition system was used during the preliminary safety tests (see Section 3.1). These tests helped to confirm safety features which satisfy a part of Objective 1 (Section 1.3), namely that the device must be “patient safe”. Note that EMG did not directly verify safety of the device, but was merely used as an input for control of device movement during the preliminary safety tests. Safety was verified by observation that the device - especially safety features such as the safety buttons - operate as intended without malfunction. Safety features will be discussed in Section 2.2.3.

Certain design philosophies were adopted as guiding principles during planning and development of the system. These were in addition to the basic engineering and clinical requirements and constraints of the system, such as safety and functionality. These important philosophies were as follows:

- The system should, if possible, not be intimidating to the participant. For examples the use of plastic components where possible, instead of metal, so that the device appears less “industrial”.
- The system should be easy to operate and require minimal training for the clinical staff.
- The system should be easy to manufacture. Where possible, design should minimize specialized components.

### **2.1.1. Coordinate system**

A rotational coordinate convention was adopted to specify device joint position, to indicate various levels of anatomical joint flexion and extension, and to indicate directions of applied forces or torques. Joint positions are measured from straight (i.e. aligned with the forearm), with positive angles indicating flexion (see Figure 2.1). For example, if the fingers were stated to be at +45 degrees, it meant that they were flexed at 45 degrees from straight. If the wrist is stated to be as -10 degrees, it means that the joint is extended to a position of 10 degrees from straight.

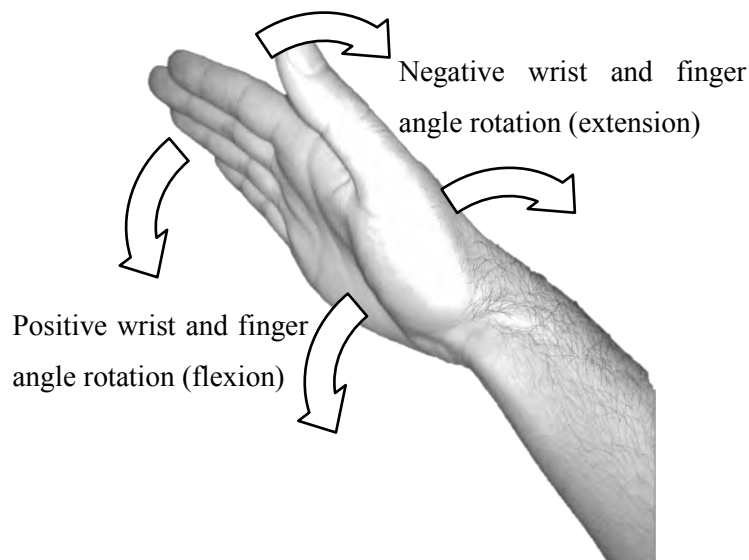


**Figure 2.1** Convention for specifying joint rotational position and velocity.

## 2.2 Device Construction

### 2.2.1. Overview of System Components

For images of the system, see Figures 2.2 to 2.4. The device was invertible, meaning that it could be used to interface with either the left or the right hand of the participant. The system was designed to comfortably but firmly manipulate the wrist or finger joints in flexion or extension. The device components were subdivided into the following categories (see Figure 2.6):

- Main structural components – Plastic or aluminium. These connect, locate and support the motors and other components and provide a framework and base upon which to stand
- Force sensing elements – Aluminium. Fitted with strain gauges for the purposes of measuring load applied to them (i.e. force transducers).
- Interface elements – Aluminium. These directly interface with the participant, lined with foam rubber for comfort

Parts of the base and main structural components were fabricated of poly(methyl methacrylate) – also known as PMMA, or as its trade name „Perspex“ – to be in line with the design philosophy of using plastic components where possible. The force transducer elements and interface elements, however, were fabricated of aluminium due to space limitations necessitating compactness and strength. All surfaces that interfaced with the participant were coated in soft foam for comfort.

The flow diagram for the integration of these components is shown in Figure 2.5.

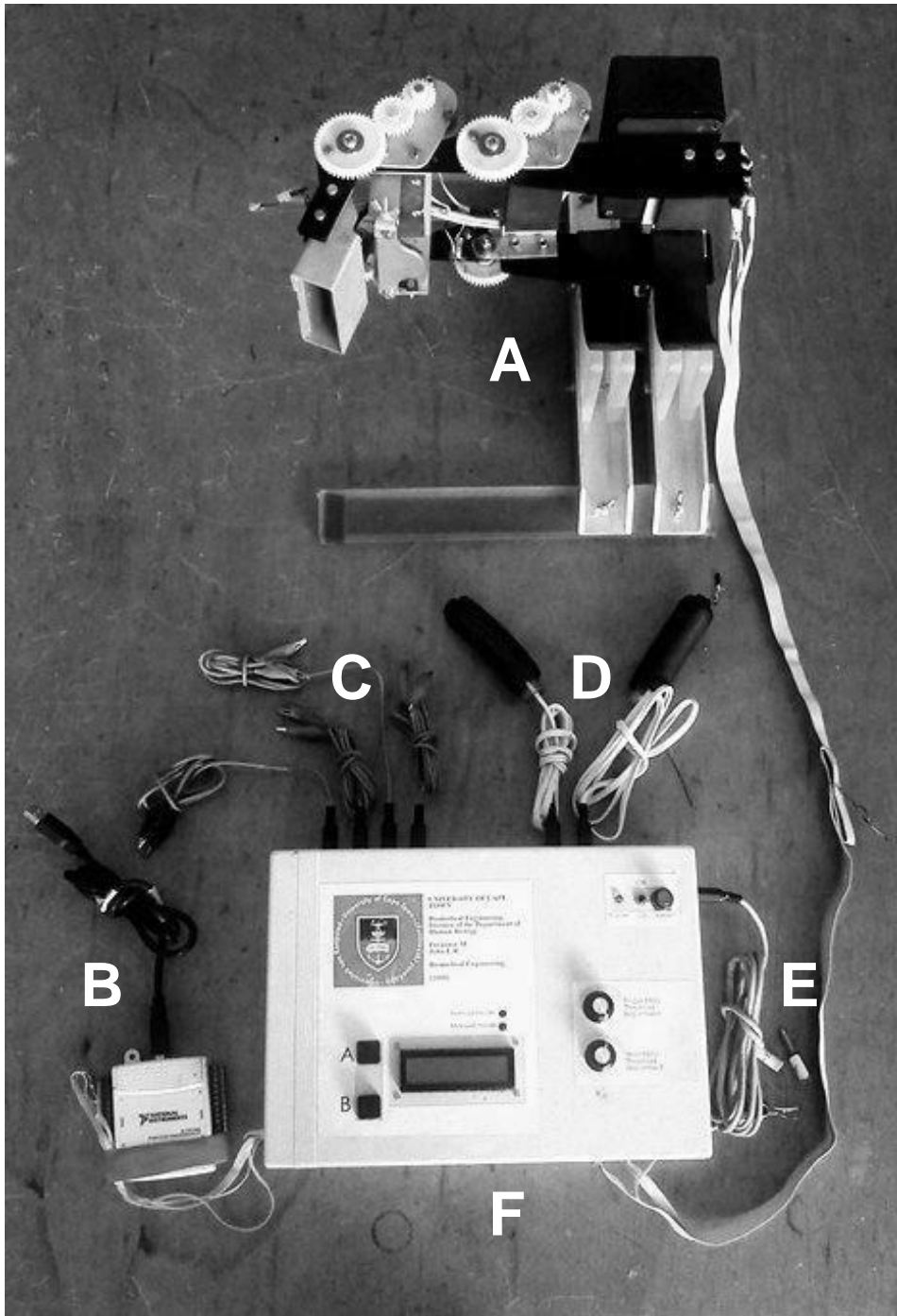


**Figure 2.2** Overview of all components making up the system: (A) Mechanical components of the system (i.e., „the device“), (B) data logger for USB for connection to PC, (C) cables for EMG electrodes, (D) safety buttons, (E) power input, (F) main control box housing electronic components (except strain gauge amplifiers which were located on the device rather than in the control box).

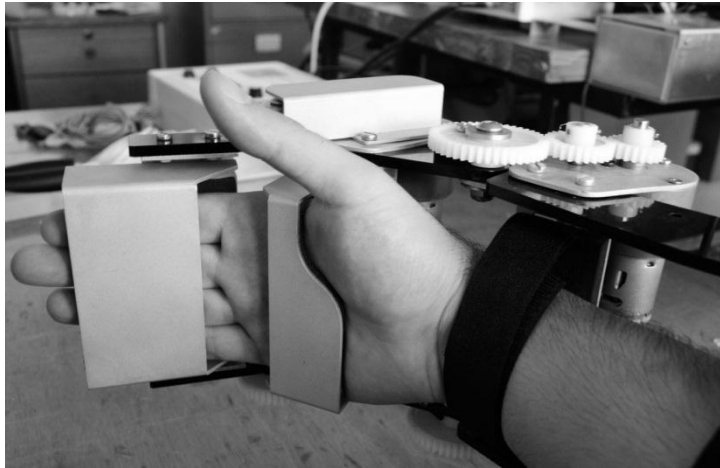


**Figure 2.3** The neutral position of the device (wrist at 0°, fingers at +45°) illustrating how the participant's hand was secured.

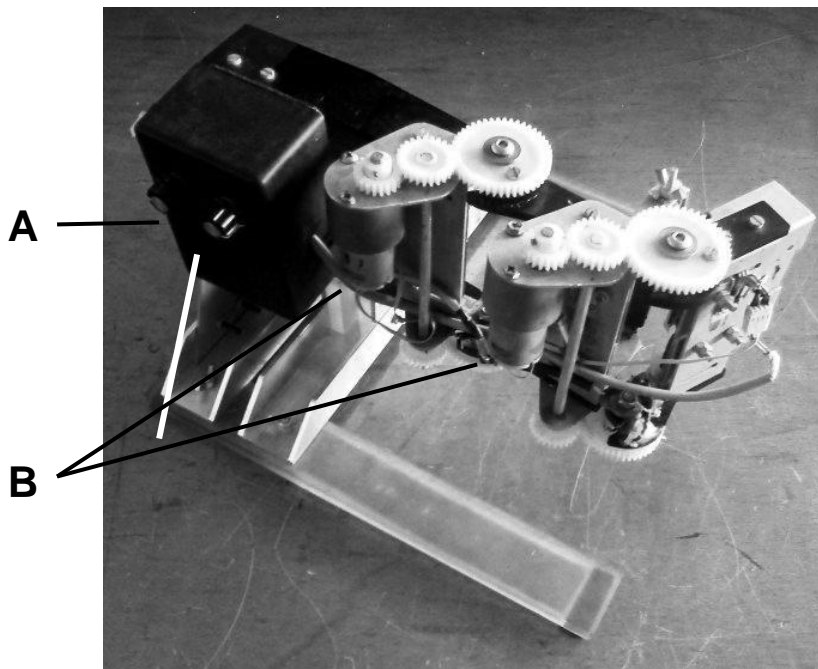


**Figure 2.4** Back view of device, illustrating the enclosure housing the strain gauge amplification circuitry (A), and the motors (B).

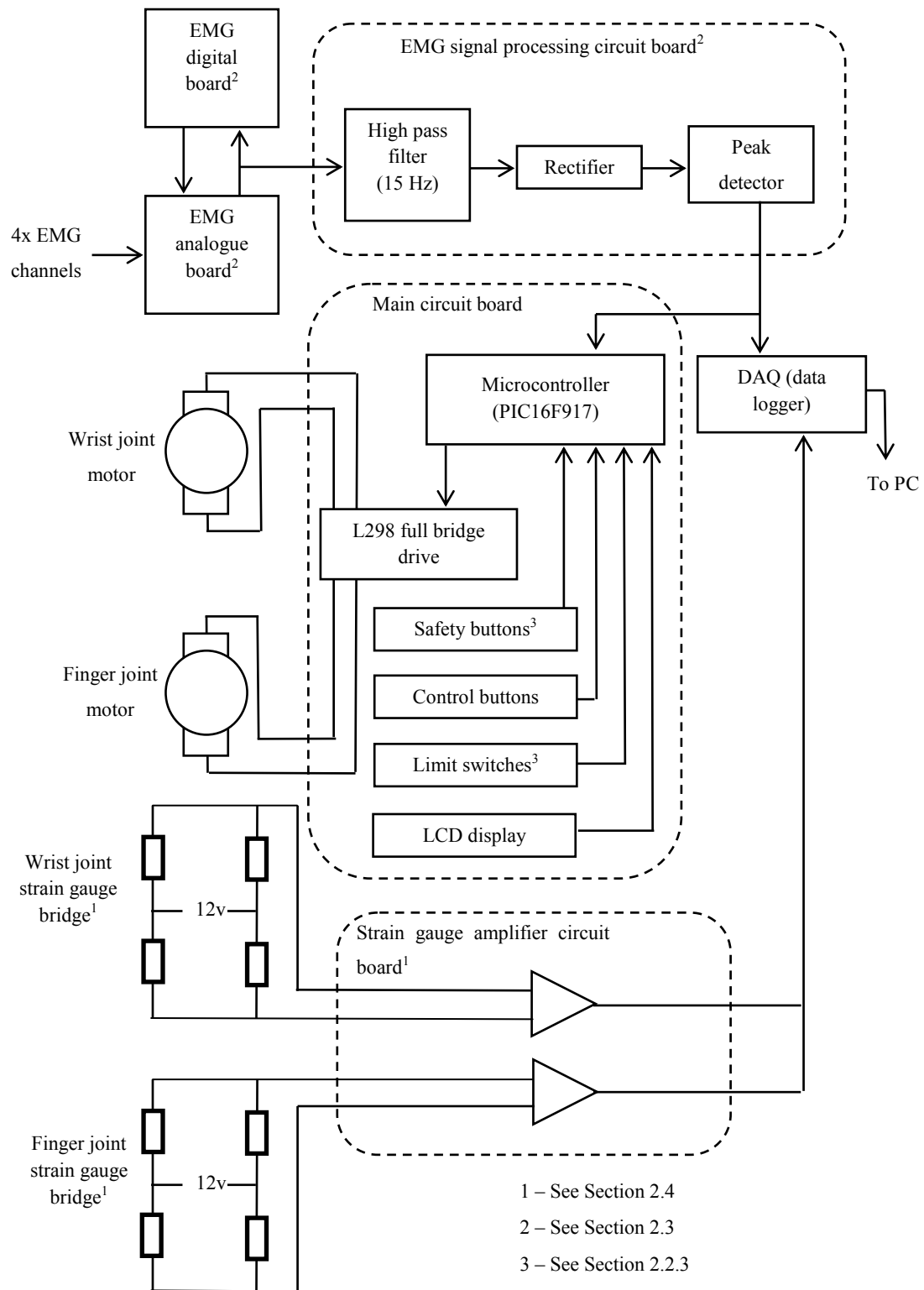


**Figure 2.5** Functional overview of the components of the system (power management circuits not shown).

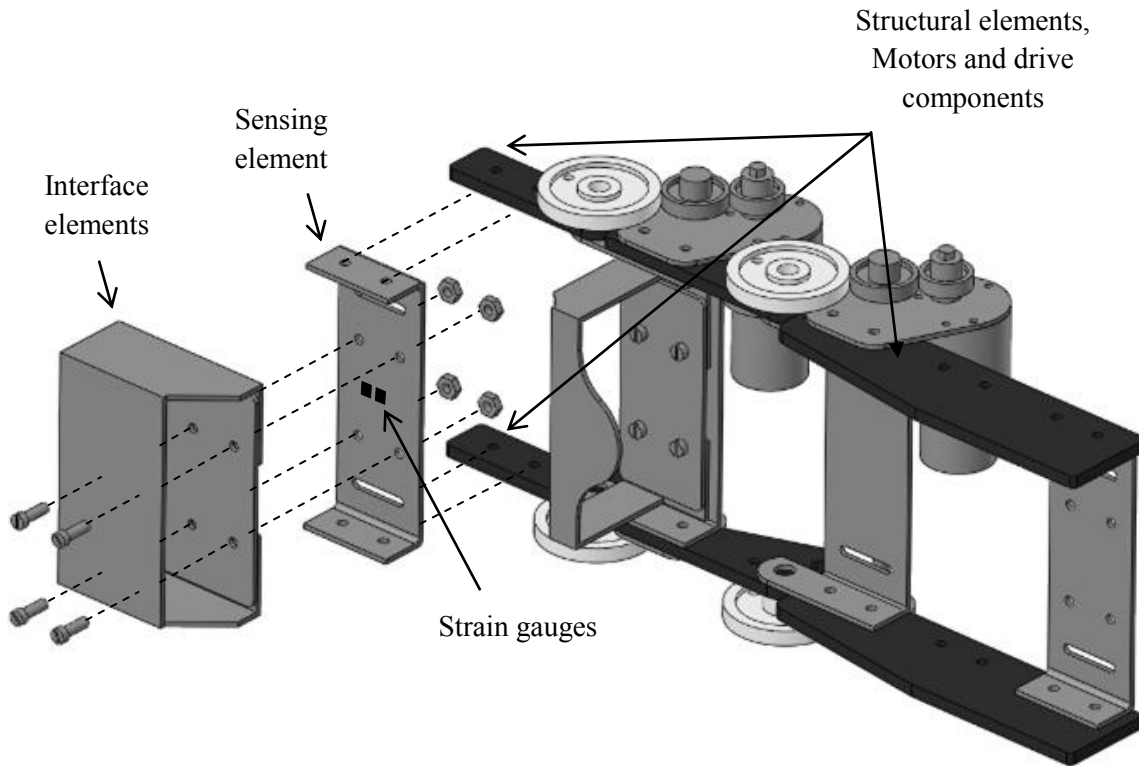


**Figure 2.6** Exploded view of structural, force transducer and interface components of the device finger joint (some components have been omitted for clarity of illustration).

### 2.2.2. Torque and Speed Specifications

The finger and wrist joint actuators were identical – geared, brushed DC electric motors. The use of somewhat limited motor power was intentional, for participant safety. It was recognised that the joint velocity might fluctuate due to resistance from participants when using motors of limited power. Participant safety was a priority, however, and more powerful motors would have introduced a substantial risk.

Two types of motors were used at different points in the study. With the slower motors, a maximum rotational speed of both the finger and wrist joints (after power transmission through the gear train) was 4.4 rpm (26.6°/s), and the rated torque at these joints was 1.32 N.m. With the faster motors, the maximum speed of each joint was 9.6 rpm (57.8°/s) and the available torque of each was 4.0 N.m. The use of these motors at different times during testing will be discussed in Section 3.2.

### 2.2.3. Safety Features

Safety was a priority in the design of each element of the system. Safety features primarily guarded against application of excessive torque to the participant's hands, but also against device malfunctions, hyperextension, and electric shock. These safety features are discussed here.

Two safety buttons were included in the design. These were simple push-buttons mounted on a handle (see Figure 2.2 and Figure 2.5). These buttons were required to be held to enable device movement. The buttons were operated by the participant as well as by the examiner. If either became uncomfortable with the any aspect of using the system, the button could be released and movement would immediately cease.

The method of implementation of the safety buttons was twofold: when a button was released, software algorithms (microcontroller implemented) as well as hardwired electronics (L298 dual bridge driver) ceased power to the motors (see Figure 2.7). For the latter the safety buttons were connected to the „enable“ pins of the L298 IC. By releasing the button the enable pins were pulled low thereby deactivating the motors' power source.

Features guarding against hyperextension included the mechanical stops (see Figure 2.8). The various structural elements were designed such that they physically obstructed rotation of the joint beyond the defined limits. This was designed to guard against the event that the limit switches fail to cease movement.

The mechanical range was pre-determined and not adjustable in this prototype. The finger joint's mechanical stops engage to only allow motion between  $0^\circ$  and  $+90^\circ$ , and the wrist's mechanical stops engage to only allow motion between  $-45^\circ$  and  $+90^\circ$ . Although the actual limits of operation of the wrist in practice were narrower due to the use of electrical limit switches (see Figure 2.9). The limit switches limited operation of the wrist to between  $+70^\circ$  to  $-35^\circ$ .

Certain design choices were also motivated by safety. As stated in Section 2.2.2, the motor torque was deliberately limited even though this may have slightly affected rotational speed of the joints against varying resistance. Also, electrical limit switches were necessary to cut motor power when the ranges of motion had been reached. The choice to wire them such that engaging the switch opened the circuit (rather than closing it) was made with safety in mind: a faulty connector or broken wire would not maintain voltage to the microcontroller. This potentially dangerous fault would not be detected if the unengaged state of the limit switch was chosen to be open circuit.

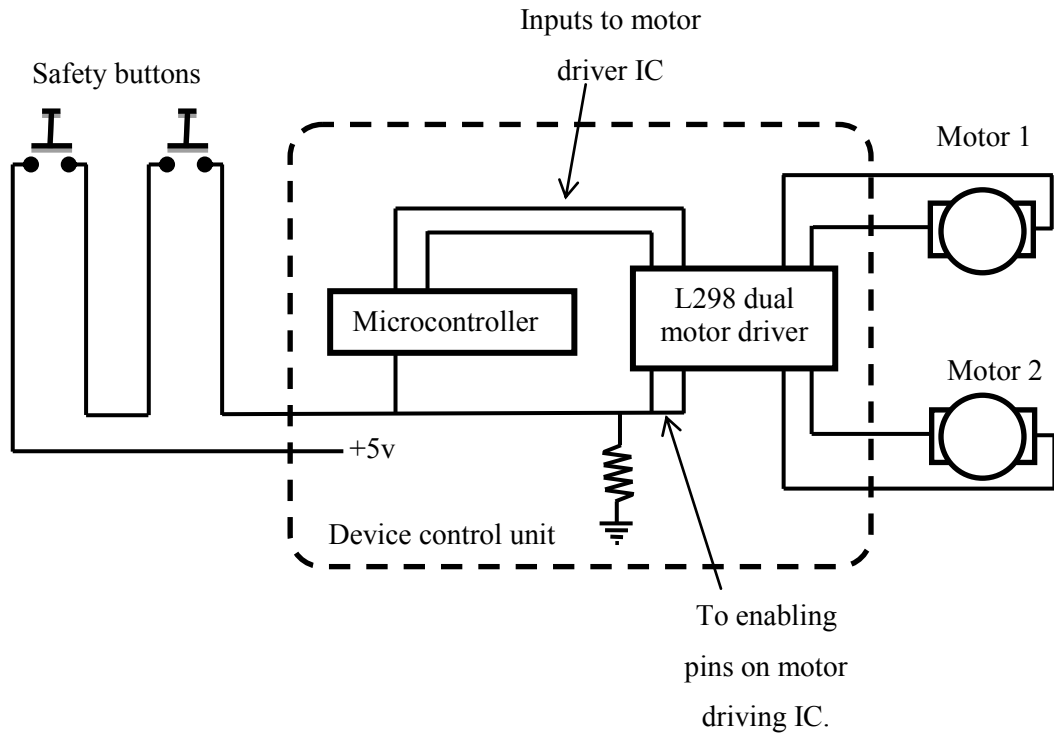


**Figure 2.7** Diagram illustrating how handheld safety buttons have redundancy in how they interrupt motor power.

### 2.3. EMG Signal Acquisition and Processing

An EMG signal acquisition system was included such that muscle activity could be recorded during tests. The observed EMG would be useful for distinguishing between neural and non-neural joint resistance (see Section 1.1.1). Non-neural joint resistance (such as due to soft tissue changes) would not be accompanied by electrical muscle activity. EMG data was useful to aid interpretation of the force data collected during the pilot clinical trials.

EMG was acquired using a bandwidth-modified version of the open source Modular-EEG boards (“The OpenEEG project,” 2013). See Appendix B for details about the OpenEEG boards, and Appendix C for details about the bandwidth modifications made.

The signal produced by the OpenEEG amplifier board was recorded by the DAQ without any alteration. It was also processed by a dedicated circuit board before being sent to the microcontroller (see Figure 2.5).

This EMG signal processing was performed with analogue electronics. It consisted of the following steps (see Figure 2.10):

- Additional high-pass filtering of the signal with a cut-off frequency of 7.3 Hz to remove low frequency components such as motion artefact.
- Rectification of the signal using a precision rectifier to avoid loss of information
- Peak detection to provide an „envelope“ for microcontroller processing.

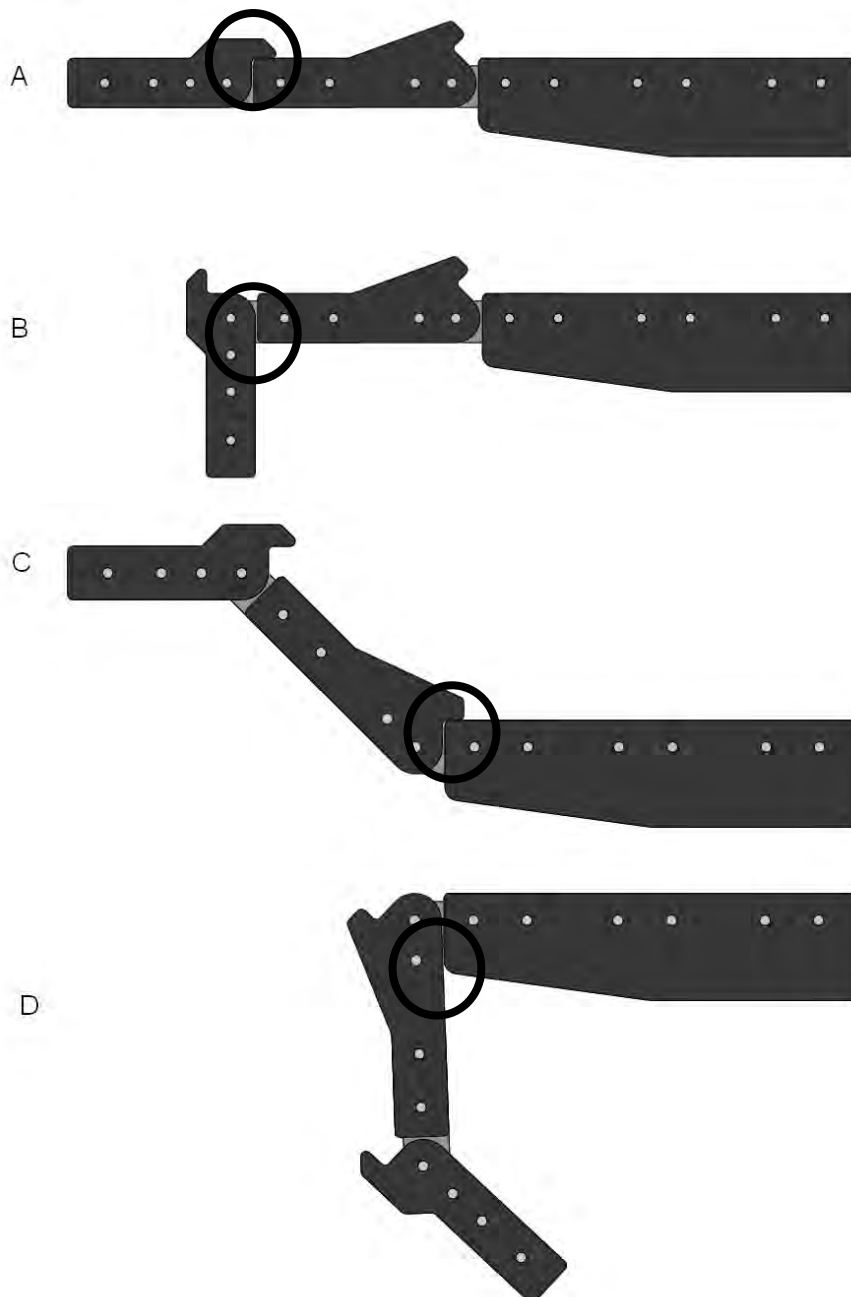


**Figure 2.8** CAD images showing a top view of selected structural components indicating how hyperextension blocks limit range of motion: (A) device finger and wrist joints at  $0^\circ$ , (B) device finger joint at  $90^\circ$  and wrist joint at  $0^\circ$ , (C) device wrist joint at  $-45^\circ$  and finger joint at  $+45^\circ$ , (D) device wrist joint  $+90^\circ$  and finger joint  $+45^\circ$ .

Four separate channels of EMG were available to be recorded, each connected to a dedicated analogue input pin on the microcontroller. In software, the analogue EMG signals were compared to the voltage set by user-controlled EMG activation threshold adjustment potentiometers to determine when a muscle was deemed active.

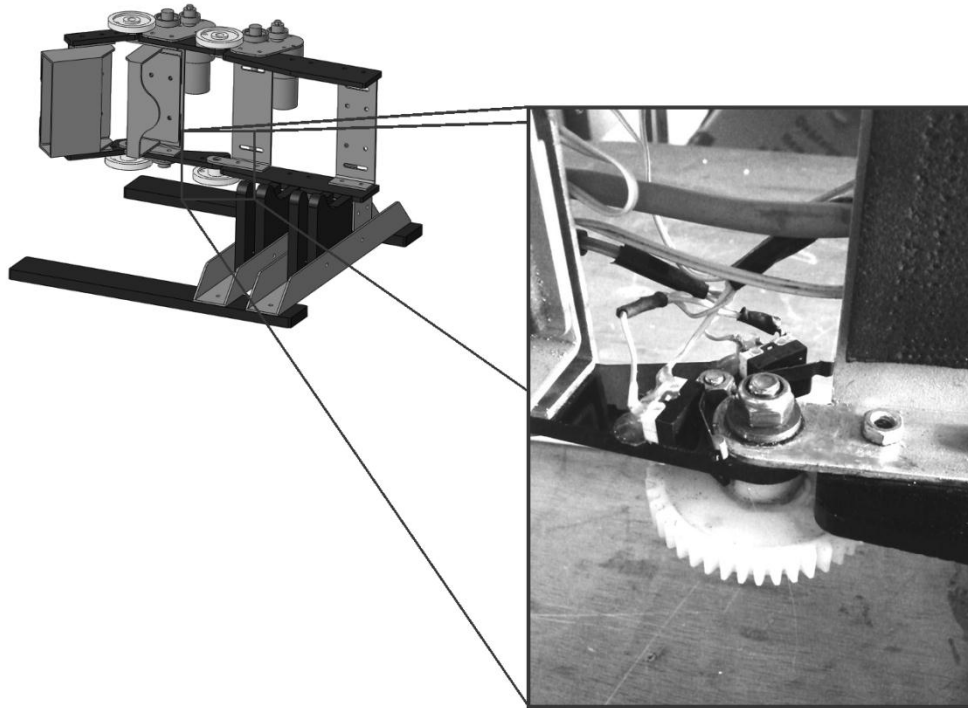


**Figure 2.9** Limit switches for wrist flexion and extension, engaged when wrist was flexed to +90 degrees or extended to -35 degrees respectively.

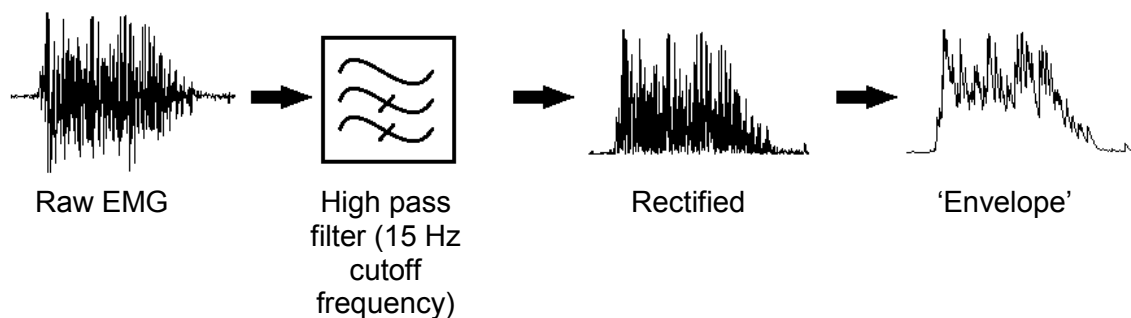


**Figure 2.10** Analogue EMG signal processing performed by the dedicated analogue EMG processing circuit board

For this comparison of EMG to the threshold, a double threshold system was applied to the EMG signals in software on the microcontroller. This was essentially a software implementation of an

electronic circuit known as a Schmitt trigger (see Horowitz and Hill, 1989). For the output to change from low to high, the EMG envelope must exceed the higher of two thresholds. However, in order for the output to return to the low state, the input must drop below the lower threshold. This prevented chatter which is observed in a single-threshold system. The upper threshold was set by the user by adjusting the threshold adjustment knobs on the control box. The lower threshold was set in software to be 20% of the upper threshold setting, which was decided following experimentation with different values. The end result of the analogue EMG signal processing was a boolean value for each muscle, with the high value indicating activity. The microcontroller uses the processed EMG data to determine which joint gesture is being attempted by the participant, and react accordingly (see Table 2.1). If the wrist flexor muscle being monitored (flexor carpi radialis) was deemed active, the wrist joint on the device was rotated. Similarly, if the wrist extensor muscle (extensor carpi radialis longus) was deemed active, the device's wrist joint was extended. If both were deemed active no action was taken. This was because, in a biomechanical sense, the co-contraction of agonist and antagonist muscles acts to stabilize a joint and no net rotation is produced.

Similarly, if the finger flexor muscles were deemed active, then the wrist extensor muscle EMG was ignored. This was because, if contracted in isolation, the finger flexor muscles also have a moment arm at the wrist joint. If only finger flexion is desired, then wrist extensor muscles are recruited to stabilize the wrist joint and a small amount of wrist extensor EMG is seen during finger flexion. Similarly, if finger extension muscles were deemed active, wrist flexion EMG was ignored.

### **2.3.1. EMG Safety Features**

Important safety features formed integral parts of the modified OpenEEG boards. These include optical isolation, for example, to isolate and protect the participant from current surges in the event of electronic failure.

Safety was also a factor when developing the experimental protocols which included EMG data collection. For example, the data collection electrodes should always be placed on the same limb as the noise cancelling ground electrode (also known as the DRL electrode – see Section 3.2.1). If one were to collect EMG data of a muscle on the contralateral arm to the ground electrode, the potential exists for a fault to allow electrical current to pass through the heart. This, while extremely unlikely, could be a potentially lethal event and all precautions should be taken to guard against it.

**Table 2.1** Truth table for sensed EMG and joint activity

wrist extensor	wrist flexor	finger extensor	finger flexor	Deemed activity:
0	0	0	0	no activity
1	0	0	0	wrist extension
0	1	0	0	wrist flexion
1	1	0	0	no activity (wrist stabilized)
0	0	1	0	finger extension
0	0	0	1	finger flexion
0	0	1	1	no activity (fingers stabilized)
0	1	1	0	finger extension only
1	0	0	1	finger flexion only

## 2.4. Force Transducers and Associated Electronics

The force sensing elements were fabricated from 1050-H14 sheet aluminium. The thickness was selected such that a measurable strain would be produced when the expected force was applied (estimated to be 30 N). The calculations for the thickness are presented in Appendix A.

Four strain gauges were adhered to the force sensing elements, into which the wrist and the finger interface elements transmitted force, and each strain gauge set was in a full bridge configuration, arranged to detect bending loads. The output of each bridge was amplified in analogue electronics (see Figure 2.11) before being recorded by the DAQ.

The amplifier circuit used an INA114BP instrumentation amplifier integrated circuit (IC) with a gain of 76.8 (660 $\Omega$  external resistor,  $R_G$ , used for gain selection - see Figure 2.11 and Appendix B). A potentiometer was used for DC offset adjustment. The output voltages were not set to zero, but rather a reference voltage of approximately 2 V so that the output may swing „negative“ to indicate forces in the extension direction. This offset was later digitally subtracted.

All operations performed in the calculation are linear. The output voltage was to be expected to be approximately proportional to the stress in the transducer over the working stress range.

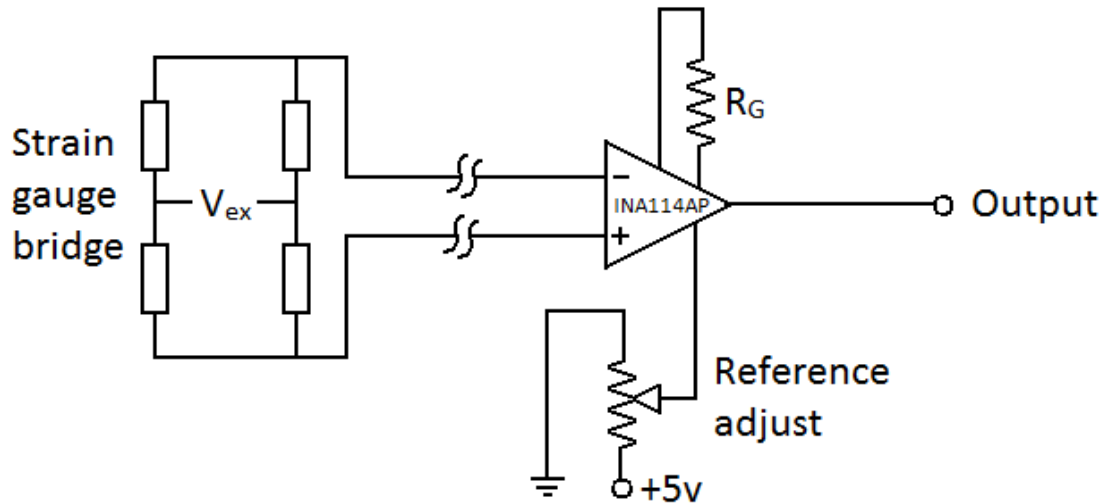


**Figure 2.11** Schematic diagram of a strain gauge gauge amplifier circuit. Identical circuits were used for the wrist and finger force transducers (see Figure 2.5).

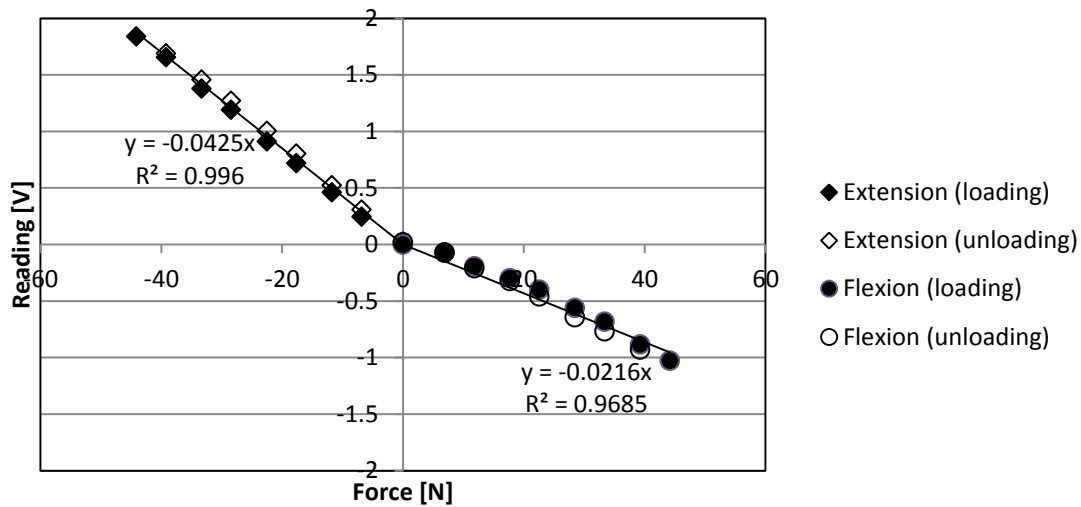
Certain factors could have affected the relationship, however, such as electronic component or part manufacturing uncertainty, the “toe” region in the stress-strain curve of the sensing element material. In light of these factors, a calibration was performed to determine the actual voltage response to applied force (see Appendix A) for details of the calibration process. The calibration curves are shown in Figure 2.12.

## 2.5. Data Logging and PC Software

PC software was required to record, process and display data in real time. All PC software for data logging was written using National Instruments Labview by Dr. Lester John of the University Of Cape Town Department Of Human Biology, Biomedical Engineering Division.

The data logger used in the system was a 12-bit National Instruments DAQ, which sampled at 10 kHz and interfaced with a PC by USB. Only data logging was performed by the DAQ because later prototypes of the system might need to perform all functions independently. PC based control of the device was avoided.

## Finger Joint Transducer Calibration Curve



## Wrist Joint Transducer Calibration Curve

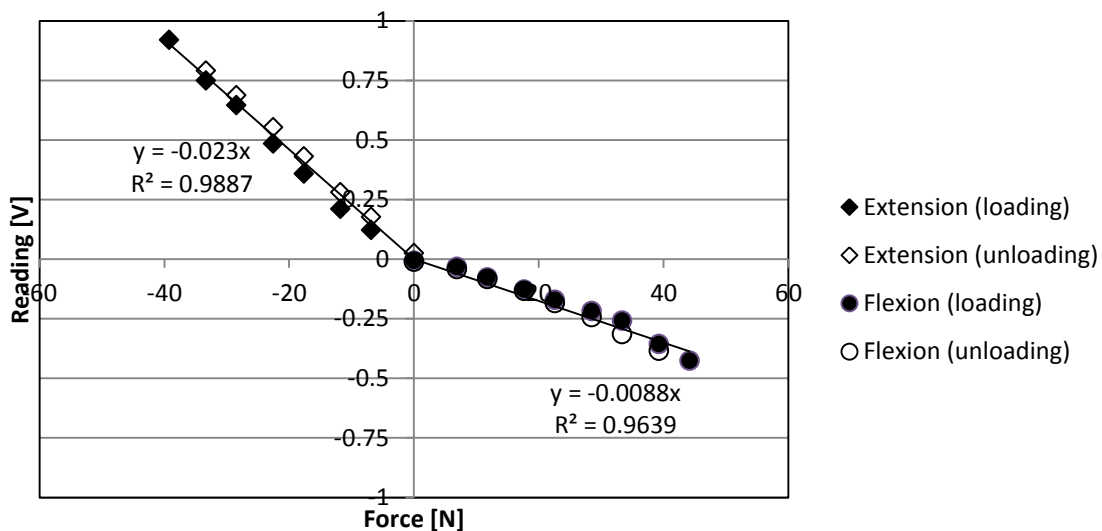


**Figure 2.12** Force amplifier calibration curves showing measured amplifier output for applied load to the interface components of the device's finger joint (top) and wrist joint (bottom). Loads were applied in steps to the interface components and the relevant voltage was recorded. Positive loads indicate that they were applied in the flexion direction (in keeping with the convention). Also shown are linear trend lines using the least squares method, with the equation and  $R^2$  values shown. The trend line was constrained to pass through the origin, since the data was zeroed in post-processing. Loading and unloading curves show minimal hysteresis and trend lines take both loading and unloading into account. For more information on the calibration, see appendix A.

The sampling rate of data logging was 1000 Hz. The following values were recorded:

- Elapsed time since the beginning of the recording
- 4x EMG data channels
- 2x participant force data channels
- 2 x EMG threshold data channels

During the clinical tests it was useful to be able to visualize these recorded values in real time. Graphical user interface (GUI) software was written to accompany the data logging software (see Figure 2.13).

The GUI contains real time plots of a short time window of EMG and force data, with the EMG activation threshold overlaid onto the EMG plots. The GUI also contains text fields for input of participant information and notes about the current recording. The GUI also featured control elements such as clickable pushbuttons to begin and terminate recordings, etc.

Data was stored in text files on the PC hard drive. These were later imported into Matlab for data processing (see Section 3.3).

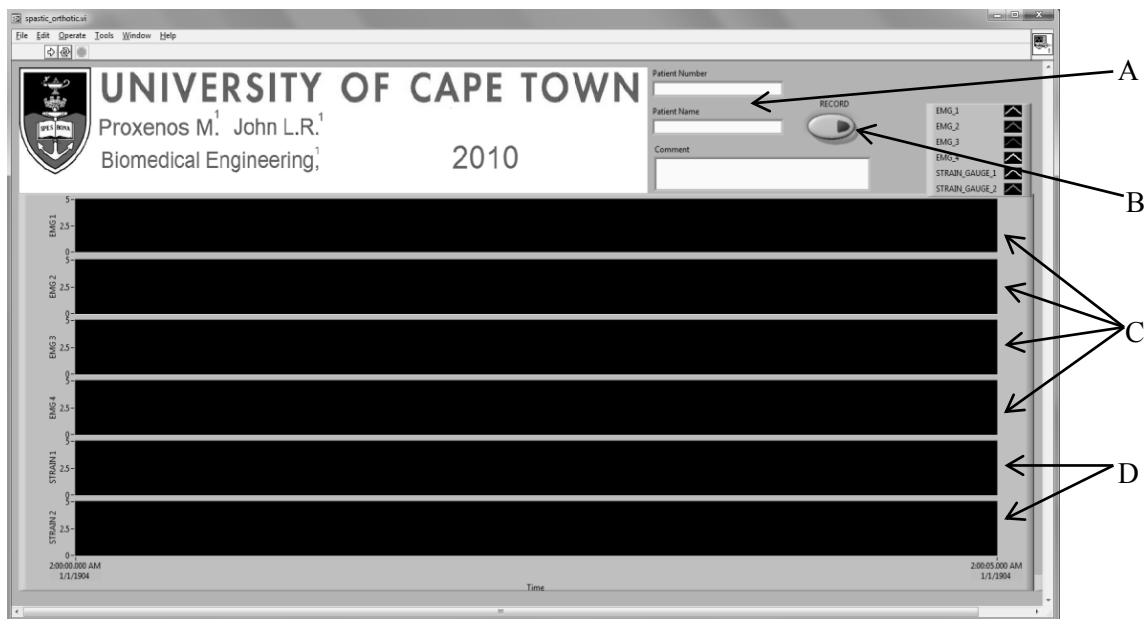


**Figure 2.13** Screenshot of the GUI. (A) Text fields for patient details and user comments. (B) Clickable button to begin or terminate a recording. (C) EMG plot areas. (D) Force plot area.

## **2.6. Modes of Operation**

The device had the ability to operate in two modes, named the „evaluation mode“ and „EMG mode“.

In evaluation mode the device would passively manipulate the participant's hand through prescribed motions while involuntary resistance was recorded.

When operated in EMG mode, the system used the EMG data acquisition system (see Section 2.3) to move the device joints in response to participant volition. If the EMG envelope signal exceeded the activation threshold, the device would respond by manipulating the appropriate joint.

[This page is intentionally left blank]

### 3. Methodology

This chapter outlines the experimental procedures that were carried out, as well as precautions that were taken.

#### 3.1. Methodology Overview

Figure 3.1 illustrates a graphical overview for the methodology, indicating various stages of apparatus development and testing.

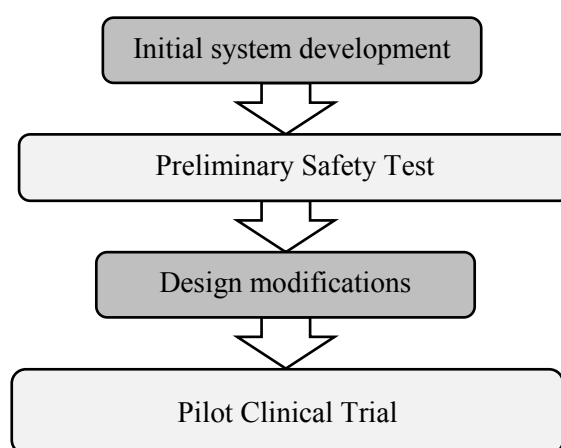


**Figure 3.1** Overview of the various phases of development and testing of the system, indicating how the design was modified as progress occurred.

The study consisted of a preliminary safety test followed by the pilot clinical trial (see Figure 3.2 and Figure 3.3). The participants in the preliminary safety test were healthy adults, while those in the pilot trial had histories of mild to moderate hypertonia of the hand and wrist. Participants in the pilot trial were assigned pseudonyms “Participant A”, “Participant B”, etc., to protect anonymity.

The study began with the preliminary safety tests, in which the system was used in EMG mode. Participants were asked to contract certain muscles with the goal of effecting specific actions of flexion and extension of the corresponding device joints. For ethical and safety reasons, participants’ interactions with the device during this phase were intentionally limited. Participants were not strapped into the device but rather were only fitted with the EMG electrodes for electrophysiology data acquisition (see Section 3.2.1 for the detailed experimental procedure). The outcomes of these tests were largely qualitative (see Section 4.1), demonstrating the ability of the device to perform the

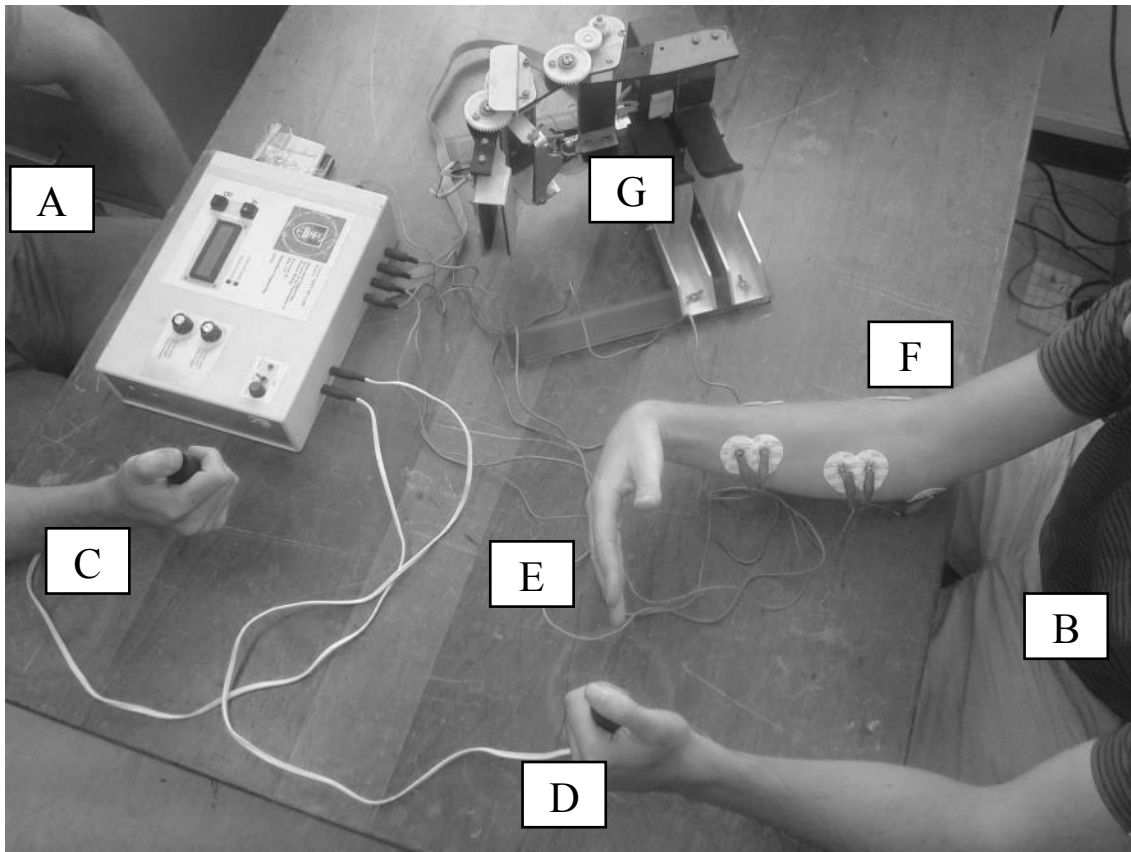


**Figure 3.2** Image illustrating the experimental setup for the preliminary safety tests. The examiner (A) and the participant (B) are seated at a table. Both are holding the safety buttons (C and D) while the participant performs tasks of wrist and/or finger flexion (E). EMG activity is measured (F), and results in movement of the device joints (G).

intended tasks safely and verification that features operated as intended, especially the safety features as outlined in Section 2.2.3. These tests also demonstrated that the system could use EMG as a control input to flex/extend the fingers/wrist, thereby demonstrating the potential use of the device as a task-oriented therapy tool. Further development in this regard is beyond the scope of this research, however, and is discussed as a recommendation for future work (see Section 5.3). Following the preliminary safety tests, areas for design improvement were identified and modifications were implemented (see Section 3.2).

The pilot trial was conducted once these modifications had been implemented (see Section 3.2.2 for the detailed experimental protocol). The system was tested with 6 participants with varying levels of hypertonia (MAS scores ranging between 0 and 3). The device manipulated the participant's hand while their involuntary resistance to passive motion was recorded. For the first three tests the finger

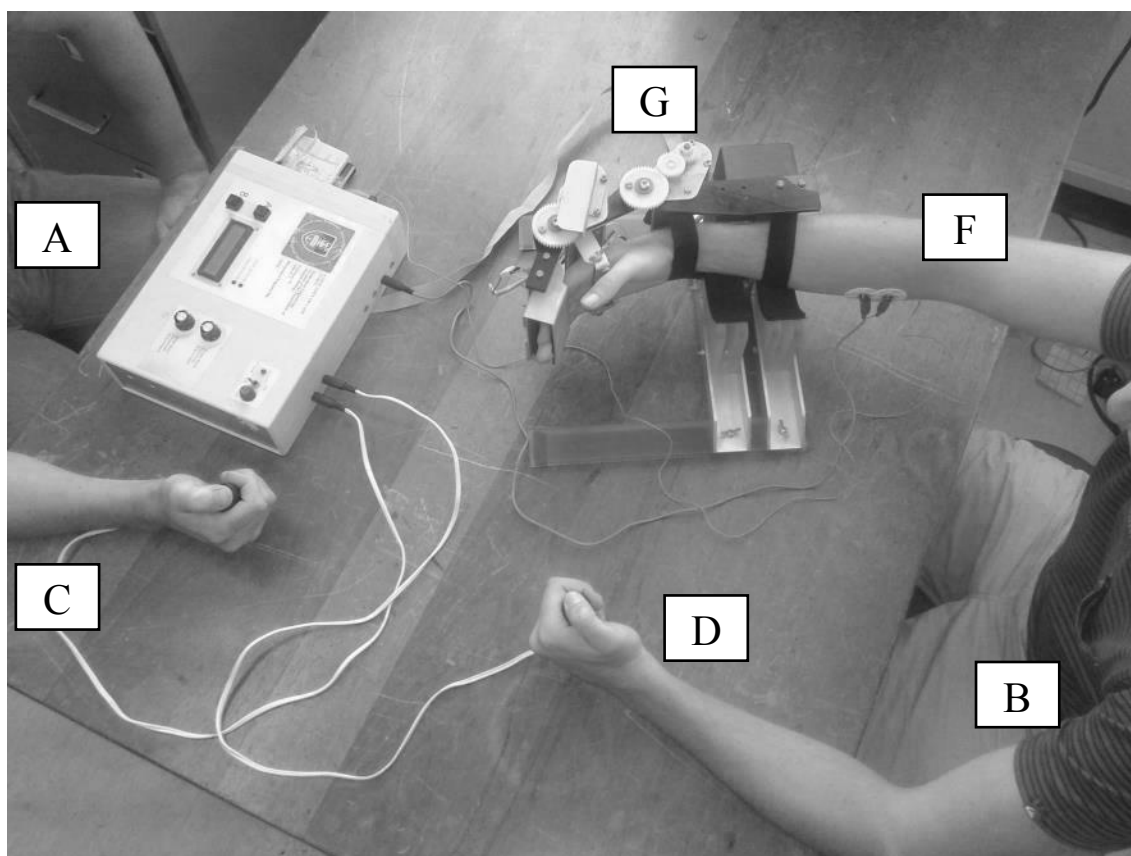


**Figure 3.3** Image illustrating the experimental setup for the pilot clinical trial. The examiner (A) and participant (B) were seated at a table. Both were holding the safety buttons (C and D). If necessary, a supervising therapist would hold the participant's safety button for him/her.

joint was extended, followed by the wrist joint. A problem encountered during these tests, however, was that the participant's fingers were slipping out place as the device finger joint was moved. Finger manipulation was therefore abandoned from the testing protocol for the remainder of the tests, and only wrist manipulation was performed for subsequent tests. Following the second test, it was further decided that EMG data would be advantageous to collect. EMG recordings for the wrist flexor (flexor carpi radialis) muscle were collected for the last four tests.

Offline force and EMG data processing was performed in Matlab to filter and remove any artefact associated with electromagnetic interference (EMI). For EMG, this consisted of applying a 50 Hz notch to remove excessive electrical noise from the mains, as well as processing to compute EMG amplitude before amplification. The latter involved spectral scaling to correct for the gains of the EMG amplifiers. The gains were frequency-dependent so spectral scaling was implemented (see Appendix E). The corresponding force data processing is summarized and discussed in Section 3.3.2.

### 3.1.1. Participants Inclusion/Exclusion Criteria

Participants in the preliminary safety test were all adult volunteers: 13 male and 2 female, average  $25.4 \pm 2.7$  years old, recruited from among the staff and students at the University of Cape Town's Department of Human Biology.

The participants in the pilot clinical trial were all adult volunteers: 2 males, 4 females, average age  $51.33 \pm 22.9$  years. Participants were recruited from the among the patients at the Departments of Physiotherapy and Occupational Therapy at Groote Schuur Hospital, as well as from Life Vincent Pallotti Hospital, both in Cape Town. The participants had a history of hypertonia in either the left or right hand. One healthy male individual was included with the six volunteers. Recorded MAS scores are presented in Table 4.2.

The inclusion criteria were as follows:

- All must be 18 years of age or older
- All must have must have read, understood and completed the consent form
- For the preliminary safety test only, all were required to be in good health and have no history of any disorder affecting the use of either hand/wrist.
- For the pilot trial, all were required to have a MAS score of 3 or less, as rated by a clinician prior to testing
- All were required to have sufficient range of motion of the fingers and wrist joints:
  - Wrist joint range of motion:  $+70^\circ$  to  $-35^\circ$
  - Finger joint range of motion:  $0^\circ$  to  $+90^\circ$

The exclusion criteria were as follows:

- None may have any history of diseases that could compromise safety. Each case was be assessed individually, both by the researcher and by a clinician present at testing. Examples of excluding conditions are:
  - Osteoporosis or arthritis of the affected hand
  - Pain during finger/wrist joint manipulation
  - Contractures
  - Tendonitis of the hand or wrist tendons
  - Carpal tunnel syndrome
  - Altered sensation and/or proprioception may or may not constitute exclusion, at the discretion of the researcher and physician
- No cognitive disorders or impaired communication capacity for any reason

### 3.1.2. Muscles for EMG acquisition

The muscles that were monitored during the study are shown in Table 3.1.

**Table 3.1** Summary of the actions of the muscles monitored in both the preliminary safety tests and the pilot trial

Muscle	Primary Actions	Phases of testing in which muscle was monitored
Flexor carpi radialis	Flexion (and radial abduction) of the wrist joint.	Both
Flexor digitorum superficialis	Flexion of the middle phalanges at the proximal interphalangeal joint. Under continued action, it also flexes the metacarpophalangeal joint and wrist joint.	Preliminary safety test Only
Extensor carpi radialis longus	Extension (and also abduction) of the wrist joint.	Preliminary safety test Only
Extensor digitorum	Extension of the phalanges.	Preliminary safety test Only

### 3.1.3. Design Modifications Following the Preliminary Safety Test

Modifications to the system were made based on the observations noted in the preliminary safety tests. After reviewing performance, clinical collaborators were concerned that the device movement was too slow to elicit a stretch response. The maximum device joint velocity was 26.6°/s. A faster variant of the motors was installed, increasing the velocity to 57.8°/s (see Section 2.2.2). However, following the first three tests, there were new concerns that discomfort could have been inflicted on the participant before either safety button could be released. The system was not unsafe, but had the potential to cause discomfort. It was decided that the original, slower motors would be reinstalled to mitigate risk since it was now clear that the slower motors would be sufficient for the task (see discussion of this in Chapter 5.2.2).

Other alterations to the system were relatively minor:

- The EMG cable lengths were lengthened to provide more freedom of movement.

- The design was modified to be used with the left or right hand. In order to achieve this, a frame system was included to allow the device to be turned upside down. In addition, the interface elements that interact with the palm were modified to accommodate the thumb appropriately.
- The strain gauge amplifier circuitry was relocated to be housed on the device itself, rather than in the control box. This was motivated by noise due to EMI that was introduced in the cables between the device and the amplifier circuitry, despite the use of shielded cables. Once the circuitry was relocated, the cables were significantly shorter and this excessive noise contamination was no longer observed.
- The system was modified to record raw EMG in the pilot trial, instead of the EMG amplitude envelope.

## **3.2. Detailed Testing Protocols**

### **3.2.1. Preliminary Safety Test**

See Figure 3.2 for an illustration of the experimental setup for the preliminary safety test. The protocol was as follows:

1. The system was set up on a table. The system had been initialized in advance for use in EMG mode (see Section 2.6). A video camera was set up to record only the participant's arm and no personal identifying features were recorded. This was in accordance with the requirements for Human Research Ethics Clearance (see Appendix G).
2. The objectives and details of the test were briefly explained. If the participant agreed, then the consent form was signed (see Appendix G) and the test proceeded.
3. The EMG electrode placement sites (see Figure 3.4 and Figure 3.5) were over the following muscle bellies of the right arm: flexor carpi radialis, flexor digitorum superficialis, extensor carpi radialis longus, extensor digitorum. An additional electrode was to be placed over the medial epicondyle of the humerus (i.e. a bony landmark on the body), as the active common mode noise cancelling ground electrode, typically referred to as a "driven right leg" or DRL based on terminology from electrocardiology. Note that for the preliminary safety tests, the right arm was used. In the pilot trial, however, the arm that was affected by increased tone was used. The ground electrode was always placed on the same arm as the other electrodes.
4. The areas where self-adhesive EMG electrodes would be attached were prepared by carefully abrasion to remove the top layer of the skin. The area was cleaned using an alcohol swab to remove natural skin oils. The EMG electrodes were then placed for bipolar EMG recording.

The inter-electrode distance was 20mm, and the contact impedance for each electrode pair was measured, and confirmed to be below 10 kOms per electrode pair, as is recommended by Fridlund and Cacioppo (1986) (see Figure 3.4 and Figure 3.5).

5. The participant was asked to contract the various muscles without holding the safety buttons, in order to confirm that these buttons were functional (i.e. no device movement was produced). This safety check was performed despite the participant not being strapped into the device. The same was repeated while the safety buttons were being held to observe that the device responded to EMG.
6. The participant was then asked to contract the various muscles while holding the safety buttons. The EMG threshold adjustment knob was used to find comfortable muscle activation thresholds. These thresholds were used to make only simple inferences of muscle activity in a binary fashion („active“ or „not active“). The exact level of the threshold depended on participant comfort. A comfortable threshold was one that was high enough that it wasn't accidentally exceeded by system noise or disturbances (i.e. motion artefact), but low enough that the participant could easily elicit an action in the device.
7. At this point, the test could begin. The video recording was initiated.
8. The participant was asked to perform three different tasks of flexion and extension, while a video recording of the test was captured for later review. The three tasks were as follows:
  - Five repetitions of flexion and extension of the device finger joint, without moving the device wrist joint if possible
  - Five repetitions of flexion and extension of the device wrist joint, without moving the device finger joint if possible
  - Five repetitions of flexion and extension of the device wrist and finger joints simultaneously
9. The video recording was terminated.
10. The device was turned off and the electrodes were removed. The test was complete.

### **3.2.2. Pilot Clinical Trial**

See Figure 3.3 for an illustration of the experimental setup for the pilot clinical trial. The protocol was as follows:

1. The system was set up on a table. The system had been initialized in advance for use in evaluation mode.
2. As with the procedure for the preliminary safety tests, a brief introductory discussion with the participant was held prior to testing. The purpose of the study was discussed, and all the

safety features were described (see Section 2.2.3). If the participant agreed, then the consent form was signed (see Appendix G) and the test proceeded. This discussion, while necessary in terms of regulations regarding human research ethics, was also important for calming the participant and relieving anxiety since psychological factors can aggravate hypertonia.

3. Assessments by three physiotherapists or occupational therapists were performed to determine the wrist flexor MAS score. Each rater was blind to the others' results.
4. EMG activity of the wrist flexor muscle, flexor carpi radialis, was recorded for all tests following Participant B (see Table 3.2). Skin preparation and EMG electrode placement was performed as for the preliminary safety tests (see Section 3.2.1). Note that the test was performed with the arm affected by hypertonia. Furthermore, for the tests for which EMG was recorded, electrodes were only placed over the flexor carpi radialis muscles and medial epicondyle of the humerus. This was unlike the preliminary safety tests which also included EMG recording of the flexor digitorum superficialis, extensor carpi radialis longus and extensor digitorum muscles, and were always performed with the right arm.
5. The EMG cables from the control box (see Figure 2.2) were attached to the electrodes. The participant was asked to contract the target muscles so that EMG signals were displayed on the GUI on the computer screen (see Figure 2.13).
6. The strain gauge offsets were adjusted until the signals were approximately mid-range (2V in the 0V – 5V system). The precise offset was unimportant, as these would later be zeroed in software (See Section 3.3.2).
7. The participant's hand was placed into the device and the straps were secured.
8. The test commenced. The participant was asked to relax and to hold the safety button with their unaffected hand while the test was in progress. If necessary, the safety button was held by a supervising clinician. The examiners safety button was also held. The initial protocol included evaluation of the finger and wrist joints, although it was found that the participants' fingers were slipping out when the device finger joint was moved. After Participant C, finger manipulation was excluded from the protocol (see Table 3.2). The precise set of prescribed movements were as follows:
  - a. For protocols included finger and wrist manipulation, the starting position was with both joints straight (0°). The protocol was as follows (see Figure 3.6):
    - i. The device flexed its finger joint from the starting position (0°) to full flexion (+90°) in preparation for the test.
    - ii. The fingers were extended from +90° back to 0°.
    - iii. The finger joint was then flexed from 0° back to +45° to allow for comfortable manipulation of the wrist joint (simultaneous full extension of

both the wrist and finger joints can cause discomfort in participants with moderate hypertonia).

- iv. The wrist joint was flexed from the starting position (0°) to +70°.
  - v. The wrist joint was extended through the full range of motion from +70° to -35°.
  - vi. The wrist was flexed back to the starting position (0°).
  - vii. The finger joint was extended from +45° to the starting position (0°).
- b. For protocols including only wrist manipulation, the starting position was with the wrist straight and with the fingers flexed to +45°. The protocol was as follows: (see Figure 3.7):
- i. The wrist joint was extended from the starting position (0°) to -35°.
  - ii. The wrist joint was flexed from -35° to +70°.
  - iii. The wrist joint was extended from +70° to -35°.
  - iv. The wrist joint was flexed from -35° to the starting point (0°).
9. Three repetitions of step 7 were performed with each participant, although only the data from the last repetition would be recorded and used for analysis. A similar approach is taken by clinicians when performing traditional MAS assessments (see Section 1.1.5).
10. Once the last repetition had been performed, data recording was terminated. The participant's hand was removed from the device.
11. The device was turned off and the electrodes were removed. The test was complete.

The various combinations of speed and/or testing protocol were used are summarised in Table 3.2.

Summary of testing protocols in the pilot trial, indicating EMG data collection, finger and/or wrist protocol, and joint speed combinations. Note the change in joint speed that was implemented after Participant C when the original, slower motors were reinstalled.

**Table 3.2**

Participant:	A	B	C	D	E	F
<b>EMG collected:</b>	No	No	Yes	Yes	Yes	Yes
<b>Fingers/Wrist protocol:</b>	Both	Both	Both	Wrist only	Wrist only	Wrist only
<b>Joint speed (torque):</b>	57.8°/s (4.0 N.m)	57.8°/s (4.0 N.m)	57.8°/s (4.0 N.m)	26.6°/s (1.32 N.m)	26.6°/s (1.32 N.m)	26.6°/s (1.32 N.m)

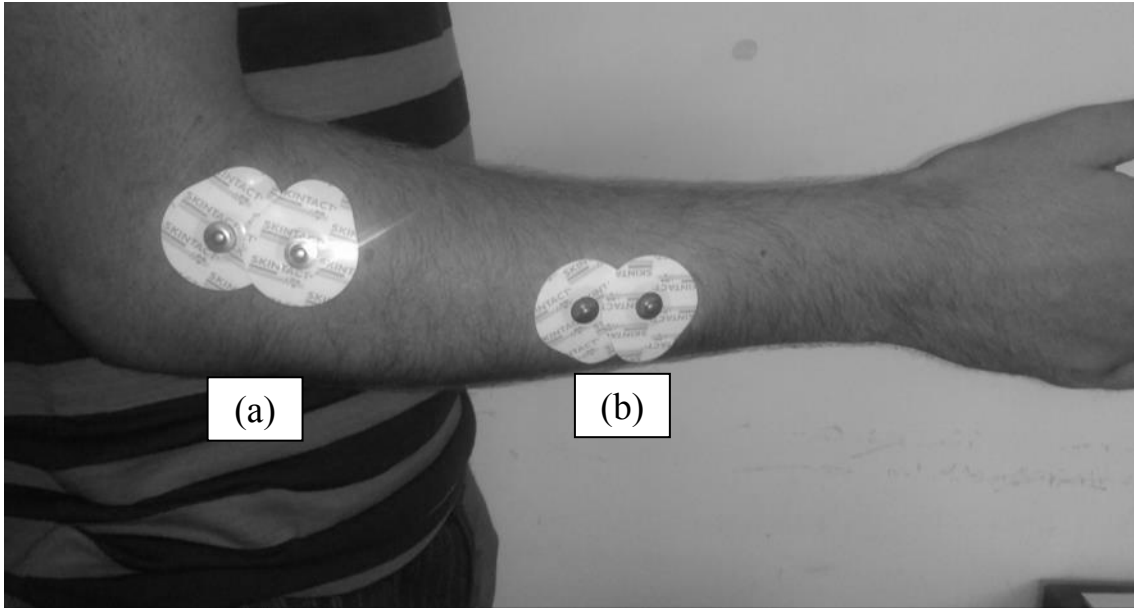


**Figure 3.4** The positions of bipolar EMG electrodes monitoring selected muscles in the extensor compartment of the forearm: (a) extensor carpi radialis longus, (b) extensor digitorum.

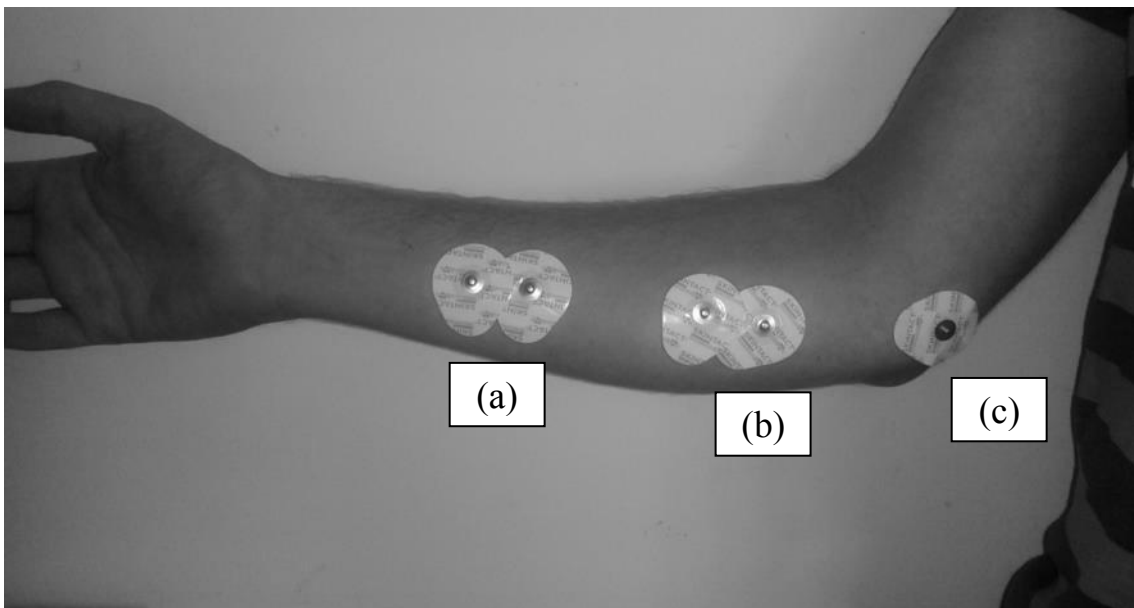


**Figure 3.5** The position of bipolar EMG electrodes monitoring selected muscles in the flexor compartment of the forearm, as well as the DRL electrode: (a) flexor digitorum superficialis, (b) flexor carpi radialis, (c) ground on the medial epicondyle of the humerus.

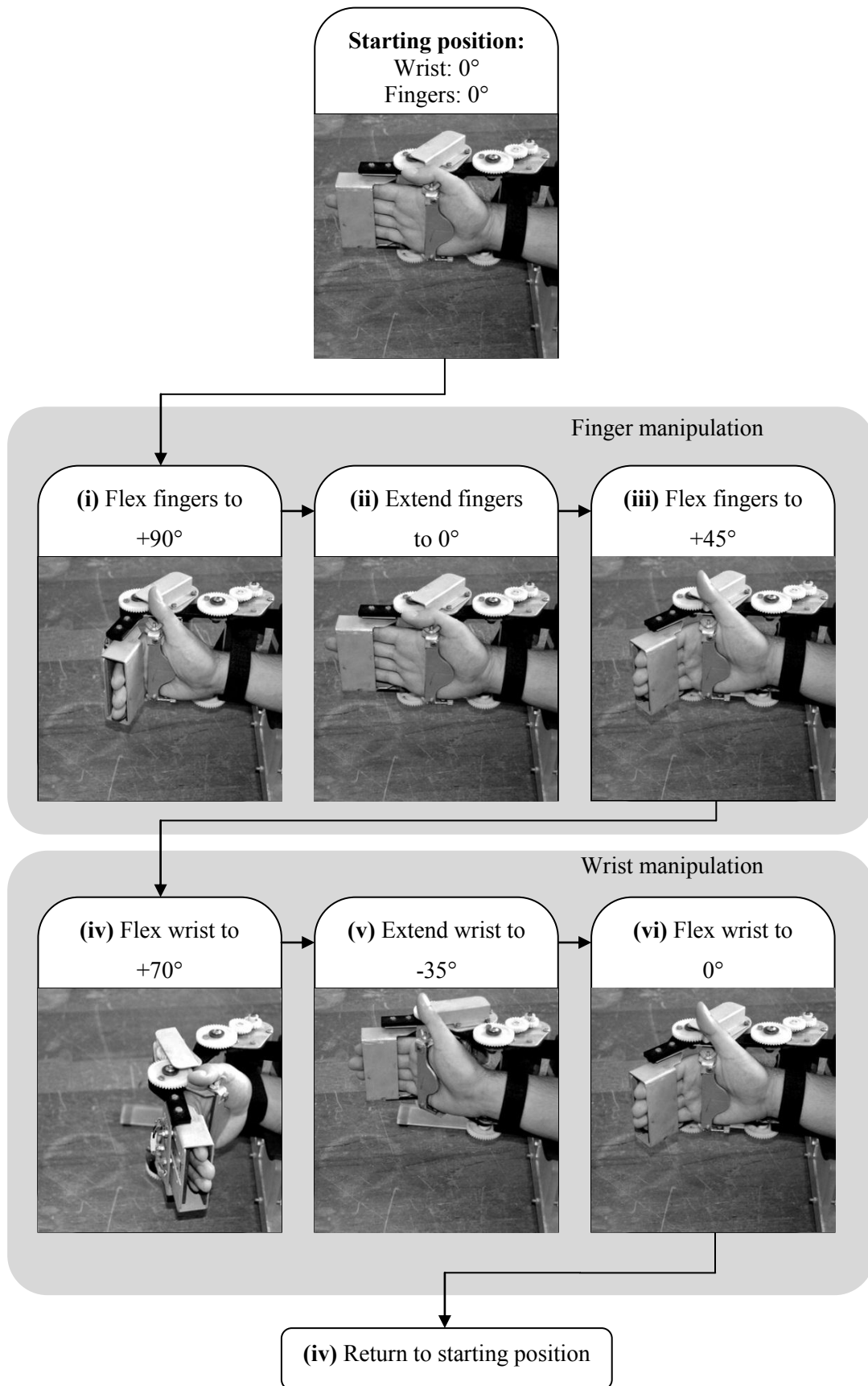


**Figure 3.6** Flow chart illustrating the various prescribed movements for the protocol including wrist and finger manipulation.

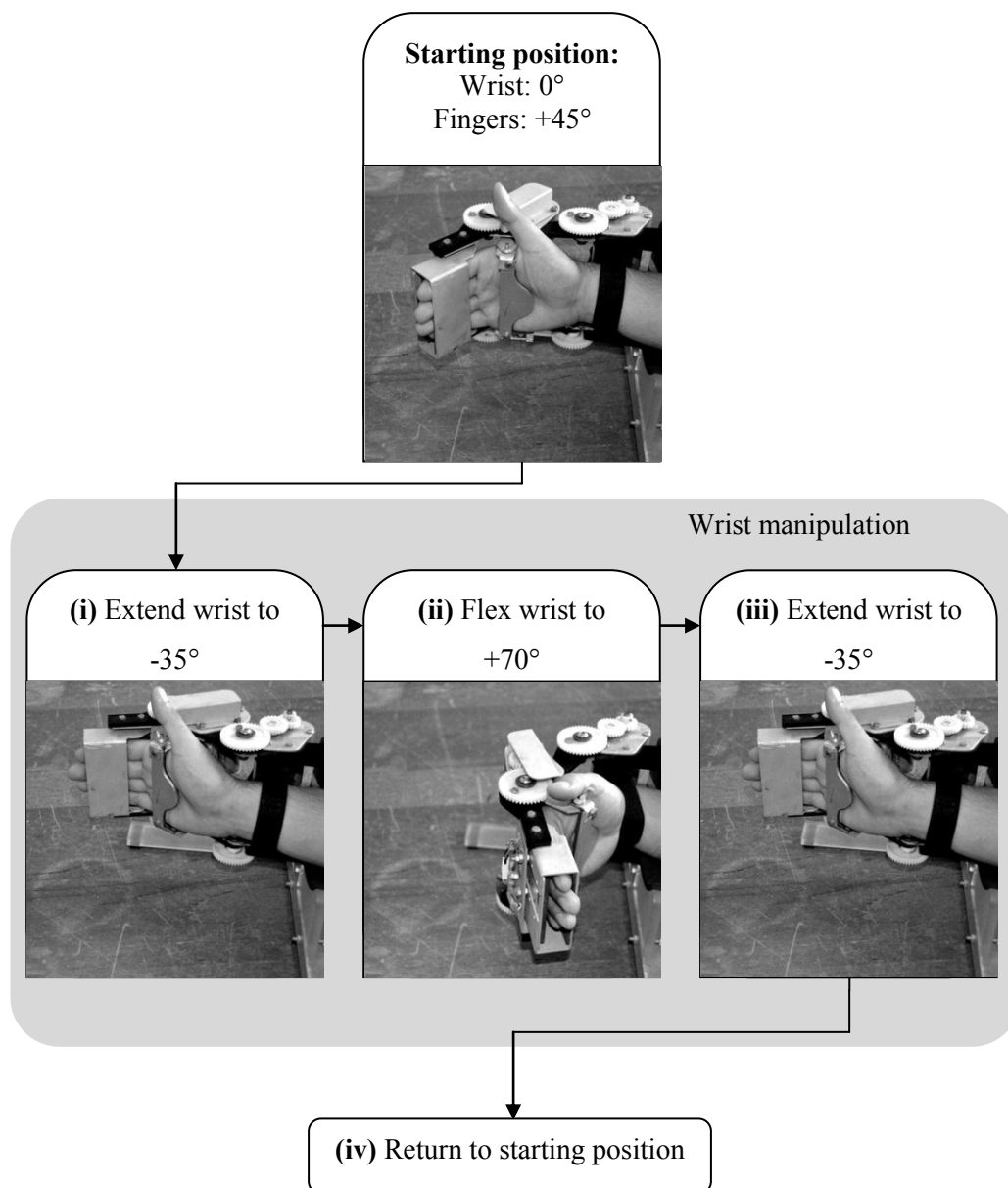


**Figure 3.7** Flow chart illustrating the various prescribed movements for the protocol including only wrist manipulation.

### **3.3. Data Processing**

#### **3.3.1. Preliminary Safety Tests**

The preliminary safety tests served as a demonstration of the various features of the device. The outcomes were largely qualitative (see results in Section 4.2). Observations regarding potential design modifications were noted (see Section 3.2), and it was verified that no unexpected behaviour of the device occurred, and that all safety features functioned as intended. To extract quantifiable data from the tests, the video recordings of the tests were reviewed. The times to complete the various repetitions of each of the tasks were noted (see Section 4.1).

#### **3.3.2. Pilot Clinical Trial**

EMG and force data were processed in Matlab. This was automated using scripts, the corresponding code for which is presented in Appendix F. The procedure for processing of the EMG data is presented in Appendix E.

Note that a part of the code is dedicated to the removal of what is referred to as „force drift“. It was found that, when the device was operated without a participant’s hand secured, force readings were registered even though no external force was applied. Force recordings obtained when operating the device without a participant secured clearly depicts the force drift (see Figure 3.8). Ideally, such recordings would reflect no activity. The main causes of this noise were EMI from the motors as well as shifting weight as the device joints moved. The latter caused a redistribution of the stress in the force transducer components which manifested as artificial readings.

The low frequency component of this artificial force reading was highly repeatable (Figure 3.8 shows repeat recordings), and so digital subtraction from the final data was possible (see Figure 3.9). The higher frequency noise, also due to EMI from the motors, was filtered using a low pass filter. The signal associated with applied force was expected to be of relatively low frequency. It was found that a cutoff frequency of 200 Hz was effective in removing EMI while preserving the components of the signal associated with applied force.

The high frequency noise component (that was removed) was also used to infer the activity of the motors for the purposes of segmenting the data: by observing the noise due to motor activity, and with knowledge of the programmed sequence of device joint actions, the specific action being carried out at each time in the test could be inferred.



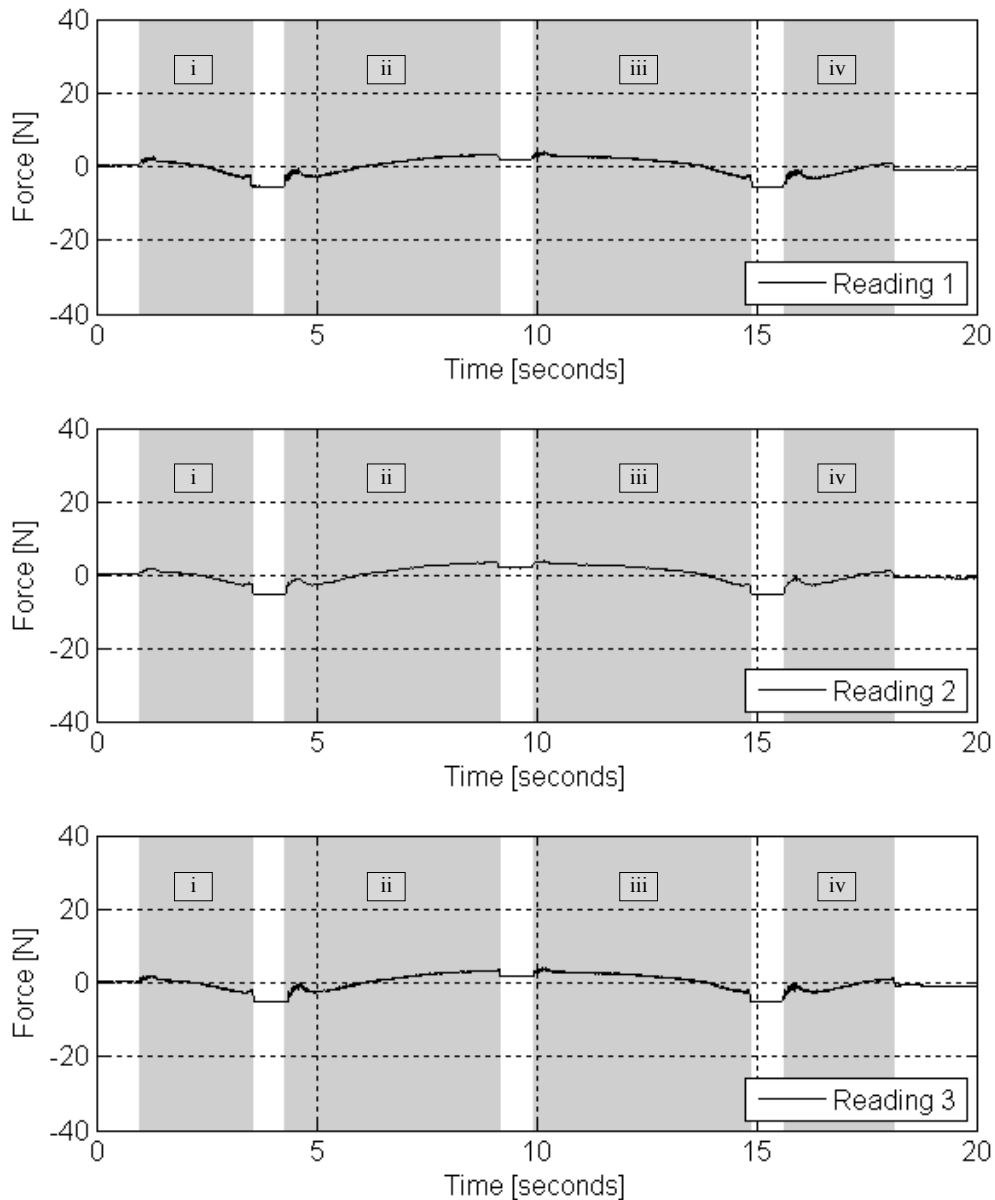


**Figure 3.8** Plot illustrating the repeatability of the drift observed in the force readings with device joint movement. Three plots of different force readings for wrist transducer were obtained during “evaluations” performed without a participant secured into the device. (i) extension of the device wrist joint from  $0^\circ$  to  $-35^\circ$ , (ii) flexion of the device wrist joint from  $-35^\circ$  to  $+70^\circ$ , (iii) extension of the device wrist joint from  $+70^\circ$  to  $-35^\circ$ , (iv) flexion of the device wrist from  $-35^\circ$  to  $0^\circ$  (see Figure 3.7). Note the drift in the reading, as well as the “stop/start” artefact introduced due to the pauses which occur roughly at  $t=3.5s$ ,  $t=9s$  and  $t=15s$ . The drift is highly repeatable, and it was possible to subtract it from recorded force data from the pilot trial (see Figure 3.9). This digital subtraction was performed in offline in software.

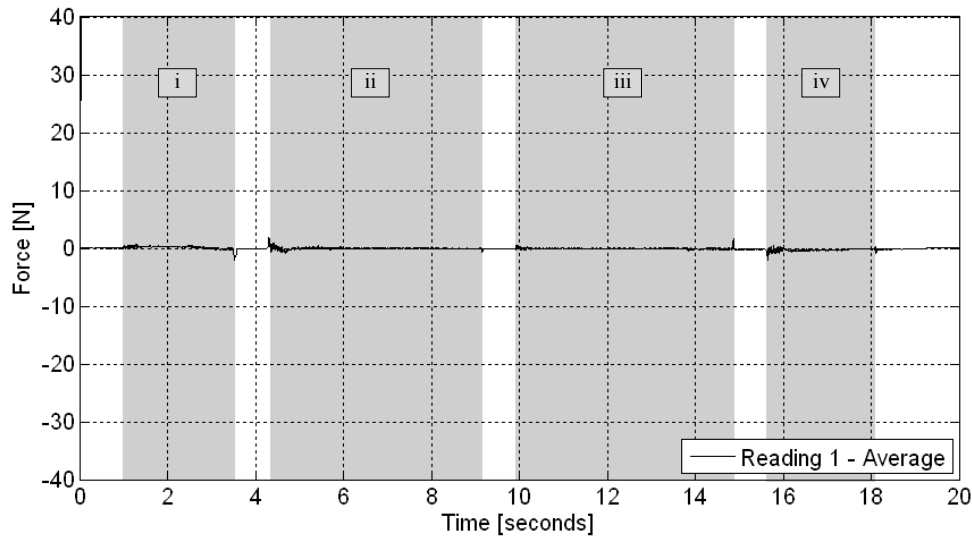


**Figure 3.9** Plot illustrating the effectiveness of digital subtraction to correct for artificial force drift. The plot shows the corrected force reading for the wrist transducer obtained during an “evaluation” performed without a participant secured into the device (see Figure 3.8). Correction was performed by digitally subtracting the average of the three readings shown in Figure 3.8. (i) extension of the device wrist joint from  $0^\circ$  to  $-35^\circ$ , (ii) flexion of the device wrist joint from  $-35^\circ$  to  $+70^\circ$ , (iii) extension of the device wrist joint from  $+70$  to  $-35^\circ$ , (iv) flexion of the device wrist from  $-35^\circ$  to  $0^\circ$  (see Figure 3.7).

The Matlab code, executed separately for each participant’s recording, performed the following tasks (in order):

1. The following data was imported:
  - Force data recorded during tests with participants
  - The force data from an identical test, recorded without a participant strapped into the device (referred to as the force drift data)
2. The force baseline was calculated as being the average of the first 1000 milliseconds of the recording. This was subtracted from all recordings for that test, such that the force data was zeroed (see the experimental protocol in Section 3.2.2), specifically step 5, stating that the force recordings would be digitally zeroed in post-processing. Note that this step is for the removal of DC offset in the force recordings, and is not to be confused with the removal of force drift (performed in step 6).
3. The time markers for the various stages of the prescribed motion were identified for both the test data and the force drift data. This was performed by analysing only the high frequency component of the data. From EMI noise observed, it could be determined when the motors

were engaged and disengaged. Using these time markers, various data segments were identified, referred to as „phase i“, „phase ii“, etc.

4. The data was cropped to discard information occurring outside of the time window of interest: 2 seconds before the test began till 2 seconds after it was terminated.
5. Each segment of the prescribed motion in the average force drift data was resized such that it temporally matched the corresponding segment in the test data.
6. The average force drift was subtracted from the test force data (see Figure 3.8).
7. The recorded force data (in volts) was transformed into Newtons using the calibration data (see Figure 2.12).
8. The data was cropped such that only the relevant segment of the test (i.e. the wrist extension phase) was included.
9. The peak measured resistive wrist force was determined, as well as the simultaneously occurring finger force (see Table 4.1). This data would be used in the biomechanical model (see Section 3.4).
10. The data presentation (plots, etc.) was prepared (see Figure 4.4 to Figure 4.11).

### **3.4. Biomechanical Model**

In addition to the signal processing performed on the data collected in the pilot trial (Section 3.3.2), a biomechanical model was implemented to estimate the tensions in the wrist for use in statistical analysis. The following section outlines the biomechanical model used, whereby the tensions in the wrist and finger flexor tendons could be calculated. The model used only the torques at the finger and wrist joints during passive wrist extension as inputs.

The model begins with a force diagram, depicting the geometry of the system and relative forces applied (see Figure 3.10).

It is assumed that all joint velocities were slow enough that inertial effects could be ignored, and that the system existed in a state of static equilibrium. Consider a participant applying forces  $F_f$  and  $F_w$ . These are measured by the transducers, which also equal but opposite forces onto the participant's hand (see in Figure 3.10).

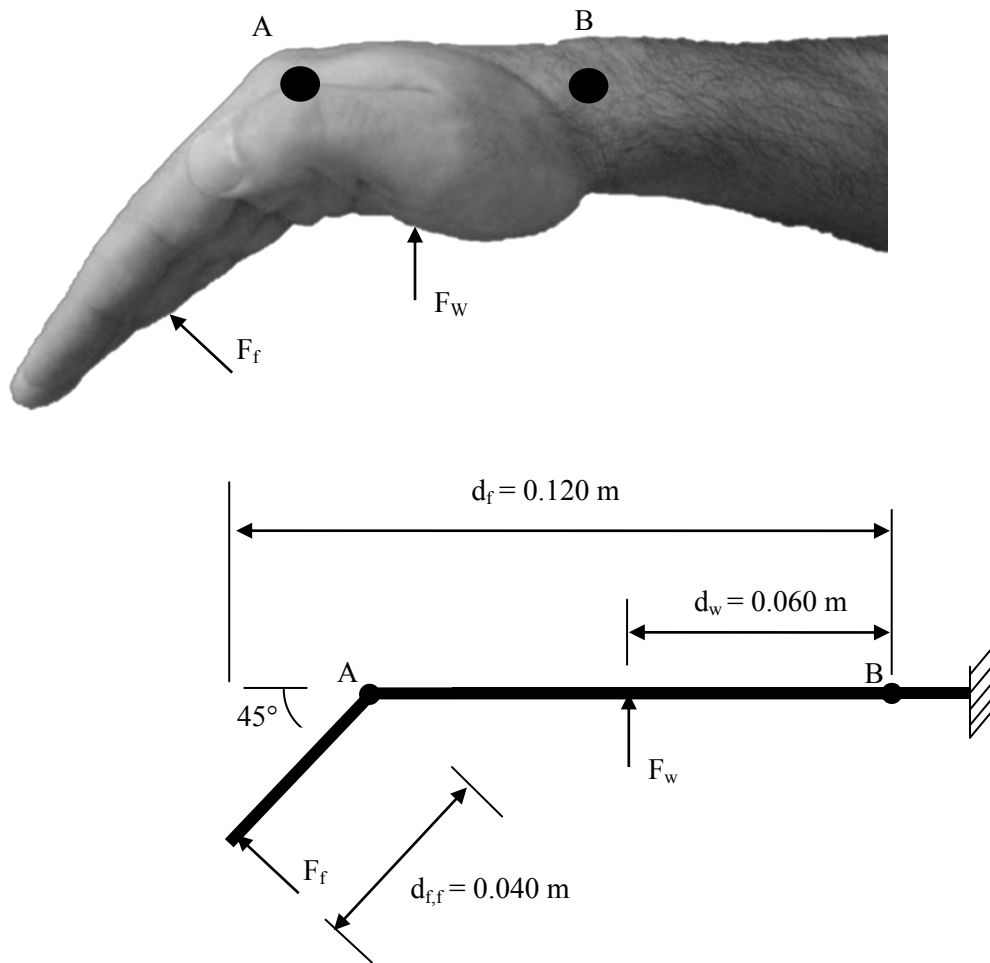


**Figure 3.10** Illustration of the participant’s hand (top) as well as force diagram for the biomechanical model (bottom). Point A corresponds to the finger (MCP) joint, and point B corresponds to the wrist joint.  $F_f$  and  $F_w$  are the forces applied to the finger joint force transducer and wrist force transducers respectively. The distances  $d_f$ ,  $d_{f,f}$  and  $d_w$  are due to the geometry of the device design (see Figure 3.3).

From the force diagram one can determine  $M_A$ , the internal moment at the participant’s finger joint due to  $F_f$ , as follows:

$$M_A = F_f \times d_{f,f}$$

The moments applied to the finger and wrist joints respectively must balance, since the system is in a state of static equilibrium. The moment  $M_A$  is balanced by tension in the participant’s finger flexor tendons. This tension can be calculated with knowledge of the tendon moment arm at the MCP joint. In their text on clinical mechanics of the hand, Brand and Hollister (1999) used the approximate values shown in Figure 3.11. These values are likely to vary between subjects, but serve as an approximation for this model.

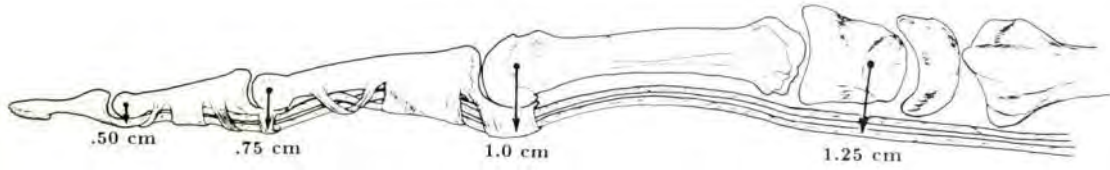


**Figure 3.11** Illustration of the various moment arms that finger flexor tendons possess at the various joints. Left to right: distal interphalangeal joint (0.05 m), middle interphalangeal joint (0.075 m), proximal interphalangeal joint (0.01 m), and the wrist joint (0.0125m). (Brand and Hollister, 1999)

The balance of moments at the MCP joint can be expressed mathematically as follows:

$$M_A = F_{tendon,finger} \times d_{tendon,finger}$$

The symbols  $F_{tendon,finger}$  and  $d_{tendon,finger}$  respectively represent the tension in the finger flexor tendons and the moment arm that the finger flexor tendons have at the finger joint (shown in Figure 3.11 to be 1.0cm). It follows that:

$$\begin{aligned} F_{tendon,finger} &= \frac{M_A}{d_{tendon,finger}} \\ &= \frac{F_f \times d_{f,f}}{d_{tendon,finger}} \end{aligned}$$

(Equation 3.1)

The internal moment  $M_B$  at the wrist joint due to the applied forced  $F_f$  and  $F_w$  can be expressed as follows:

$$M_B = F_w \times d_w + (F_f \times \sin 45^\circ) \times d_f$$

(Equation 3.2)

$M_B$  is again balanced by the tension in tendons at that joint. The wrist and finger flexor tendons both have moment arms at the wrist joint. This balance of moments at the wrist joint can be expressed mathematically as follows:

$$M_B = (F_{tendon,finger} + F_{tendon,wrist}) \times d_{tendon,wrist}$$

(Equation 3.3)

The symbols  $F_{tendon,wrist}$  and  $d_{tendon,wrist}$  respectively represent the tension in the wrist flexor tendons and the moment arm that the wrist flexor tendons have at the wrist joint. It will be assumed that the wrist

flexor tendon has the same moment arm at the wrist as the finger flexor tendon, shown in Figure 3.11 to be 1.25cm.

Rearranging, we have:

$$F_{tendon,wrist} = \frac{M_B}{d_{tendon,wrist}} - F_{tendon,finger} \quad (\text{Equation 3.4})$$

Substituting Equation 3.1 and Equation 3.2, the tension in the wrist flexors can be determined:

$$F_{tendon,wrist} = \frac{F_w \times d_w + (F_f \times \sin 45^\circ) \times d_f}{d_{tendon,wrist}} - \frac{F_f \times d_{f,f}}{d_{tendon,finger}} \quad (\text{Equation 3.5})$$

Substituting known or estimated values for  $d_w$ ,  $d_f$ ,  $d_{tendon,wrist}$ , and  $d_{tendon,finger}$ , we can show that:

$$F_{tendon,wrist} = 4.8 \times F_w + 2.79 \times F_f \quad (\text{Equation 3.6})$$

By applying Equation 3.6 with data recorded in the pilot trial (using the peak recorded force in the wrist transducer during wrist extension as  $F_w$ , and the co-occurring force measured by the finger transducer as  $F_f$ ), the peak tension in the wrist tendon during wrist extension was calculated.

### 3.5. Precautions

This section details the precautions taken during the test procedures, to ensure patient safety and to protect the integrity of the results:

#### 3.5.1. Preliminary Safety Test

- Participants were asked to refrain from moving excessively during the tests, to prevent motion artefact in the EMG recordings.
- The ground electrode for EMG recordings was always placed onto the same arm as the other EMG electrodes to prevent accidental discharge of electrical current across the heart.

It was ensured that the EMG electrodes were not touched once the test had begun, to avoid the introduction of noise.

### **3.5.2. Pilot Clinical Trial**

- A careful assessment of the participant's hand was performed to ensure that the inclusion criteria were satisfied (see Section 3.1.1) – especially the range of motion requirements.
- Participants were asked to refrain from moving excessively during the tests, to prevent motion artefact in the EMG recordings. Care was taken to ensure that the participant understood not to attempt voluntary movement during a test, since only passive (involuntary) resistance was of interest.
- The ground electrode for EMG recordings was always placed onto the same arm as the other EMG electrodes to prevent accidental discharge of electrical current across the heart.
- As for with the preliminary safety tests, it was ensured that the EMG electrodes were not touched once the test had begun, to avoid the introduction of noise.
- Care was taken to ensure that the participant was comfortably seated and positioned before the test began, because if he/she moved or shifted excessively during the test, it may have introduced motion artefact into the force and EMG recordings.
- Immediately before the test was initiated, it was ensured that the participant's thumb was not flexed and/or opposed, because it would obstruct motion of the hand during finger flexion. It was bound if necessary.

[This page is intentionally left blank]

## 4. Results

This section details the results of the experimental protocols outlined in Chapter 3. Section 4.1 presents the data collected during the preliminary safety tests, and Section 4.2 presents the data collected during the pilot clinical trial. The data presented in this section has been processed following the methods discussed in Section 3.3.

### 4.1. Preliminary Safety Tests

As was discussed in Section 3.1, the outcomes of the preliminary safety tests were qualitative, and little quantifiable data was recorded. The following observations were made regarding the safe function of the device:

- The safety buttons operated as intended – the device movement was halted when either of the buttons was released (see Section 2.2.3).
- The limit switches were effective in limiting the range of motion to between  $+70^\circ$  and  $-35^\circ$  (see Section 2.2.3 and Section 2.1).
- The EMG signal acquisition system operated as intended, and the device responded to participant EMG appropriately (see Section 2.3).

Despite the main outcomes of the preliminary safety tests being qualitative, data on the times to complete the repetitions of the tests was extracted when the videos of the tests were reviewed. As was stated in Section 3.1, the potential to develop the device as an EMG-controlled active therapy tool exists, but is beyond the scope of this research. Data on the times to complete various tasks when using the EMG control mode may prompt further development in this regard. Times to complete repetitions varied as participants „learned“ which muscle activation was related to each device joint movement (see Figure 4.1 to Figure 4.3).

The preliminary safety tests revealed no potential risks to participants. The pilot trial was subsequently conducted.

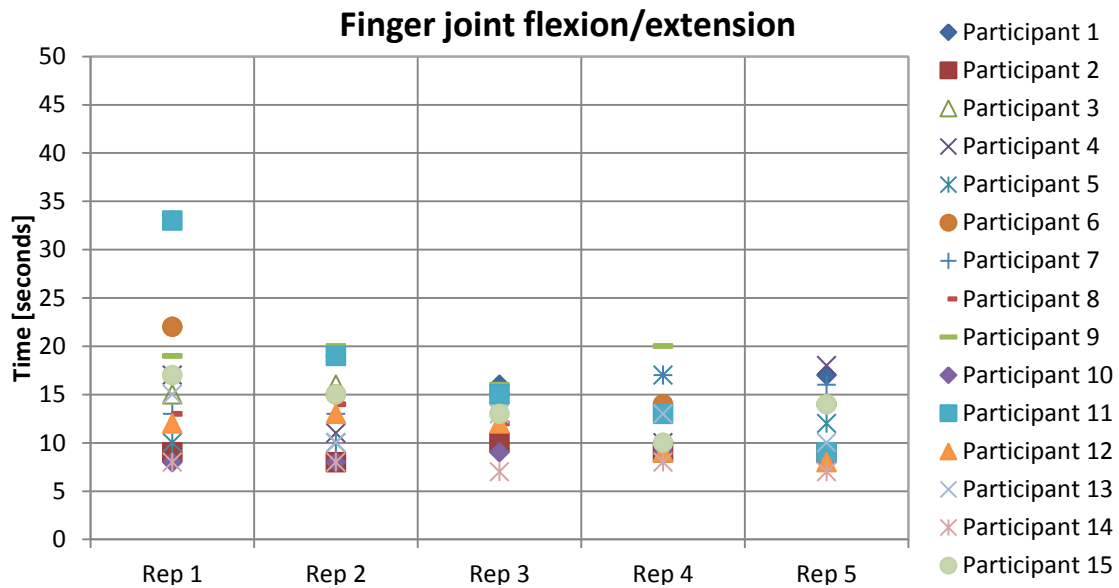


**Figure 4.1** Times to complete repetitions during the first test in the preliminary safety test – five repetitions of finger flexion and extension performed by 15 participants with no history of hypertonia (see Figure 3.2).

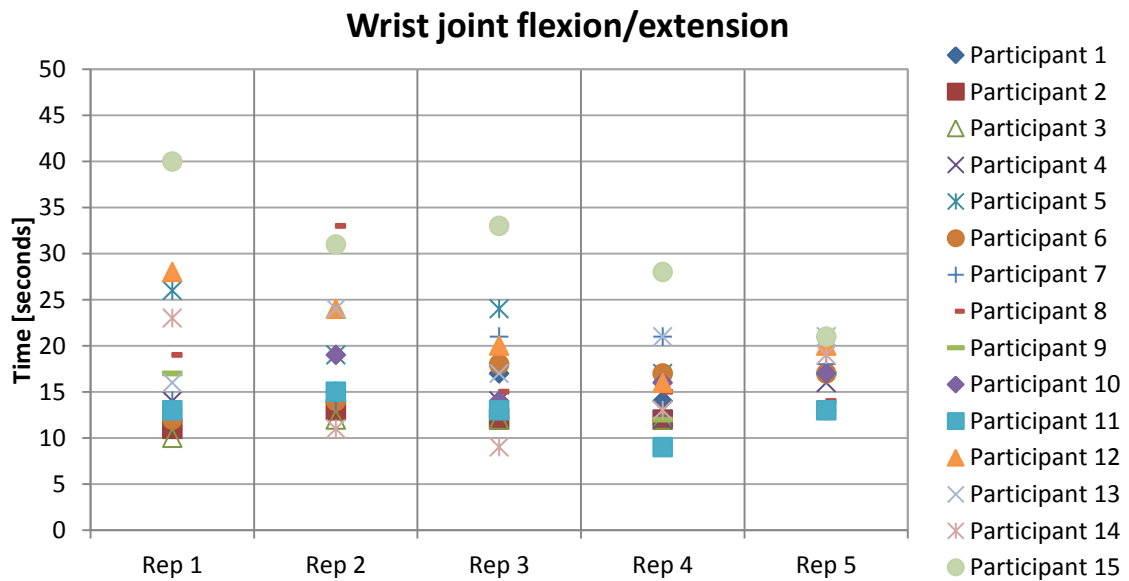


**Figure 4.2** Times to complete repetitions during the second test in the preliminary safety test – five repetitions of wrist flexion and extension performed by 15 participants with no history of hypertonia (see Figure 3.2).

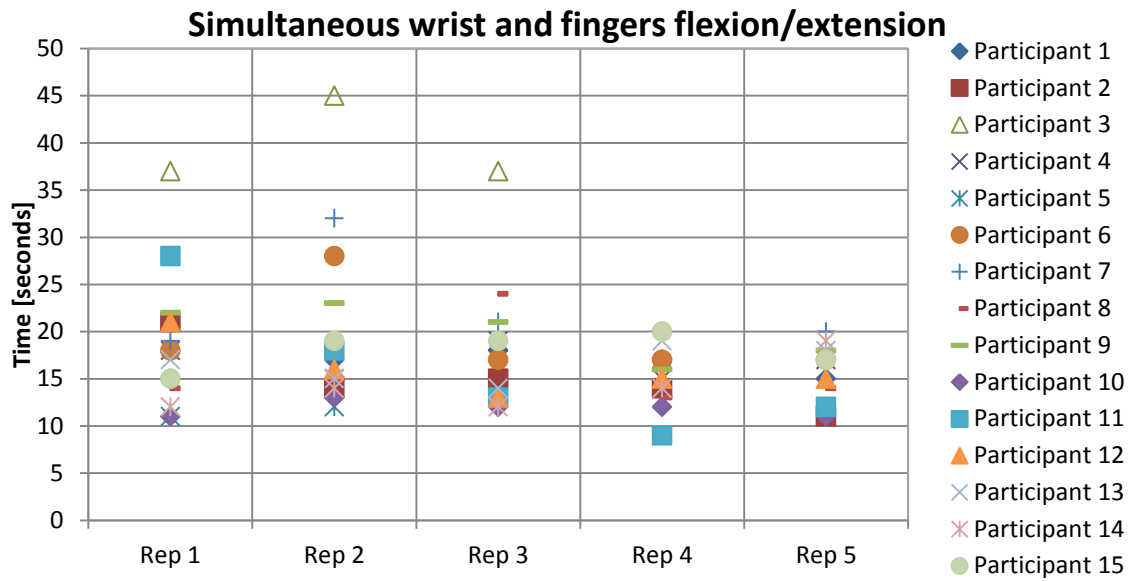


**Figure 4.3** Times to complete repetitions during the third test in the preliminary safety test – five repetitions of simultaneous wrist and finger flexion and extension performed by 15 participants with no history of hypertonia (see Figure 3.2).

## 4.2. Pilot Clinical Trial

### 4.2.1. Processed Data

Figure 4.4, to Figure 4.9 show the plots of the force (and EMG data if available) that was collected during the tests. The force data was processed in the method described in Section 3.3.2. The EMG data processing method is described in Appendix E.

**Participant A – Average MAS score: 2.17**  
**Force Recordings**

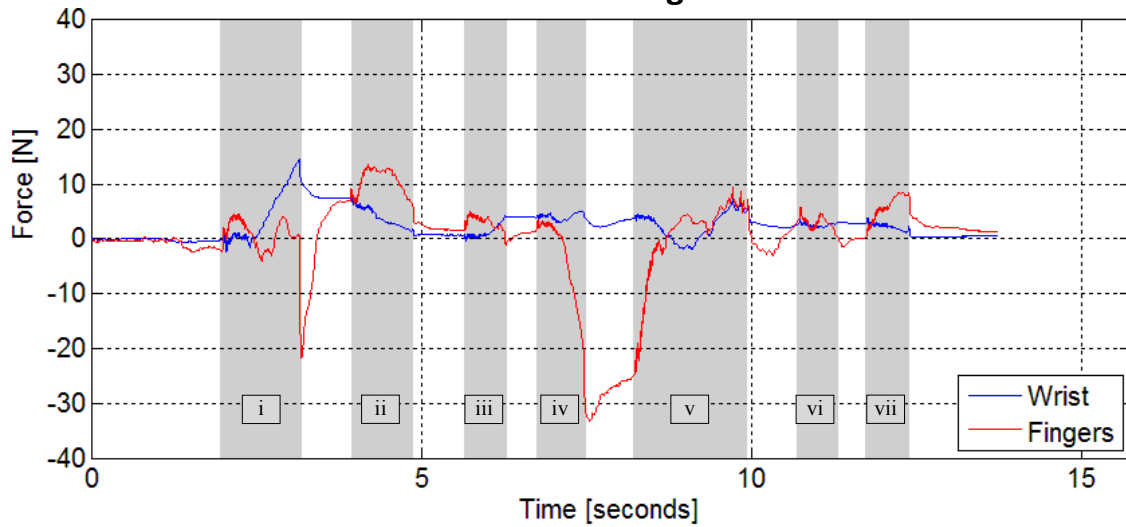


**Figure 4.4** Wrist and finger force recordings for Participant A during passive wrist and finger manipulation. Indicated are the different phases of device joint movement. From starting position (wrist and fingers at  $0^\circ$ ): (i) Flexing fingers from  $0^\circ$  to  $+90^\circ$ , (ii) extending fingers from  $+90^\circ$  to  $0^\circ$ , (iii) flexing finger joint from  $0^\circ$  to  $+45^\circ$ , (iv) flexing wrist from  $0^\circ$  to  $+70^\circ$ , (v) extending wrist joint from  $+70^\circ$  to  $-35^\circ$ , (vi) flexing wrist from  $-35^\circ$  to  $0^\circ$ , (vii) extend fingers from  $+45^\circ$  to  $0^\circ$  (see Figure 3.6). The white areas between regions i – vii represent pauses in device motion.

**Participant B – Average MAS score: 2.67**  
**Force Recordings**

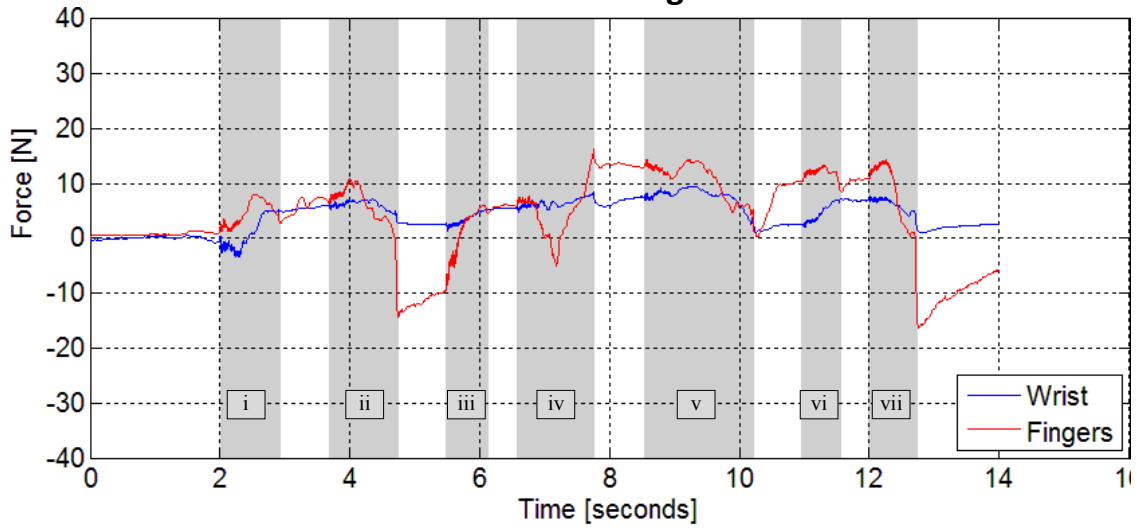
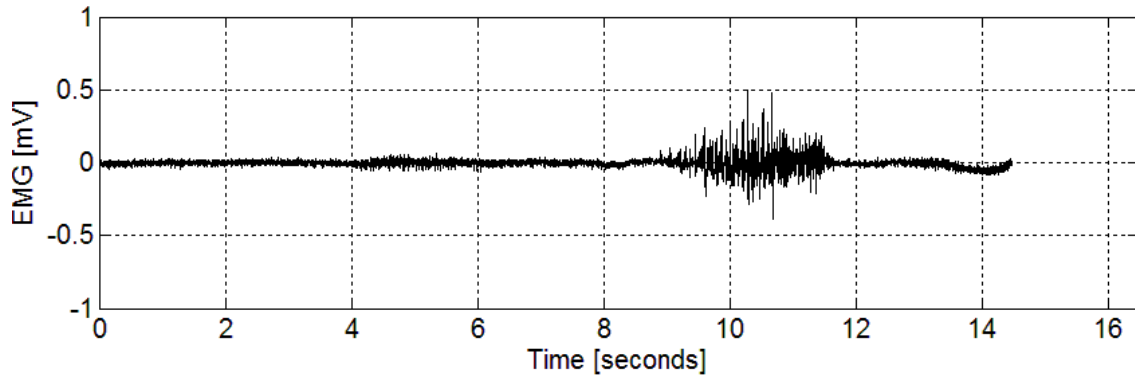


**Figure 4.5** Wrist and finger force recordings for Participant B during passive wrist and finger manipulation. Indicated are the different phases of device joint movement. From starting position (wrist and fingers at 0°): (i) Flexing fingers from 0° to +90°, (ii) extending fingers from +90° to 0°, (iii) flexing finger joint from 0° to +45°, (iv) flexing wrist from 0° to +70°, (v) extending wrist joint from +70° to -35°, (vi) flexing wrist from -35° to 0°, (vii) extend fingers from +45° to 0° (see Figure 3.6). The white areas between regions i – vii represent pauses in device motion.

**Participant C – Average MAS score: 2.67**  
**EMG Recordings for Flexor Carpi Radialis**



**Force Recordings**

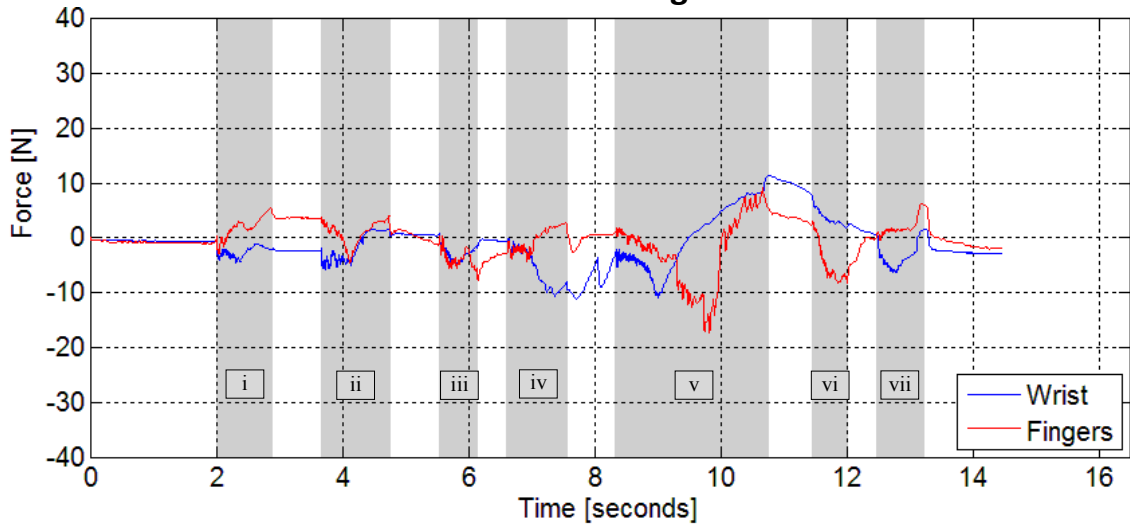
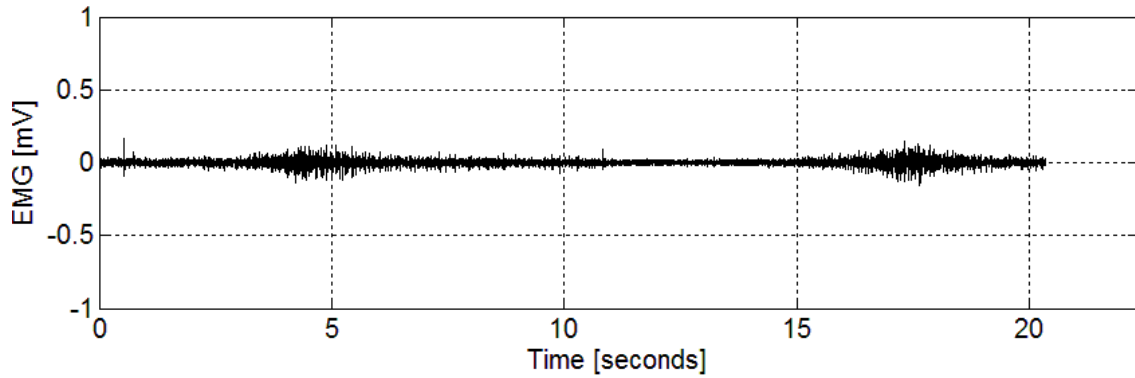


**Figure 4.6** Flexor carpi radialis muscle EMG recordings (top) and wrist and finger force recordings (bottom) for Participant C during passive wrist and finger manipulation. Indicated are the different phases of device joint movement. From starting position (wrist and fingers at 0°): (i) Flexing fingers from 0° to +70°, (ii) extending fingers from +90° to 0°, (iii) flexing finger joint from 0° to +45°, (iv) flexing wrist from 0° to +70°, (v) extending wrist joint from +70° to -35°, (vi) flexing wrist from -35° to 0°, (vii) extend fingers from +45° to 0° (see Figure 3.6). The white areas between regions i – vii represent pauses in device motion.

**Participant D – Average MAS score: 1.83**  
**EMG Recordings for Flexor Carpi Radialis**



**Force Recordings**

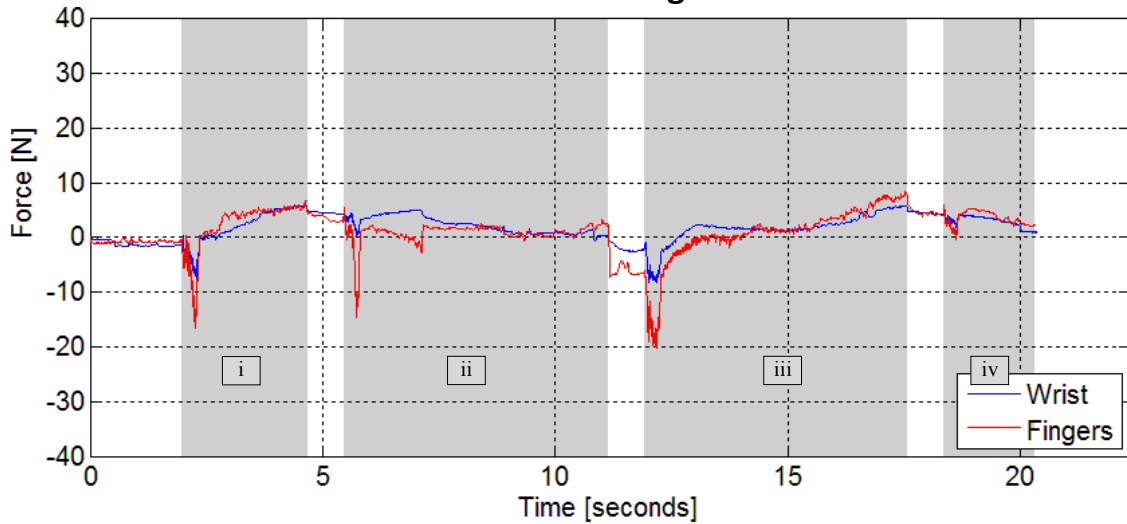
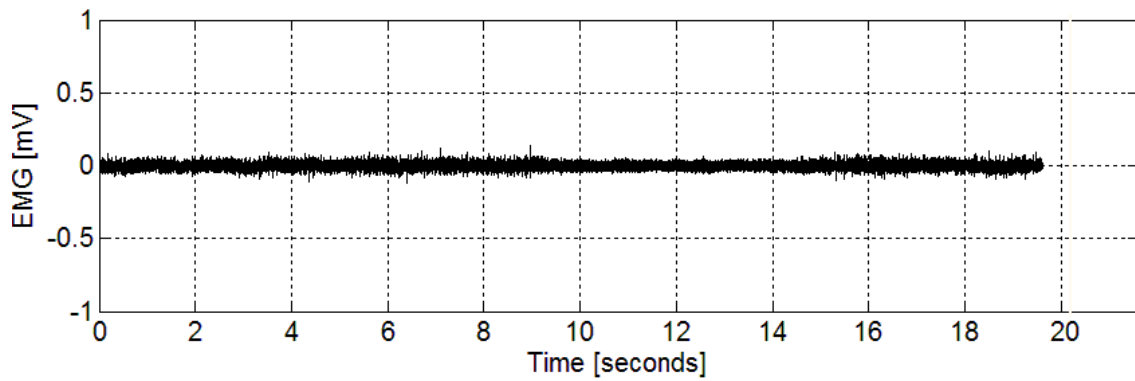


**Figure 4.7** Flexor carpi radialis muscle EMG recordings (top) and wrist and finger force recordings (bottom) for Participant D during passive wrist manipulation. Indicated are the different phases of device joint movement. From starting position (wrist and fingers at 0°): (i) Extend wrist joint from 0° to -35°, (ii) flex wrist joint from -35° to +70°, (iii) extend wrist joint from +70 to -35°, (iv) flex wrist from -35° to 0° (see Figure 3.7). The white areas between regions i – iv represent pauses in device motion.

**Participant E – Average MAS score: 2.33**  
**EMG Recordings for Flexor Carpi Radialis**



**Force Recordings**

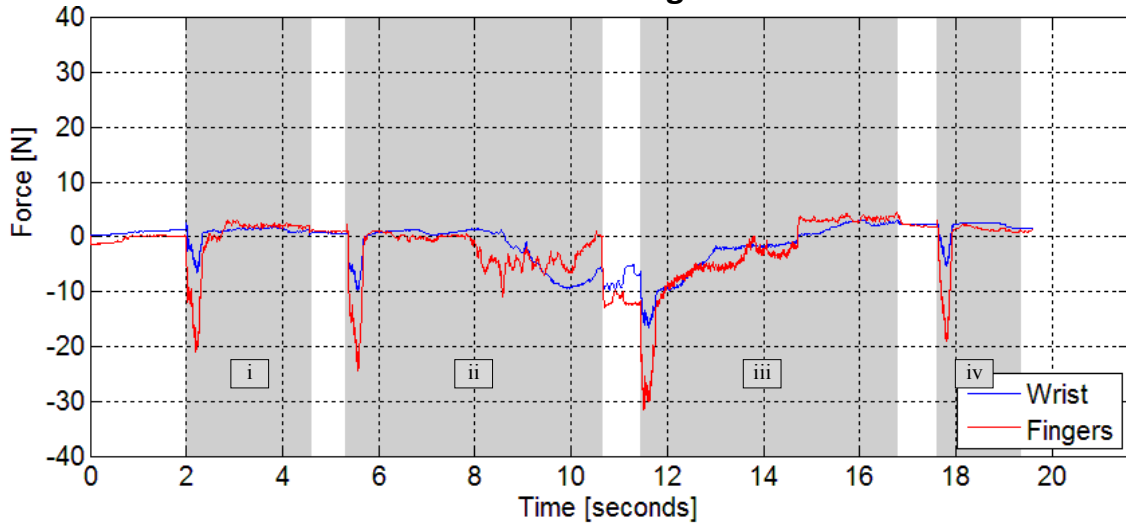
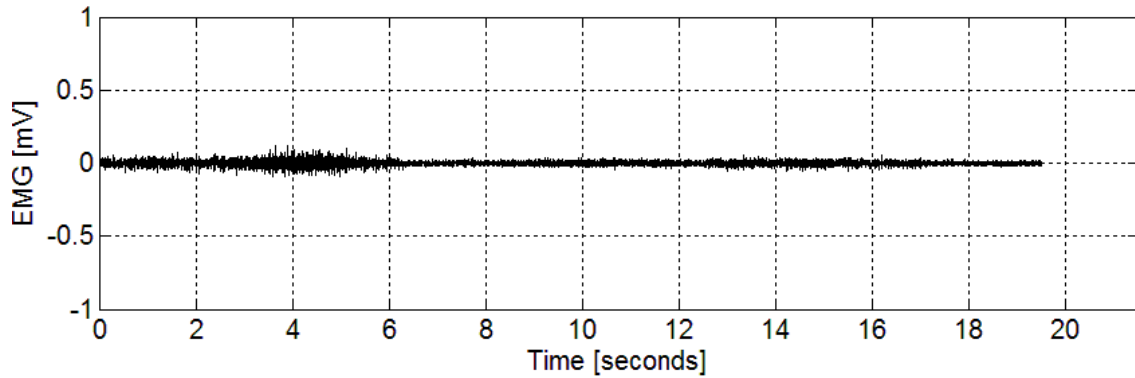


**Figure 4.8** Flexor carpi radialis muscle EMG recordings (top) and wrist and finger force recordings (bottom) for Participant E during passive wrist manipulation. Indicated are the different phases of device joint movement. From starting position (wrist and fingers at 0°): (i) Extend wrist joint from 0° to -35°, (ii) flex wrist joint from -35° to +70°, (iii) extend wrist joint from +70 to -35°, (iv) flex wrist from -35° to 0° (see Figure 3.7). The white areas between regions i – vii represent pauses in device motion.

**Participant F – Average MAS score: 0**  
**EMG Recordings for Flexor Carpi Radialis**



**Force Recordings**

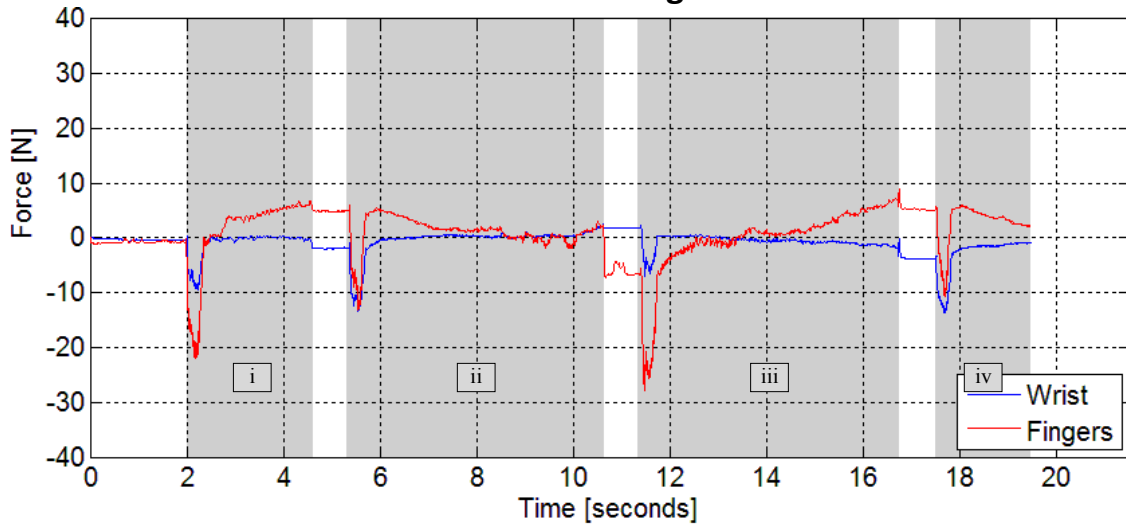


**Figure 4.9** Flexor carpi radialis muscle EMG recordings (top) and wrist and finger force recordings (bottom) for Participant F during passive wrist manipulation. Indicated are the different phases of device joint movement. From starting position (wrist and fingers at  $0^\circ$ ): (i) Extend wrist joint from  $0^\circ$  to  $-35^\circ$ , (ii) flex wrist joint from  $-35^\circ$  to  $+70^\circ$ , (iii) extend wrist joint from  $+70^\circ$  to  $-35^\circ$ , (iv) flex wrist from  $-35^\circ$  to  $0^\circ$  (see Figure 3.7). The white areas between regions i – vii represent pauses in device motion.

Table 4.1 contains the data extracted from during the pilot trial. Of interest was the peak positive force as measured by the wrist and finger force transducers, occurring during extension of the wrist joint (i.e. phase „v“ for Participants A, B and C, and then phase „vii“ for Participants D, E and F). This occurs in the segment labelled „vi“ for Figure 4.4 to Figure 4.6, and in the segment labelled „jii“ for Figure 4.7 to Figure 4.9. This information was used with Equation 3.6 from Section 3.4 to estimate the tension in the wrist flexor tendons. Equation 3.6 requires the peak resistive force measured during wrist extension, as well as the finger force measured at the time that the peak wrist force occurred. Note that the tensions in the wrist flexor tendons are generally higher than the peak measured forces. This is due to the relatively small moment arm that the tendons have at the wrist and finger joints when compared with those of the measured forces.

Table 4.1 also includes the MAS assessment scores as performed by the clinicians. Due to the testing being conducted at various institutions and at various times, the MAS assessments were not all conducted by the same clinicians in each case. MAS scores of „1+“ were assigned the value of 1.5 when calculating the average MAS score for each participant.

Figure 4.10 graphically represents the MAS scores for all participants, illustrating the variability in scores between raters.

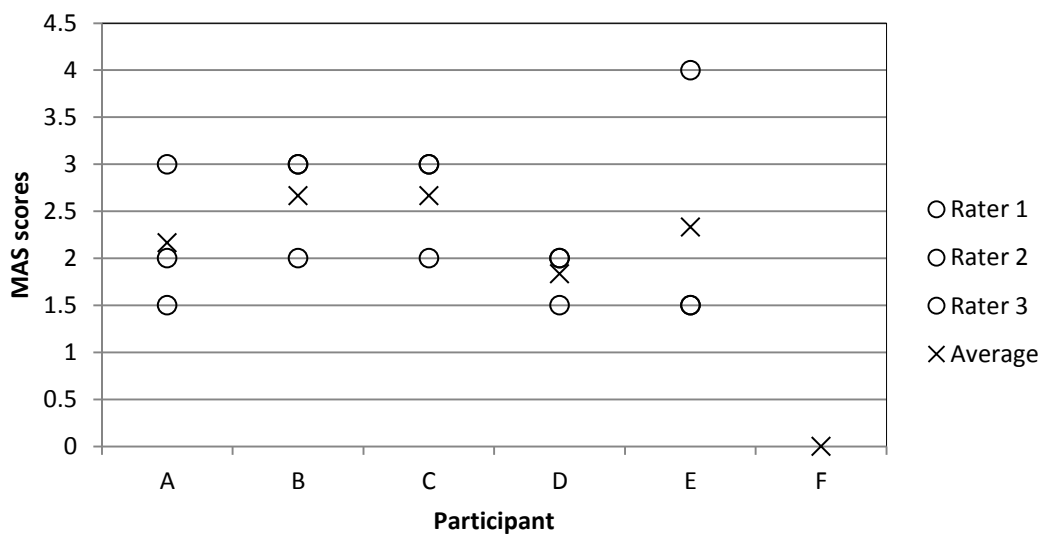


**Figure 4.10** Graphical representation of MAS scores for participants, illustrating the variability between raters.

**Table 4.1** Summary of data collected during the pilot trial.

Participant	Peak measured force during wrist extension [N]	Time at which peak wrist force during wrist extension occurs [seconds]	Simultaneous finger force when wrist peak force occurs [N]	Estimated tension in wrist flexor tendons as determined using Equation 3.6 [N]	Wrist flexor MAS scores				General description, based on MAS score
					Rater 1	Rater 2	Rater 3	Average (standard deviation)	
A	7.1	9.73	9.2	59.6	2	3	1+	2.17 (0.76)	Distinct increase in muscle tone, but affected limb still easily moved.
B	9.5	9.28	13.8	84.2	2	3	3	2.67 (0.58)	Considerable increase in muscle tone. Movement becoming difficult.
C	11.4	10.78	4.9	68.2	3	3	2	2.67 (0.58)	Considerable increase in muscle tone. Movement becoming difficult.
D	5.9	17.52	8.2	51.1	2	2	1+	1.83 (0.29)	Slight increase in muscle tone, minimal resistance through range of motion.
E	3.1	16.01	3.8	25.3	1+	1+	4	2.33 (1.44)	Distinct increase in muscle tone, but affected limb still easily moved.
F	0.6	12.55	-0.9	0.3	[healthy individual]			0	No increase in muscle tone.

#### 4.2.2. Statistical Analysis

The following section describes the statistical outcomes of the study. The statistical methods were developed with assistance from Henri Carrara, a consulting statistician from the University Of Cape Town's Health Sciences faculty.

Since the MAS scores are not normally distributed, the Spearman's Rank Correlation Coefficient was used to determine the agreement between the MAS scores and each of the two datasets<sup>1</sup>. These are namely:

1. Correlation between the average MAS assessments for each participant and the peak force measured at the wrist.
2. Correlation between the average MAS assessments for each participant and the estimated wrist flexor tension, as calculated with Equation 3.6.

The data for these comparisons can be found in Table 4.1. The correlation coefficients were calculated based on the definition of the Spearman Rank Correlation Coefficient:

$$\rho = \frac{\sum(x_i - \bar{x})(y_i - \bar{y})}{\sqrt{\sum(x_i - \bar{x})^2 \sum(y_i - \bar{y})^2}}$$

In this definition, x and y represent the ranks of the two set of variables (rather than the actual variable values), and  $\bar{x}$  and  $\bar{y}$  represent their respective rank means. The Spearman's Rank Correlation Coefficient assesses how well the relationship between two variables can be described using a monotonic function. This is in contrast to the Pearson Product Moment Correlation Coefficient, which gives a perfect value when the relationship between the variables is linear, rather than monotonic.

---

<sup>1</sup> A commonly used method for measuring the agreement between two clinical measures is a Difference plot (Bland and Altman, 1986). Such a plot quantifies the agreement (rather than correlation) between two clinical measures. Measures that show a high degree of agreement can be used interchangeably in the field (for example, two methods of measuring blood pressure). In the case of this research, the data being compared (forces and MAS scores) cannot be used interchangeably, and so the Difference plot is not applicable. If a repeatability study is performed, however, consecutive assessments made with the same participant can be compared for agreement with a difference plot.

For both of the correlation analyses performed, the correlation coefficient  $\rho$  was shown to be 0.81. Due to the nature of the Spearman Rank Correlation Coefficient using ranks rather than the actual values of the variables, the correlation coefficients for the two comparisons were identical. That is to say, even though the variables varied in relation to each other, their ranks within their respective datasets were the same, and as such the correlation coefficients were identical too.

For the purposes of determining statistical significance, the Student's t value and corresponding p value were calculated. Similarly, the t and p values calculated were identical for the two correlations analysed. They were as follows:

- $t = 2.78$
- $p = 0.0498$

The p value is below 0.05, indicating statistical significance.

As was stated in Section 4.2.1, one of the MAS assessments for Participant E contradicted other observations (see table 4.1). One rater assigned a MAS score of 4, which is intended to indicate rigidity in both flexion and extension (see Table 1.2). Both other raters scored the participant as „1+“, indicating a slight catch followed by a minimal resistance across the range of motion. It should be noted that this participant's peak wrist force during wrist extension was the second lowest observed, second only to the healthy participant (see Table 4.1), and the EMG recording showed little activity in the flexor carpi radialis muscle during the test (see Figure 4.8).

To augment the statistical analysis, the correlations were recalculated with the anomalous MAS assessment for Participant E omitted. The new average MAS score, calculated from the remaining two raters' assessments, was 1.5. For both of the correlation analyses that were recalculated, the correlation coefficient  $\rho$  was shown to be 0.99. As with the original correlations, the ranks for each variable in the calculation, and thus the correlation coefficients themselves, were identical. The corresponding t and p values were as follows:

- $t = 11.66$
- $p = 0.0003$

The p value is below 0.05, again indicating statistical significance. The results of the analysis are summarised in Table 4.2

**Table 4.2** Summary of the results of the statistical analysis

	Peak wrist force [N]	Peak Estimated Wrist Flexor Tension [N]
Spearman's Rank Correlation Coefficient with average MAS scores (primary result)	0.81	0.81
t-value	2.78	2.78
p-value	0.048	0.048
Spearman's Rank Correlation Coefficient with average MAS scores, omitting anomalous MAS assessment	0.99	0.99
t-value, omitting anomalous MAS assessment	11.66	11.66
p-value, omitting anomalous MAS assessment	0.0003	0.0003

[This page is intentionally left blank]

## 5. Discussion

This section contains an analysis of the design, experimental methodology and results. It will begin with the preliminary safety tests, and proceeding to the pilot clinical trial. Lastly, recommendations for future work will be presented.

### 5.1. Preliminary Safety Tests

As was stated in Section 4.1, all safety features operated as intended. The aim of the preliminary safety tests was achieved: to demonstrate that the device is safe and functions as intended (see Objective 1 in Section 1.3). In addition to this, various other observations were made about the functioning of the device.

One such observation was that there was a clear trend towards faster times to complete tests, as is illustrated in Figures 4.1 to 4.3. Participants quickly learned to control device joint movements, even in this short exposure (performing a total of only 15 repetitions of various given tasks). The fact that participants had initial difficulty in controlling the device, however, is an indication that the devices interpretation of participant gestures may not be optimum. In the ideal case, this gesture recognition would be seamless, and the device would recognise any wrist flexion, not just flexion performed in a particular way. For instance, one participant reported that trying to move his “thumb towards [his] elbow” helped achieve the task of device wrist joint flexion better than simply flexing his wrist. This action forces a stronger activation of the flexor carpi radialis muscle, and as such produces a stronger measurable EMG signal.

Some participants reported difficulty isolating activation of one device joint from the other. For example, in trying to perform tasks of device finger joint flexion, some participants accidentally activated device wrist joint flexion too. This may indicate EMG cross talk between two channels, since the wrist and finger muscles lie in close proximity to one another. It may also be due to co-activation of these muscle groups, since performing finger flexion usually necessitates stabilizing of the wrist joint which elicits EMG from the flexor carpi radialis muscle.

The lack of a dedicated threshold adjustment for each EMG channel impeded performance in this regard. One threshold was shared between the wrist flexor and extensor channels, and another between the finger flexor and extensor channels. This arrangement was implemented due to microcontroller limitations. EMG signal strength, however, was affected by relative anatomical size and position of the target muscles. A common EMG threshold was often a compromise in

effectiveness for each channel. The inclusion of a dedicated EMG threshold for each channel is recommended for future work (discussed further in Section 5.3).

Overall, the preliminary safety tests indicated that no safety risks were present and that the device functioned as intended. While some design modifications were implemented before the pilot trial (see Section 3.1.3), these were not motivated by safety concerns but rather by improved device functionality and noise reduction. Once these modifications were completed, the pilot trial could proceed.

## **5.2. Pilot Clinical Trial**

### **5.2.1. Test Count and Statistical Analysis of the Results:**

The tests show strong correlations between resistive force and MAS scores, which is to be expected. Furthermore, this is in agreement with Lindberg et al. (2011), who reported that their study of the Neuroflexor device showed a “strong correlation” between resistive force and MAS ( $r > 0.6$ ,  $P < 0.001$ ). As Damiano et al. (2002) point out, isokinetic measurements and MAS scores both measure resistance to passive stretch, so it is logical to assume that they would be correlated. They also found strong correlations between these two measures. However, the results of the pilot trial (Section 4.2.2) suggest that there is no increase in the accuracy of wrist tone assessments made using estimated wrist flexor tension as opposed to peak force applied at the wrist. This is despite the moment arm that the finger flexor muscles may have at the wrist joint. This suggests that the effect that the finger flexors have at the wrist is negligible when compared to the wrist flexors. Certain factors relating to the experimental protocol and statistical analysis should be considered, however.

Testing was terminated after 6 participants due to a lack of volunteers that met the inclusion criteria for the study. Volunteers for the pilot trial were sought from amongst the in- and out-patients at three care facilities in Cape Town: Groote Schuur Hospital, Life Vincent Pallotti Hospital and the Western Cape Rehabilitation Centre (see Appendix G for documentation regarding clearance to conduct research at these facilities). Suitable volunteers were successfully recruited from only the first two of these facilities. Willing volunteers were often available, but most did not meet the inclusion criteria of having comfortable (i.e. pain free) range of motion up to  $35^\circ$  in extension. This was despite the range of motion criteria for the study being the same as that required by similar research in literature, such as studies with the NeuroFlexor device by Lindberg et al. (2011). The work by Pizzi et al. (2005) also suggested that those with mild to moderate hypertonia in the wrist would have sufficient range of motion to participate (see Figure 1.4). It was suspected that individuals with larger ranges of motion

and with less pain are likely to be discharged earlier and are less likely to be encountered at a care facility. It is possible that the volunteers were recruited for this research from a population with anomalously low ranges of motion relative to their MAS scores.

Despite statistical significance, the low test count may have influenced the statistical analysis. Consider also that the Spearman’s Rank Correlation Coefficient correlates the ranks of the variables in two datasets, rather than the variables themselves. Due to the relatively small test count, the ranks of the two values being compared in this research (wrist force and the wrist flexor tendon tension) are likely to be similar, even if their actual values relate to the MAS score differently. As an illustrative example, consider the hypothetical variables Y1 and Y2 that increase linearly and exponentially with variable X respectively (see Figure 5.1 and Table 5.1). Despite having different mathematical relationships with X, the variables Y1 and Y2 have identical ranks within each paired dataset. Each would produce perfect (and identical) Spearman’s Rank Correlation Coefficients with variable X, despite not being identical functions of X. Similarly, the peak wrist forces and estimated wrist tensions measured in the trial could be expected to produce identical correlation coefficients when compared to the MAS scores. With a higher test count, however, identical ranking is unlikely and differences in correlation would become apparent.

Another point for consideration is the use of average MAS scores as a gold standard. The MAS score has been criticized for its unreliability (see section 1.1.5). Even the average of three raters’ MAS scores may not be reliable enough to serve as a proxy for hypertonia severity. Achieving statistical significance suggests that that the sample size (n=6) is large enough that the probability of the observed correlations being due to anomalous recordings is small (less than 5%). The effect of the unreliable MAS score, however, is illustrated by the marked difference that a single score had on the outcome. When a score from one rater was omitted for only one participant (see Section 4.2.2), the overall correlation coefficients increased from 0.81 to 0.99 – an increase of 22.2%. For experimental robustness, the outcome should not be so reliant on individual observations so much as overall trends. Despite the results indicating statistical significance at this sample size, experimental robustness could be improved by increasing the test count or by replacing the MAS score as the gold standard for analysis.

**Table 5.1** Hypothetical variable X, Y1 and Y2, illustrating that the ranks of the variables are identical

X	Y1	Y2	Rank of Y1 (lowest to highest)	Rank of Y2 (lowest to highest)
1	1	1	1	1
2	2	4	2	2

3	3	9	3	3
4	4	16	4	4
5	5	25	5	5

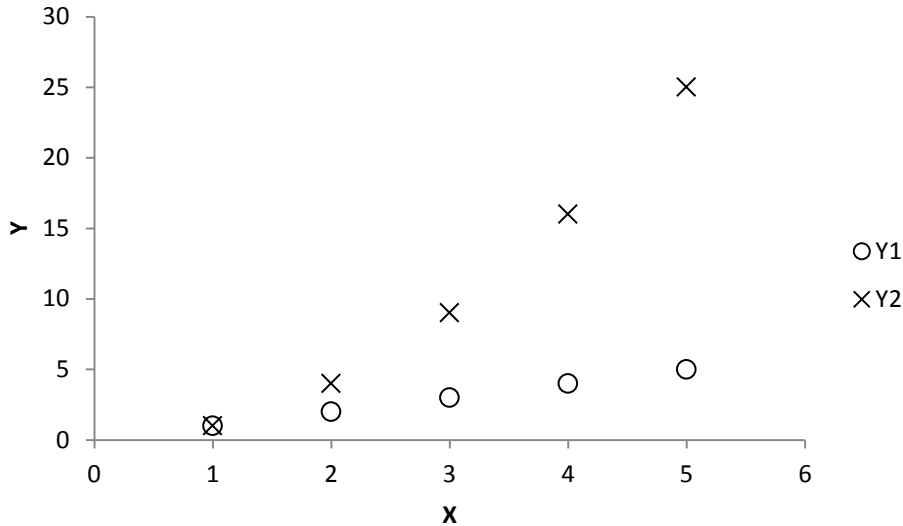


**Figure 5.1** Hypothetical variables Y1 and Y2 which vary linearly and exponentially with X respectively

### 5.2.2. Force Recordings

The estimate of the expected peak force of 30 N (with a safety factor) was appropriate. The highest recorded force was from Participant A, who exerted a peak of 33.32 N in extension (i.e. a negative recorded force) to the finger joint transducer. Participant A had an average MAS score of 2.17. The values recorded were in agreement with the data presented by Lindberg et al. (2011). In their study, the highest resistive force recorded was approximately 37 N from a participant with a wrist MAS of 3.

In general, the observations follow intuition. Participants with a higher average MAS score generally also exhibit more fluctuant force activity. This is evident when one compares Figure 4.9 to Figure 4.5 or Figure 4.6 (the lowest and highest MAS scoring participants). The expectation was that clear force peaks would be observed during wrist extension, and that these peaks would be more pronounced in those with higher MAS scores. This is observed most clearly in Participant C and Participant D, for whom recordings show clear force activity during wrist extension (see Figure 4.6 and Figure 4.7). Note that the peak force observed by participant C occurs exactly as peak wrist extension occurs, and subsides partially during the subsequent pause. This is consistent with the velocity dependent component of UMNS.

Furthermore, periods of EMG activity can clearly be seen to coincide with rises in recorded force. This indicates that these forces are at least partially neural in origin (for example, see Figure 4.6). Note that almost no wrist flexor EMG activity or wrist flexor force activity was observed for Participant F (Figure 4.9), who had a MAS score of 0. Some finger force activity was observed, although without finger flexor and/or extensor EMG recordings one cannot say definitively whether the activity observed is neural in origin. Since this participant had no history of hypertonia, it is probable that this force was due to viscoelastic effects.

The reduction of motor speed that was implemented following testing with Participant C (see Section 3.1.3) is a possible factor that must be considered. The modifications were necessary to avoid unnecessary discomfort to participants. They may, however, have influenced the results since some features of UMNS - such as spasticity - are velocity dependent. This variation in motor speed was therefore not ideal. It may be reasonable to expect that tests with slowed motors (Participant D, E and F) would result in smaller peak wrist and finger forces. While this is indeed reflected in Table 4.1, it should also be noted that these participants also had the lowest average MAS scores. While it is uncertain whether this velocity dependence is so strong that results would be affected considerably, this is one of the factors preventing definitive conclusions from being drawn. Due to the low test count, data could not be pooled by velocity for separate analysis. See Section 5.2.1 for a discussion of the test count. As such, the results from this study represent preliminary findings, and the various recommendations for future work in Section 5.3 include maintaining of consistent velocities during tests as well as pooling of tests by velocity. Lastly, the presence of artefact was noted in the force readings. This is especially pronounced in results from tests with the slower motors installed (Participants D, E and F - see Figures 4.7 to Figure 4.9). The artefact occurs at the beginning of each phase of movement and is visible as a strong negative dip in the recordings. This is a result of EMI from the motors that occurs on start up. It is apparent that the slower motors radiate substantially higher levels of EMI. This duration of the effect was prolonged by pulse width modulation implemented at the beginning of each movement as a „soft start“ to prevent violent jerking of the device joints. Note that none of the peak wrist or finger forces that were extracted from the data (Table 4.1) occurred during these periods. It is possible, however, that the artefact was masking forces that could otherwise be observed.

EMI from the motors introduced noise into the strain gauge bridges and the cables that carry signals to the force amplifiers. While shielding mitigated this effect, it did not eliminate it. The signals in these cables had a very low signal-to-noise ratio, and were especially susceptible to EMI. This noise could be reduced by using motors that create lower levels of EMI (e.g. stepper motors), and by relocating them such that they are not in such close proximity to the sensitive force transducers. This is discussed further in Section 5.3 on recommendations for future work.

### 5.2.3. Biomechanical Model

The outcomes of the biomechanical model follow intuition. That is to say, the estimated wrist flexor tensions have approximate magnitudes that are of the expected order. Consider that the highest tension in the wrist flexors estimated by the model was 84.2 N. If we assume that this load was shared evenly between the two prime wrist flexors (flexor carpi radialis and flexor carpi ulnaris), and that each tendon had a round cross section of 5mm diameter, the tension in each would be 2.14 MPa. For comparison, the ultimate tensile strength of the flexor carpi radialis muscle has been shown to be at least 51.6 MPa (Loren and Lieber, 1995). The highest tension estimated by the model represents 5.1% of the load capability of the tendon, which follows intuition and lends credence to the model.

The assumptions on which the model relies should be considered. These are namely:

1. The assumption of a system in a state of static equilibrium (i.e. inertial effects were small).
2. Simplification of joint morphology: in the model, joints are treated as simple hinges when in reality the centre of joint rotation (and tendon moment arms) vary with joint angle.
3. The assumption that all participants had similar joint morphologies. Common values for finger and wrist flexor moment arms were adopted for all participants (i.e. the values for  $d_{\text{tendon, finger}}$  and  $d_{\text{tendon, wrist}}$ ).

The first two assumptions are unlikely to appreciably affect the model; the device acceleration was slow enough that inertial effects could be ignored, and the treatment of the joint as a simple hinge was deemed acceptable. A possible improvement, however, might be to compensate for biomechanical effect of different hand sizes. Measurements of participants' hands could be used to scale the assumed tendon moment arms, and provide more accurate estimates. This is included in recommendation for future work.

### 5.2.4. EMG and Neural vs. Non-neural Hypertonia

A rise in wrist flexor EMG was observed to be accompanied by a positive wrist flexor force in almost all instances where EMG was collected. The exception was with Participant F (see Figure 4.9) - no rise in wrist force was observed to coincide with the observed EMG activity at the end of phase i. Note that Participant F had no history of hypertonia. In healthy individuals, EMG activity is a normal response only to high velocity stretch (i.e. the knee-jerk reflex). It should not be observed in passive stretch of healthy muscle. The observed EMG may be a result of the participant stabilizing their wrist

(a voluntary action). Such wrist flexor activity would result in no net wrist force, since it would be opposed by wrist extensors.

There is, however, a rise in Participant F's finger force at the end of phase i, which is again observed to rise and peak towards the end of phase iii. The rise in finger force seen at these points might be attributable to viscoelastic joint/muscle properties. Without finger flexor EMG, however, the possibility of the force being neural in origin cannot be ruled out. Regardless, these increases in finger force did not affect the results: the biomechanical model required the magnitude of the finger force at the time when the peak wrist force during wrist extension occurs. For Participant F, this occurs before the rise in finger extension is observed.

For Participant E (see Figure 4.8), a low level of EMG activity was present even before the start of phase i. This activity can be seen to subside slightly at the end of phase ii and resume during phase iii. That is to say, the EMG subsided when the wrist joint was flexed. A negative force (i.e. a force in the extension direction) was observed to occur simultaneously. This may be explained by the process by which the force readings were zeroed. Recall that in Section 3.3.2, it was stated that the baseline for force recording was obtained by averaging the first 1000ms of data in each recording. The recordings only began, however, once the participant had already been strapped into the device. If a force was applied to the device during the 1000ms interval, the baseline would not represent a zero value. In addition, flexion of the joint might relieve tension in the wrist and finger flexors. Hypertonia is a stretch response, so the relief in tension would result in an observed reduction in both EMG and force. It is recommended that protocols for future research be constructed such that force baseline recordings are captured during a time when the participant is not secured into the device (see Section 5.3).

### **5.2.5. MAS Scores**

There is little agreement between the three raters regarding the MAS scores (see Table 4.1 and Figure 4.10). In no instance did all three raters agree on a single score for a participant. The average standard deviation of MAS scores was 0.73, which represents almost a full step on the 5-point ordinal scale. This poor interrater MAS agreement is corroborated by other analyses in literature (e.g. (Blackburn et al., 2002; Ansari et al., 2006; Alibiglou et al., 2008; Mutlu et al., 2008). The study by Mutlu et al (2008), for instance, states that MAS scores are “not very reliable and assessments of spasticity using these scales should be therefore interpreted with great caution”. This lack of agreement from raters corroborates research that suggests that the MAS score is unreliable. It underscores the need for an objective measure of muscle tone.

The high variability of MAS scores also may have had an effect on the results of this study. This is apparent in Section 4.2.2 when the correlation coefficients were recalculated omitting an anomalous MAS score. The results were dramatic – the correlation coefficient increased by 22% (discussed in Section 5.2.1). The fact that a single MAS score had such a pronounced effect indicates a potential lack of robustness in the experimental protocol. It is possible that even the average of three independent MAS scores is not a reliable proxy for the severity of hypertonia, and does not serve as a reliable gold standard for research. Potential solutions to this may include replacing the MAS score with another measure of muscle activity – such as EMG activity – or to increase the test count such that individual scores have less of an effect on research outcomes.

Note that the tests were performed at various facilities, and at various times. The same raters were not available to perform assessments for all participants. Individual MAS assessments cannot be compared across participants to identify trends. That is to say, one cannot determine from the results of this study if one rater consistently scores participants as having higher or lower muscle tone.

It should also be noted that there appears to be no standardised procedure for the method of performing the MAS assessments. In the publication where the MAS score was first described (Bohannon and Smith, 1987), assessments of elbow flexor tone were performed. There was no description of a standard method for wrist assessment. For example, some assessors may extend the wrist joint while holding the finger joint in a fixed angle. Others may allow the finger joint to move freely. The effect of this is that some clinicians may be allowing finger flexor hypertonia to influence wrist joint assessments, while others may not. While the results of this research indicate that there is no improvement in accuracy when comparing biomechanical results to the average MAS score, this may not be true of individual raters (see Section 5.3.3). Investigation into the development of a standardized method for MAS assessment is recommended for future work.

### **5.3.6. Ergonomics**

Manipulation of the finger joint was abandoned from the protocol due to design issues with finger ergonomics (see Section 3.2.2). Movement of the device finger joint often resulted in the participants' fingers slipping out of place. This is a result of the lack of adjustability for various hand sizes, and was more likely to occur with participants with smaller hands.

The inclusion of finger manipulation would have allowed further analysis of data in this study. Finger flexor tone could have been assessed in the same way as was performed with the wrist. Such data could have been used to further confirm methods ability to accurately assess hypertonia. Such data

would also have helped provided a more complete clinical picture for each participant. This issue should be addressed in future design revisions.

Note also that the current ergonomic design made it difficult to position the hands of participants with extreme weakness. Specifically, participants were often unable to hold their fingers rigid for insertion into the device components. While this lead to difficulty during setup, it did not impede testing or affect the results. This should also be a factor for consideration for future design revisions (see Section 5.3).

### **5.3. Recommendations for Future Work**

The results indicate no improvement in assessment accuracy when using the device and the biomechanical model (see Section 4.2.1). However, certain factors could have affected the results (see Section 5.2). This section provides a discussion of recommendations for future work based on these points.

#### **5.3.1. Device Design Modifications**

The recommended changes are intended to improve recording quality (e.g. reduction of noise) and ergonomics. They are as follows:

- Replacement of brushed DC electric motors with a different actuation method. It is recommended that stepper motors be considered. Various advantages would be offered by such a modification:
  - Noise due to EMI in the force recordings would be reduced.
  - Velocity management would be improved, allowing more uniformity across participants.
  - Joint position could be digitally monitored, and setting of limits of the range of motion could be applied and adjusted in software. Hardware implementation (limit switches) do not offer such adjustability. Recall that range of motion was the leading factor in exclusion of volunteers (see Section 5.2.1). Adjustability would allow testing with a greater number of participants.
- Removal of actuators away from the force transducers. This would further reduce noise in the force recordings due to EMI. Furthermore, relocation of the actuators would minimize unnecessary weight being shifted during device joint manipulation – a factor which contributed to force drift (see Section 3.3.2).

- Improvement of ergonomics. Redesign of the ergonomic components is recommended. It is recommended to use detachable components that may easily be secured onto the participant's hand without complication. These components could then be easily attached to the structure of the device. The system should also be adjustable such that various hand sizes can be accommodated.
- Inclusion of dedicated EMG activation threshold adjustment knobs. Each EMG channel should have its own dedicated EMG activation threshold adjustment.

### 5.3.2. Experimental Protocol

The following points should be considered for future revisions of the experimental protocol:

- Uniform velocity for all participants. It was unavoidable in the experimental protocol that the joint velocity of the device be altered after testing with Participant C (see Section 3.1.3). This was not ideal, since some features of UMNS are a velocity dependent. It is recommended that future experimental protocols be conducted at uniform velocities across participants. Furthermore, for each participant tests should be repeated at various velocities – using the same velocities across participants – such that resistance profiles at each velocity can be compared.
- Use multiple measures to validate readings. Since the reliability of the MAS score has been shown to be questionable (see Section 1.1.5), it is not suitable as a validation technique. Alternative validations should be sought. Possible measures include EMG power, the use of varying velocities (to test velocity dependence), and more reliable scales such as the Tone Assessment Scale. Ideally, a combination of validations should be used.
- EMG for both wrist and finger flexors and extensors should be recorded. The results depict relatively large forces in the extension direction (see Section 4.2.1). In tests that include EMG recordings, only wrist flexor activity was recorded to reduce discomfort associated with skin preparation. Without EMG recordings of the wrist extensor muscles as well as finger flexors and extensors, the distinction between neural and viscoelastic force cannot be made.
- Separate recording of the force transducer baseline. A recording for the baseline of the force transducers (later used to zero the recordings) should be performed before the participant is secured into the device (see Section 5.2.4).

### **5.3.3. Other Recommendations**

Although results suggest no effect of finger flexor torque at the wrist when forces or tensions are correlated with the average MAS score, this may not necessarily be the case for individual MAS score correlations. It was not possible to compute individual MAS score correlations in this study because the individual MAS assessments were not performed by the same raters across all participants.

It is hypothesised that individual MAS scores correlated with wrist flexor tension would vary significantly between raters. If so, that would support not only the use of objective quantitative devices but also more standardization of the MAS method for the wrist joint (see Section 5.2.5).

### **5.3.4. Opportunities for Further Research and Development:**

In addition to the objectives presented in Section 1.3, other research and development aims could be perused. Examples of these include, but are not limited to, the following:

- Once developed further, the device should be investigated for repeatability. One possible approach is to perform consecutive recordings using the device, and to analyse the results with a difference plot (Bland and Altman, 1986)
- The device could be used to analyse the effect of various available treatment paradigms being implemented in the field. Muscle tone of individuals could be assessed as they undergo various interventions to determine the relative effectiveness of each. This includes physical therapy as well as pharmacological interventions.
- The device could be developed to include functionality as a task-oriented therapy aide for hemiparetic patients. The results of the preliminary safety test confirm that the device can be controlled using EMG as an input. Development of this system may allow hemiparetic participants to undergo task-oriented therapy with assistance from the device, which has been shown to improve therapy outcomes (Smith et al., 1999; Bayona et al., 2005).

[This page is intentionally left blank]

## 6. Conclusions

The research presented in this thesis set out to prove the hypothesis that a robotic device for wrist flexor hypertonia that compensates for the effect of finger flexor torque at the wrist joint can provide more accurate wrist flexor muscle tone assessments than one that does not. The first objective was to design, construct and test a patient-safe device for the evaluation of wrist flexor muscle tone. The second objective was to compare the MAS score for volunteers with hand/wrist hypertonia against two methods of evaluation with the device - peak wrist force during passive wrist extension and estimated peak wrist flexor tendon tension using a biomechanical model.

The first objective was achieved, and a device capable of measuring wrist and finger force during joint manipulation was constructed, although opportunity for design improvement exists. Noise in the force recordings could be mitigated by implementation of a different actuation method. Similarly, design alterations such as adjustable range of motion would allow for more extensive testing – since there was a lack of volunteers that met the range of motion inclusion criteria.

The second objective showed that the methods of tone assessment with the device, using peak wrist force and peak wrist flexor tendon tension, both correlated strongly – and identically – to the MAS assessments. These findings suggest that the either method may provide acceptably accurate assessments of muscle tone. Furthermore, the results suggest that the influence of the finger flexor hypertonia on wrist joint torque is small relative to that from the wrist flexors themselves. Factors that should be considered, however, include the fact that the MAS score itself is unreliable, and that even the average of three MAS scores for each participant may not be a suitable proxy for hypertonia severity. Similarly, elements of the experimental protocol may have influenced the results (most notably, the non-uniform joint velocities for various tests). While these factors prevent definitive conclusions from being drawn, the results do, however, provide motivation for continued investigation.

[This page is intentionally left blank]

## References

- Albani, G., Cimolin, V., Galli, M., Vimercati, S., Bar, D., Campanelli, L., Gandolfi, R., Lombardi, R., Mauro, A., 2010. Use of Surface EMG for Evaluation of Upper Limb Spasticity During Botulinum Toxin Therapy in Stroke Patients. *Functional Neurology* Vol. 25, p103.
- Alibiglou, L., Rymer, W., Harvey, R., Mirbagheri, M., 2008. The Relation Between Ashworth Scores And Neuromechanical Measurements of Spasticity Following Stroke. *Journal of NeuroEngineering and Rehabilitation* 5.
- Ansari, N.N., Naghdi, S., Moammeri, H., Jalaie, S., 2006. Ashworth Scales are Unreliable for the Assessment of Muscle Spasticity. *Physiother Theory Pract* 22, 119-125.
- Barnes, M.P., Johnson, G.R., 2001. *Upper Motor Neurone Syndrome and Spasticity*. Cambridge University Press.
- Barnes, M.P., Kent, R.M., Semlyen, J.K., McMullen, K.M., 2003. Spasticity in Multiple Sclerosis. *Neurorehabil Neural Repair* 17, 66-70.
- Bayona, N., Bitenski, J., Salter, K., Teasell, R., 2005. The Role of Task-Specific Training in Rehabilitation Therapies. *Top Stroke Rehabil* 12, 58-65.
- Biodex Dynamometers [WWW Document], 2014. . URL <http://www.biodex.com/physical-medicine/products/dynamometers>
- Bizzini, M., Mannion, A., 2003. Reliability of a new, hand-held device for assessing skeletal muscle stiffness. *Clin Biomech (Bristol, Avon)* 18, 459-61.
- Blackburn, M., van Vliet, P., Mockett, S.P., 2002. Reliability of Measurements Obtained With the Modified Ashworth Scale in the Lower Extremities of People With Stroke. *Phys Ther* 82, 25-34.
- Bland, J., Altman, D., 1986. Statistical Methods for Assessing Agreement Between Two Methods of Clinical Measurement. *The Lancet* 327, 307-310.
- Bohannon, R.W., Smith, M.B., 1987. Interrater Reliability of a Modified Ashworth Scale of Muscle Spasticity. *Phys Ther* 67, 206-207.
- Boiteau, M., Malouin, F., Richards, C.L., 1995. Use of a Hand-held Dynamometer and a Kin-Com® Dynamometer for Evaluating Spastic Hypertonia in Children: A Reliability Study. *Phys Ther* 75, 796-802.
- Bovendeerd, T., Newman, M., Barker, K., Dawes, H., Minelli, C., Wade, D., 2008. The Effects of Stretching in Spasticity: A Systematic Review. *Archives of Physical Medicine and Rehabilitation* 89, 1395-1406.
- Brand, P., Hollister, A., 1999. *Clinical Mechanics of the Hand*, 3rd ed. Mosby.
- Brashear, A., Zafonte, R., Corcoran, M., Galvez-Jimenez, N., Gracies, J.-M., Gordon, M.F., McAfee, A., Ruffing, K., Thompson, B., Williams, M., Lee, C.-H., Turkel, C., 2002. Inter- and Intrarater Reliability of the Ashworth Scale and the Disability Assessment Scale in Patients with Upper-limb Poststroke Spasticity. *Archives of Physical Medicine and Rehabilitation* 83, 1349-1354.
- Burgar, C.G., Lum, P.S., Shor, P.C., Machiel Van der Loos, H.F., 2000. Development of Robots for Rehabilitation Therapy: the Palo Alto VA/Stanford Experience. *J Rehabil Res Dev* 37, 663-673.
- Damiano, D., Quinlivan, J., Owen, B., Payne, P., Nelson, K., Abel, M., 2002. What does the Ashworth scale really measure and are instrumented measures more valid and precise? *Dev Med Child Neurol*. 44, 112-8.
- Duncan, P.W., Propst, M., Nelson, S.G., 1983. Reliability of the Fugl-Meyer Assessment of Sensorimotor Recovery Following Cerebrovascular Accident. *PHYS THER* 63, 1606-1610.
- Fleuren, J., Voerman, G., Erren-Woltrers, C., Snoek, G., Rietman, J., Hermens, H., Nene, A., 2009. Stop Using The Ashworth Scale for the Assessment Of Spasticity. *Journal of Neurology, Neurosurgery & Psychiatry* 81, p46-53.
- Fridlund, A., Cacioppo, J., 1986. Guidelines for Human Electromyographic Research. *Psychophysiology* 23, 567-89.

- Gäverth, J., 2013. Development and Evaluation of a New Method to Objectively Measure Spasticity.
- Hesse, S., Werner, C., Pohl, M., Rueckriem, S., Mehrholz, J., Lingnau, M. I., 2005. Computerized Arm Training Improves the Motor Control of the Severely Affected Arm After Stroke A Single-Blinded Randomized Trial in Two Centers. *Stroke* 36, 1960-1966.
- Hogan, N., Krebs, H.I., Sharon, A., Charnnarong, J., 1995. Interactive robotic therapist.
- Horowitz, P., Hill, W., 1989. *The Art Of Electronics*, 2nd ed. Cambridge University Press.
- Ibrahim, I., Berger, W., Trippel, M., Dietz, V., 1993. Stretch-induced Electromyographic Activity and Torque in Spastic Elbow Muscles. Differential Modulation of Reflex Activity in Passive and Active Motor Tasks. *Brain* 116, 971-989.
- Jobin, A., Levin, M., 2000. Regulation of stretch reflex threshold in elbow flexors in children with cerebral palsy: a new measure of spasticity. *Developmental Medicine & Child Neurology* 42, 531-540.
- Juvinall, R., Marshek, K., 2011. *Fundamentals of Machine Component Design*, 5th ed. Wiley.
- Kollen, B.J., Lennon, S., Lyons, B., Wheatley-Smith, L., Scheper, M., Buurke, J.H., Halfens, J., Geurts, A.C.H., Kwakkel, G., 2009. The Effectiveness of the Bobath Concept in Stroke Rehabilitation. What is the Evidence? *Stroke* 40, e89-e97.
- Krebs, H.I., Ferraro, M., Buerger, S.P., Newbery, M.J., Makiyama, A., Sandmann, M., Lynch, D., Volpe, B.T., Hogan, N., 2004. Rehabilitation Robotics: Pilot Trial of a Spatial Extension for MIT-Manus. *Journal of NeuroEngineering and Rehabilitation* 1, 5.
- Krebs, H.I., Hogan, N., Aisen, M.L., Volpe, B.T., 1998. Robot-aided Neurorehabilitation. *Rehabilitation Engineering, IEEE Transactions on* 6, 75 -87.
- Krebs, H.I., Volpe, B.T., Williams, D., Celestino, J., Charles, S.K., Lynch, D., Hogan, N., 2007. Robot-Aided Neurorehabilitation: A Robot for Wrist Rehabilitation. *Neural Systems and Rehabilitation Engineering, IEEE Transactions on* 15, 327 -335.
- Lance, J.W., 1980. The Control of Muscle Tone, Reflexes, and Movement: Robert Wartenberg Lecture. *Neurology* 30, 1303-1313.
- Lehohla, P., 1998. Census 1996: Census in Brief. *Statistics South Africa*.
- Lehohla, P., 2003. Census 2001: Census in Brief. *Statistics South Africa*.
- Lehohla, P., 2012. Census 2011: Census in Brief. *Statistics South Africa*.
- Levin, M., Feldman, A., 1994. The role of stretch reflex threshold regulation in normal and impaired motor control. *Brain Res* 657, 23-30.
- Lindberg, P.G., Gaverth, J., Islam, M., Fagergren, A., Borg, J., Forssberg, H., 2011. Validation of a New Biomechanical Model to Measure Muscle Tone in Spastic Muscles. *Neurorehabilitation and Neural Repair* 25, 617-625.
- Logan, L.R., 2011. Rehabilitation Techniques to Maximize Spasticity Management. *Top Stroke Rehabil* 18, 203-211.
- Loren, G., Lieber, R., 1995. Tendon Biomechanical Properties Enhance Human Wrist Muscle Specializaion. *Journal of Biomechanics* 28, 791-9.
- Malhotra, S., Pandyan, A.D., Day, C.R., Jones, P.W., Hermens, H., 2009. Spasticity, an Impairment That is Poorly Defined and Poorly Measured. *Clin Rehabil* 23, 651-658.
- Marieb, E.N., Hoehn, K., 2006. *Human Anatomy & Physiology*, 7th ed. Benjamin Cummings.
- Matweb Material Property Data Website [WWW Document], 2014. . URL <http://www.matweb.com/>
- Mirbagheri, M., Barbeau, H., Kearney, R., 2000. Intrinsic and reflex contributions to human ankle stiffness: variation with activation level and position. *Exp Brain Res* 4, 423-36.
- Mirbagheri, M., Kearney, R., Barbeau, H., 1998. Stretch reflex behavior of spastic ankle under passive and active conditions. *Proceedings of the 20th Annual International Conference of the IEEE Engineering in Medicine and Biology Society* 20.
- Mutlu, A., Livanelioglu, A., Gunel, M., 2008. Reliability of Ashworth and Modified Ashworth Scales in Children with Spastic Cerebral Palsy. *BMC Musculoskeletal Disorders* 9, 44.
- NeuroFlexor Online Brochure [WWW Document], 2012. . URL [http://www.aggeromedtech.com/wp-content/uploads/2011/06/NeuroFlexor-brochure\\_090312.pdf](http://www.aggeromedtech.com/wp-content/uploads/2011/06/NeuroFlexor-brochure_090312.pdf)
- Paci, M., 2003. Physiotherapy Based on the Bobath Concept for adults with Post-stroke Hemiplegia: a Review of Effectiveness Studies. *J Rehabil Med* 35, 2-7.

- Pandyan, A., Gregoric, M., Barnes, M., Wood, D., Van Wijck, F., Burridge, J., Hermens, H., Johnson, G., 2005. Spasticity: Clinical Perceptions, Neurological Realities and Meaningful Measurement. *Disabil Rehabil* 27, p2-6.
- Pandyan, A.D., Johnson, G.R., Price, C.I.M., Curless, R.H., Barnes, M.P., Rodgers, H., 1999. A Review of the Properties and Limitations of the Ashworth and Modified Ashworth Scales as Measures of Spasticity. *Clinical Rehabilitation* 13, 373-383.
- Pizzi, A., Carlucci, G., Falsini, C., Verdesca, S., Grippo, A., 2005. Evaluation of Upper-limb Spasticity After Stroke: A Clinical and Neurophysiologic Study. *Archives of Physical Medicine and Rehabilitation* 86, 410-415.
- Prange, G.B., Jannink, M.J.A., Groothuis-Oudshoorn, C.G.M., Hermens, H.J., IJzerman, M.J., 2006. Systematic Review of the Effect of Robot-aided Therapy on Recovery of the Hemiparetic arm After Stroke. *The Journal of Rehabilitation Research and Development* 43, 171.
- Riener, R., Nef, T., Colombo, G., 2005. Robot-aided Neurorehabilitation of the Upper Extremities. *Medical and Biological Engineering and Computing* 43, 2-10.
- Rizzo, M.A., Hadjimichael, O.C., Preiningerova, J., Vollmer, T.L., 2004. Prevalence and Treatment of Spasticity Reported by Multiple Sclerosis Patients. *Multiple Sclerosis* 10, 589-595.
- Sherwood, A.M., Graves, D.E., Priebe, M.M., 2000. Altered Motor Control and Spasticity After Spinal Cord Injury: Subjective and Objective Assessment. *J Rehabil Res Dev* 37, 41-52.
- Sivan, M., O'Connor, R., Makower, S., Levesley, M., Bhakta, B., 2011. Systematic Review of Outcome Measures Used in the Evaluation of Robot-assisted Upper Limb Exercise in Stroke. *Journal of Rehabilitation Medicine* 43, 181-189.
- Smedes, F., van der Salm, A., Koel, G., Oosterveld, F., 2014. Manual Mobilization of the Wrist. A Pilot Study in the Rehabilitation of the Chronic Hemiplegic Hand. *Journal of Hand Therapy*.
- Smith, G., Silver, K., Goldberg, A., Macko, R., 1999. "Task-Oriented" Exercise Improved Hamstring Strength and Spastic Reflexes in Chronic Stroke Patients 2112-2118.
- Sommerfeld, D.K., Eek, E.U.-B., Svensson, A.-K., Holmqvist, L.W., von Arbin, M.H., 2004. Spasticity After Stroke: Its Occurrence and Association With Motor Impairments and Activity Limitations. *Stroke* 35, 134-139.
- Stevenson, V., Thompson, A.J., 2006. *Spasticity Management*. CRC Press.
- Takahashi, C.D., Der-Yeghiaian, L., Le, V., Motiwala, R.R., Cramer, S.C., 2008. Robot-based Hand Motor Therapy After Stroke. *Brain* 131, 425-437.
- Takahashi, C.D., Der-Yeghiaian, L., Le, V.H., Cramer, S.C., 2005. A Robotic Device for Hand Motor Therapy After Stroke, in: 9th International Conference on Rehabilitation Robotics, 2005. ICORR 2005. Presented at the 9th International Conference on Rehabilitation Robotics, 2005. ICORR 2005, pp. 17 - 20.
- The OpenEEG project [WWW Document], 2013. . URL <http://openeeg.sourceforge.net/>
- Thibaut, A., Chatelle, C., Ziegler, E., Bruno, M.-A., Laureys, S., Gosseries, O., 2013. Spasticity After Stroke: Physiology, Assessment and Treatment. *Brain Injury* 27, 1093-1105.
- Toth, A., Fazekas, G., Arz, G., Jurak, M., Horvath, M., 2005. Passive Robotic Movement Therapy of the Spastic Hemiparetic Arm with REHAROB: Report of the First Clinical Test and the Follow-up System Improvement. *Proceedings of the 2005 IEEE 9th International Conference on Rehabilitation Robotics*.
- Volpe, B. t., Krebs, H. i., Hogan, N., Edelsteinn, L., Diels, C. m., Aisen, M. l., 1999. Robot Training Enhanced Motor Outcome in Patients with Stroke Maintained Over 3 years. *Neurology* 53, 1874-1874.
- Volpe, B.T., Krebs, H.I., Hogan, N., 2001. Is Robot-aided Sensorimotor Training in Stroke Rehabilitation a Realistic Option? *Curr. Opin. Neurol.* 14, 745-752.
- Watkins, C., Leathley, M., Gregson, J., Moore, A., Smith, T., Sharma, A., 2002. Prevalence of Spasticity Post Stroke. *Clin Rehabil* 16, p515-522.

[This page is intentionally left blank]

# Appendix A – Device Design and Manufacture

## A.1. Device Structure

The device consisted of various interacting elements. These included:

- Main structural components – Plastic or aluminium. These connect, locate and support the motors and other components and provide a framework and base upon which to stand
- Force sensing elements – Aluminium. Fitted with strain gauges for the purposes of measuring load applied to them (i.e. force transducers).
- Interface elements – Aluminium. These directly interface with the participant, lined with foam rubber for comfort

Elements are illustrated in Figure A.1, which illustrates a partially exploded view of the device.

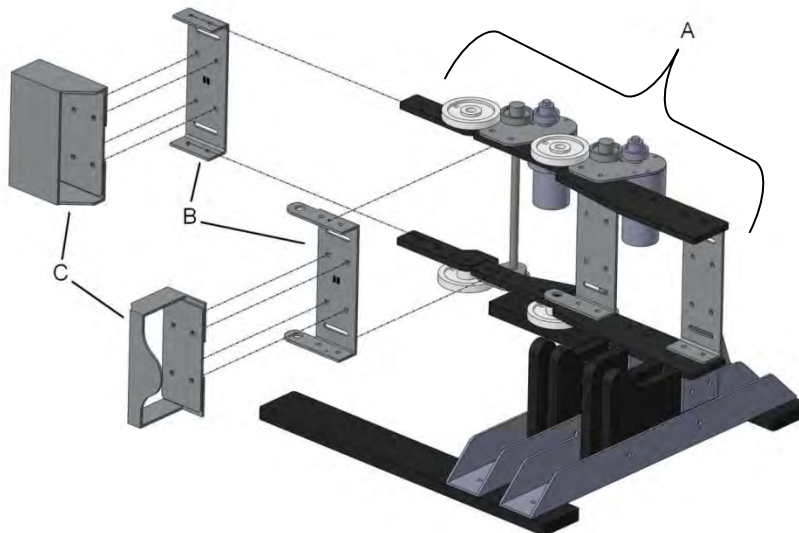


**Figure A.1** Partially exploded view of a CAD model of the device, illustrating interactions between the main structural elements (A), force sensing elements (B), and interface elements (C).

## A.2. Ergonomic Elements

The device was designed to interface with the hand and forearm (see Figure A.2), so ergonomics were a consideration.

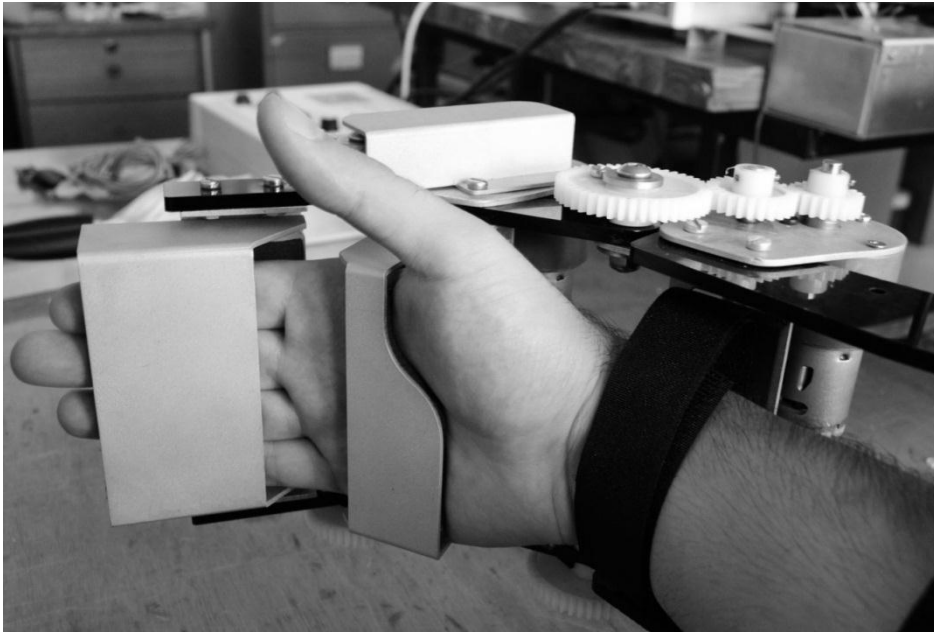


**Figure A.2** Photograph showing the device with a participant's hand secured (Reproduced from Figure 2.3)

Points for consideration were:

- The two degrees of freedom (rotation at the wrist and MCP joints) necessitated independently moving sets of interface elements.
- Force was transmitted from the interface elements to the force transducer components by means of four M4 bolts on each assembly (see Figure A.3). Spacer nuts were included to ensure no unintended contact between these components.
- The interface elements were modularly separate from the force component elements. This allowed for potential changes to be more easily implemented. This prevented the need for reapplication of the strain gauges following an interface element design revision.
- All the interface components were fabricated using folded 2 mm sheet aluminium (grade 1050-H14).
- All surfaces on the device that interface with the participant were coated with foam rubber.
- Adjustments for participant hand size were not included in this prototype design. Such adjustments are recommended to be added to future versions of the device (see Section 5.3.1).

### A.3. Design of the Force Transducer Elements

Two identical force transducer elements were required. One measured the force applied to the finger interface elements and another to the wrist elements (see Figure A.2). These consisted of folded aluminium components, referred to as force sensing elements, with strain gauges attached.

All other elements could be designed with large safety factors to ensure that they would not fail. The force transducer elements, however, were required to have thin gauge sections to allow for measurable strains of relatively small forces. These elements were designed in conjunction with the corresponding strain gauge amplification circuitry (see Appendix B).

The force sensing elements were made from 1050-H14 sheet aluminium. Calculations showed that 2mm gauge sections were appropriate (see sections A.3.1 and A.3.2).

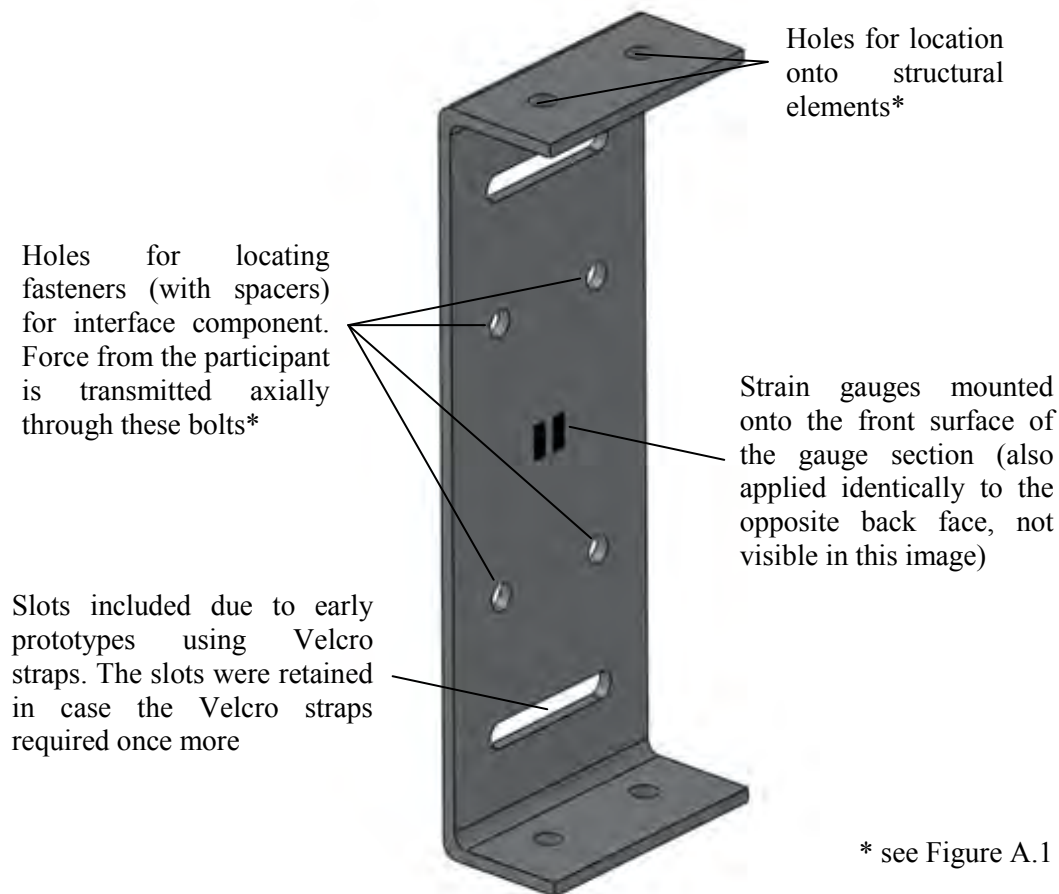


**Figure A.3** CAD model of a force sensing element indicating relevant design features

The designs of the wrist and finger transducer elements were very similar (see Figure A.3). The design consisted of a flat piece of sheet metal, with folded tabs at the ends for location to the structural elements. The interface elements were attached using bolts and spacers nearer the middle. Strain gauges were attached at the centre, on the front and back surfaces of the gauge section. These were wired into a full bridge configuration such that the bending strain in the gauge section of the material was measured.

### A.3.1. Calculation of Force Sensing Element Material Thickness

The initial estimate for the peak force from the participant would be up to 30 N, since participants for the study would have from mild to moderate hypertonia of the hand and/or wrist. Participants with more severe hypertonia were excluded from the study. The basic calculations presented here were confirmed with finite element modelling (see Section A.4) as well as empirical calibration (see Section A.3.2)

The applied force through the four bolts could be represented in cross section by a pair of equal 15 N point forces. Since the body is assumed to be in static equilibrium, and due to symmetry, the values of the reaction forces are also 15 N each. The element could be modelled as a simple beam with applied forces from the interface element, and reaction forces from the structural elements. The shear force and bending moment distributions in the part could be derived from the free body diagram (see Figure A.4).

The peak bending moment (occurring in the gauge section) was calculated to be 0.2625 N.m. This value was used in the flexure formula to calculate the bending stress in a beam at those points (Juvinal and Marshek, 2011):

$$\sigma = \frac{M \times y}{I}$$

(Equation A.1)

„M“ is the bending moment in the beam at the point of interest (in this case, the gauge section), „σ“ is the bending stress at this point, „y“ is the distance from the neutral axis and „I“ is the second moment of area about the neutral axis. Equation A.1 shows that the stress is proportional to both the bending moment and the distance from the neutral axis. The material thickness, still to be determined, was represented by the symbol „h“.

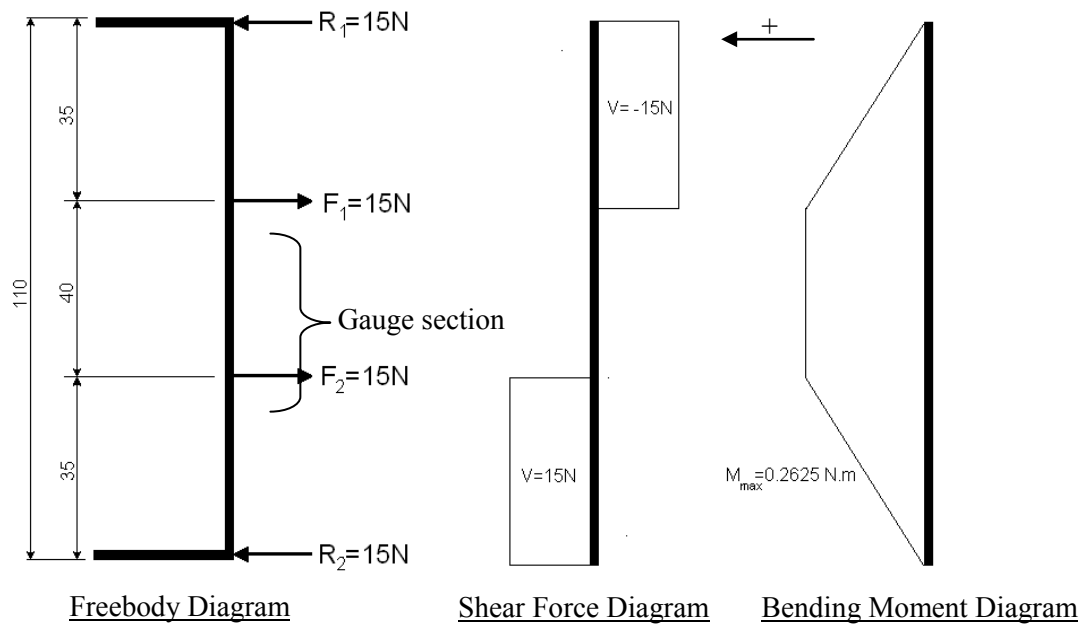


**Figure A.4** Free body diagram, shear force diagram and bending moment diagram of the force sensing element. Note that the maximum bending moment (located in the gauge section) is 0.2625 N.m.

The second moment of area for a rectangular cross section could be expressed in terms of parameter  $h$  as follows. The width of the gauge section is represented by „ $b$ “:

$$\begin{aligned}
 I &= \frac{1}{12}bh^3 \\
 &= \frac{1}{12}(0.04)h^3 \\
 &= 0.0033h^3 \text{ m}^4
 \end{aligned}$$

(Equation A.2)

Using the calculated maximum bending moment in the beam (see Figure A.4) and by substituting Equation A.2 into Equation A.1, the flexure formula could be rewritten as follows:

$$\sigma = \frac{M \times \frac{h}{2}}{\frac{1}{12}bh^3}$$

$$\begin{aligned}
&= \frac{0.2625 \times \frac{h}{2}}{\frac{1}{12}(0.04)h^3} \\
&= \frac{39.375}{h^2} Pa
\end{aligned}$$

(Equation A.3)

If  $h$  was selected to be 2mm (an available standard thickness for 1050-H14 aluminium), then the stress in the beam at the gauge section (see Figure A.4) could be calculated as:

$$\begin{aligned}
\sigma &= \frac{39.375}{0.002^2} \\
&= 9.84 MPa
\end{aligned}$$

(Equation A.4)

The yield strength of 1050-H14 sheet aluminium is specified by manufacturers to be 103 MPa (“Matweb,” 2014). The safety factor was 10.5, which was more than sufficient. It was required, however, to confirm that the strain „ $\varepsilon$ ” was high enough to allow measurement with sufficient resolution. 1050-H14 aluminium has a modulus of elasticity „ $E$ ” of 69.0 GPa, so the strain could be calculated using the following relationship between stress and strain:

$$\begin{aligned}
\varepsilon &= \frac{\sigma}{E} \\
&= \frac{9.84 MPa}{69.0 GPa} \\
&= 142.7 \mu\varepsilon
\end{aligned}$$

(Equation A.5)

The strain gauge amplification circuits had a transfer function relating strain to output voltage as follows (see Section B.4):

$$V = -1934.29 \times \varepsilon$$

(Equation A.6)

Note that this was only valid while the bending stress due to loading was within the linear range (i.e. the material was still loaded within the elastic region). For these experiments, however, the maximum expected loading was below that required to induce any plastic strains, as evidenced by the large safety factor. At the expected maximum load, the measured voltage from the strain gauge amplifier circuit was calculated to be 276.0 mV. This range was large enough to be measured with sufficient resolution but not so large as to risk saturating the data logger. 1050-H14 sheet aluminium with thickness of 2mm was deemed appropriate.

### **A.3.2. Force Transducer Calibration**

Many factors could have contributed to a deviation between real-world behaviour and the model used in section A.3.1. These include, but are not limited to:

- Non-uniform application of force to the interface element
- Stresses in the force sensing element due to other sources than the applied force, (e.g. fasteners used to locate the interface components or residual stresses from manufacturing procedures)
- Uncertainty in the accuracy of components used in the amplifier electronics (e.g. from the exact value of the external resistor used to select the gain of the amplifier)

As such, the system calibration was performed, empirically relating applied force and voltage output (see Figure A.5 for a sketch of the calibration setup). A simple system using a rope, pulley and weights was used to apply a known force to a harness attached to the interface element. The process was repeated in a similar fashion for flexion and extension of the finger and wrist force sensing elements.

The step-by-step methodology for this calibration was as follows:

1. The device finger and wrist joints were at  $0^\circ$  (i.e. aligned straight).
2. The device was positioned appropriately and a harness attached such that the tension force applied through the rope was in the appropriate direction (i.e. it was required be normal to the surface on which the strain gauges were attached).
3. The rope from the harness was run over the pulley (the cradle was not attached yet).
4. The offset on the strain gauge amplifier electronics board was adjusted until the plot of the force reading in the PC-based GUI showed approximately 2V (mid-range in the 0 – 5V system) to allow negative force recordings. This offset would later be removed in software.

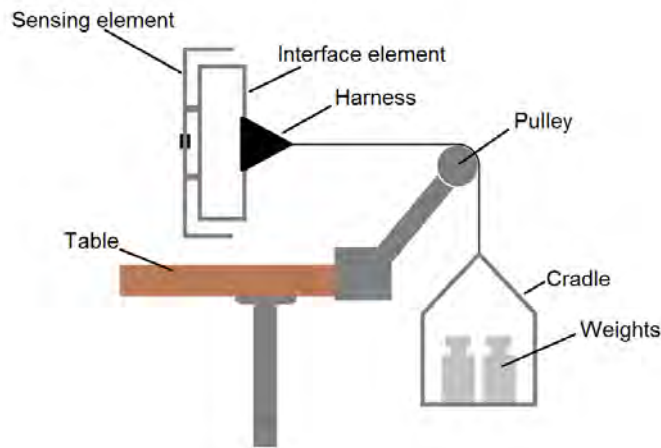


**Figure A.5** Sketch of the calibration apparatus illustrating how a known force was applied to the interface element from weights via a rope over a pulley.

5. The recording was initialized in the GUI. This was referred to as time  $t=0$  seconds.
6. No action was taken for 30 seconds, to establish a stable baseline reading.
7. At  $t=+30s$ , the cradle (weighing 0.7 kg) was attached to the end of the rope. The cradle was pressed down gently then released. This created a “spike” in the readings which was helpful for data processing later to distinguish time steps.
8. Again, no action was taken for 30 seconds for the reading to stabilize and to provide a time interval for calculation of an average value.
9. At  $t=+60seconds$ , a weight was placed into the cradle, and again the cradle was briefly pressed down gently to create a spike in the readings.
10. The total mass of the weights applied were recorded.
11. Again, a 30 second pause was observed to allow readings to stabilize and to provide a time interval for acquisition of an average value.
12. Steps 10, 11 and 12 were repeated until all weights had been applied (a total weight of 4.5 kg).
13. Using 30 second time steps in a similar fashion to the loading procedure, the weights were gradually removed until no weights remained.
14. When no weights remained, a further 30 second pause was observed to obtain a closing baseline value.
15. The recording was terminated.
16. This process was repeated for finger flexion, finger extension, wrist flexion and wrist extension.

Plots of the recorded calibration data for the wrists and fingers can be seen in Figure A.6. The data have been “zeroed”, such that they all begin at the baseline for easy comparison.

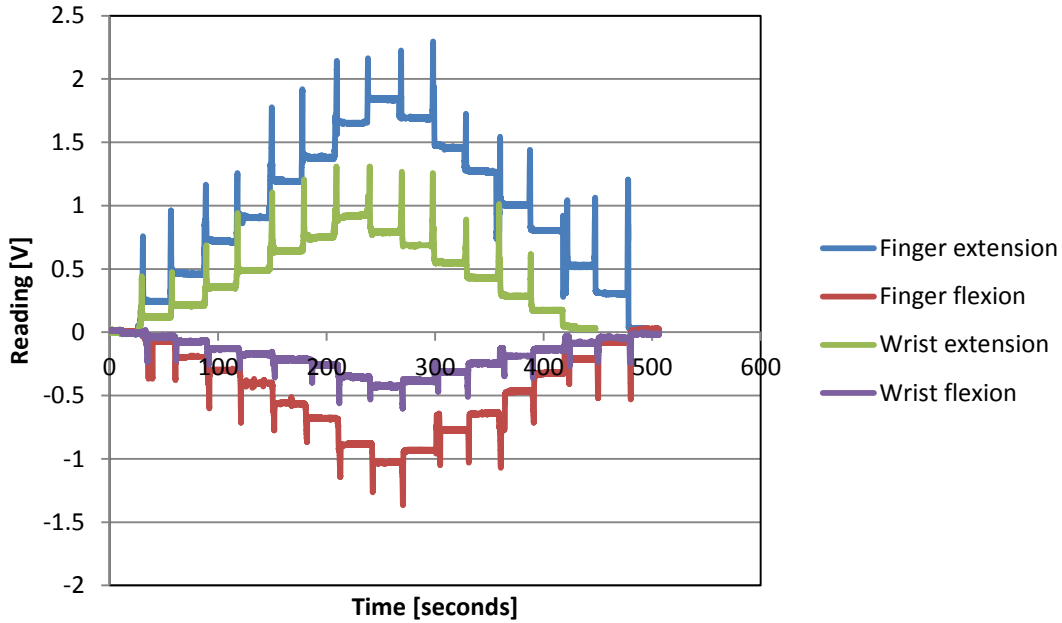


**Figure A.6** Plots of raw data collected during calibration of the force measurement system.

The calibration data was processed according to the following procedure, which was performed in Microsoft Excel 2010:

1. The data was zeroed by subtracting the average value of the data collected during the first 25 seconds of recording.
2. The spikes in the force reading associated with a change in loading were identified. The recorded data was averaged over the time interval from 15 seconds to 25 seconds after each weight was applied (i.e. a 10 second interval). These averages were manually checked to ensure that the signal had in fact stabilised and that no unwanted disturbances were present (such as due to the table being bumped). For each weight step, the average recorded voltage was noted as well as the corresponding weight applied.
3. The noted weights and corresponding voltages were plotted. A linear trend line was applied, which uses the least squares method. Since the data was zeroed before processing, the trend line was constrained to pass through the origin. The  $R^2$  value was also calculated (see Figure A.7 and Figure A.8) as a measure of the quality of the fit. Note that differences between the voltage outputs for loading and unloading curves were small. This indicated that hysteresis in the recording system was negligible.

### Finger Force Transducer Calibration Data

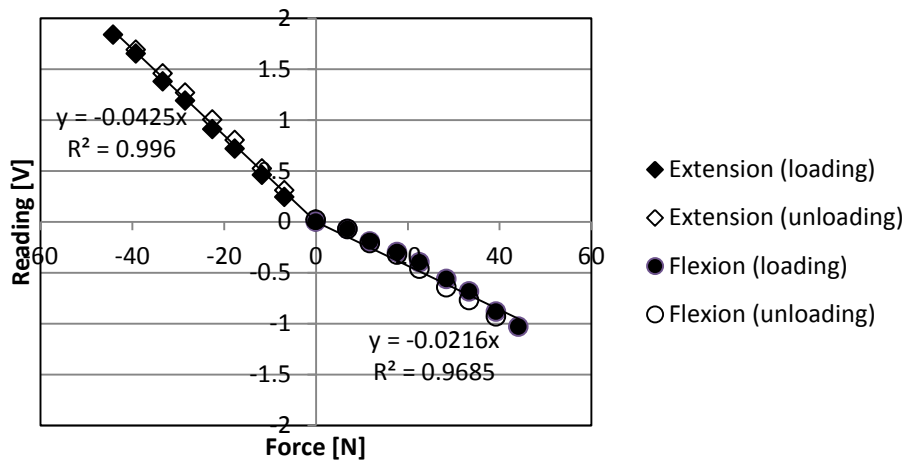


**Figure A.7** Plots of processed calibration data for the finger force transducers, indicating the relationship correlation between applied force and voltage from the strain gauge circuitry. Shown on the graph are the equations of the linear trend lines for flexion and extension, and the  $R^2$  values to indicate the quality of the trend line fit.

### Wrist Force Transducer Calibration Data

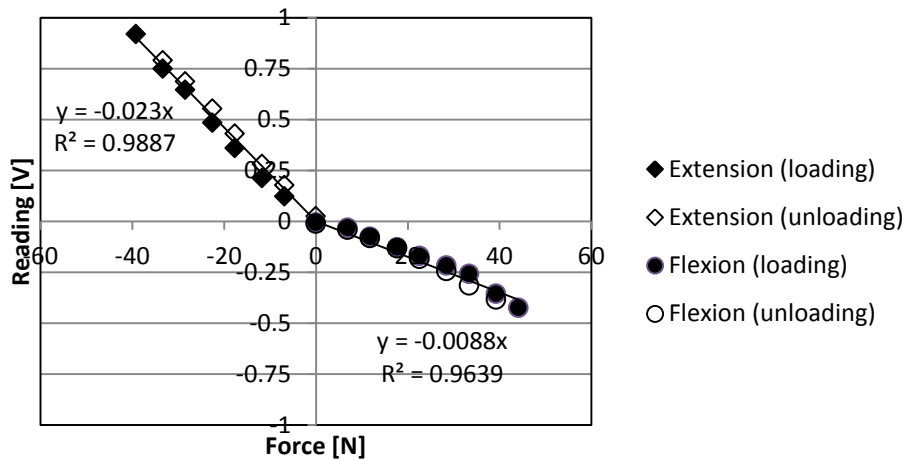


**Figure A.8** Plots of processed calibration data for the wrist force transducer, indicating the relationship correlation between applied force and voltage from the strain gauge circuitry. Shown on the graph are the equations of the linear trend lines for flexion and extension, and the  $R^2$  values to indicate the quality of the trend line fit.

## **A.4. Finite Element Analysis of Selected Components**

A simple finite element analysis (FEA) of the force sensing element components was performed to confirm design calculations. Furthermore, some certain structural components were modelled where safety was concerned (i.e. hyperextension blocks – see Section 2.2.3). This section details the process FEA analyses.

The device was designed using the SolidWorks 2011 x64 edition computer aided design (CAD) package. The program included the Simulation add-on, which was used to implement the required FEA. As with all FEA models, parameters such as material properties, part fixtures/restraints and loading were modelled. Global and site-specific controls for mesh generation of a part were applied and were analysed to ensure that the mesh did not significantly affect the results of the analysis. Each part was modelled with three meshes with incrementing coarseness. The results from the three models were compared to each other to confirm reliability.

There were three components that were modelled under expected loading: The finger force transducer sensing element as well as proximal and distal structural components.

### **A.4.1. Finite Element Analysis of the Distal Force Sensing Element**

FEA was used to model the expected peak stress and strain in the distal force sensing element to ensure that they comply with the calculations in section A.3.1. Since the geometry and loading of the wrist and finger force sensing elements were similar, only one was modelled.

The loading consisted of forces applied at the bolt holes where the interface element would be attached. The restraints were applied at the holes on the folded tabs where the component located onto the structural elements (see Figure A.10). Note that the slots were included as features of the design due to earlier versions including Velcro straps. The slots were retained in case these Velcro straps were once again required.

The part was analysed with two loading configurations: with the force applied in the positive and negative directions. This was to check that the peak stresses would be of the same magnitude, but with alternating directions (compressive and tensile).

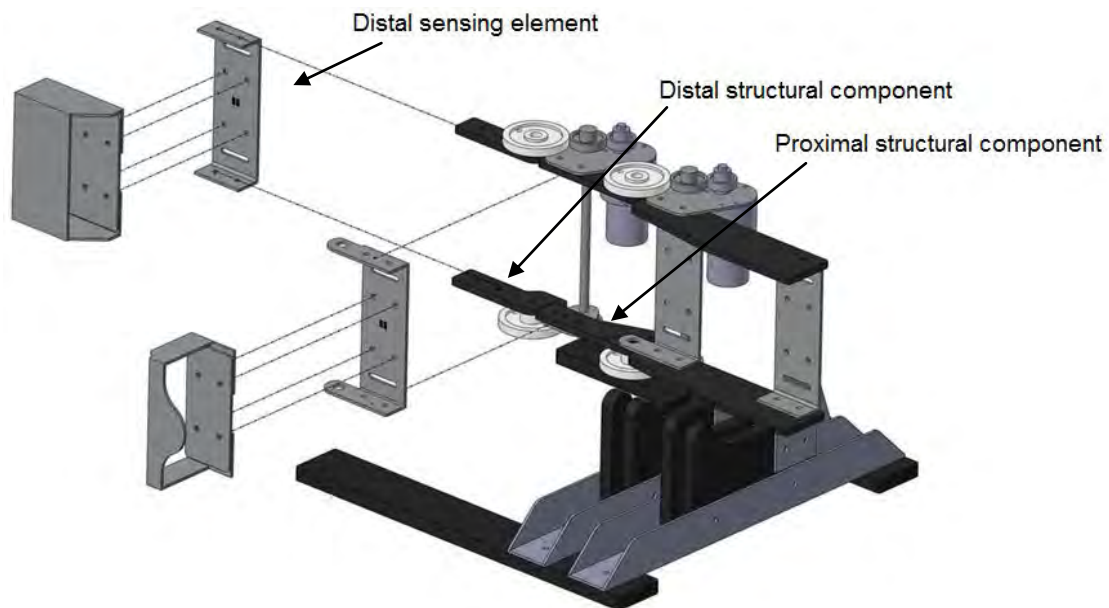
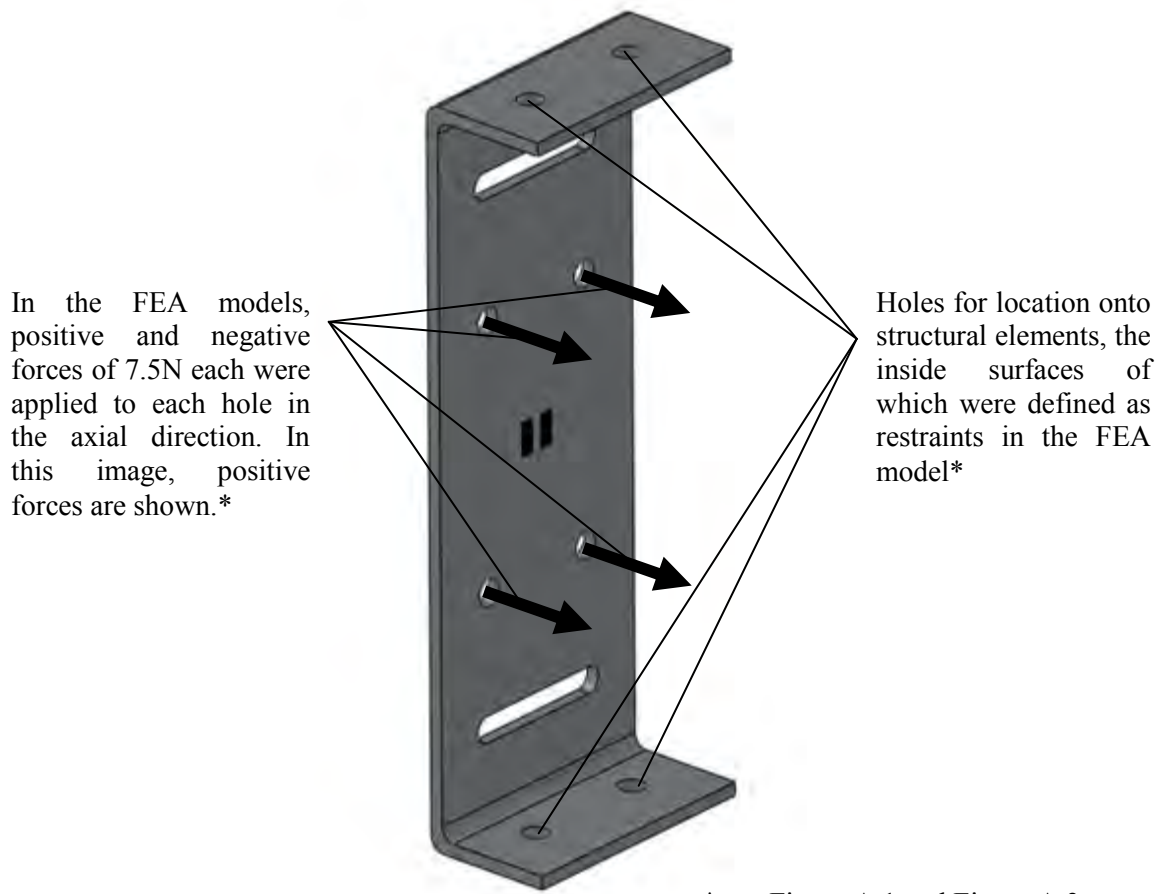


**Figure A.9** CAD model of a partially exploded assembly indicating components that were analysed using FEA models

As was stated in Section A.3.1, an expected applied load of 30N from the participant was estimated. In the model, this load was transmitted to the force sensing elements via the bolts in the holes surrounding the strain gauges (see Figure A.10). The FEA model was constructed such that the 30N force applied by the participant would be distributed evenly throughout all four bolt holes (7.5N each). Fixed geometry restraints were applied on the holes on the top and bottom and bottom folded tabs of the force sensing elements, effectively locking the inner surfaces of these holes in space.

The global element size of the primary model was set to 2mm. The part was also analysed with the element size setting set to 50% and 150% of the initial size (1mm and 3mm respectively). This was to confirm that the mesh selection had little effect on the outcomes of the model. Mesh controls were also applied such that the regions surrounding the slots and holes had a finer mesh, since stress concentrations effects near these areas were expected to cause steeper stress gradients. A finer mesh was required to accurately resolve the stress in these regions. Six models were created in total - two loading configurations (for positive and negative force directions) with three mesh coarseness settings each (see Figure A.11).



In the FEA models, positive and negative forces of 7.5N each were applied to each hole in the axial direction. In this image, positive forces are shown.\*

Holes for location onto structural elements, the inside surfaces of which were defined as restraints in the FEA model\*

\* see Figure A.1 and Figure A.3.

**Figure A.10** CAD model of a force sensing element, illustrating the loading and restraints applied in the FEA model

The outcomes of the models showed that the peak stressed did not vary considerably between models. The stress distributions on the surface of the part for the various models are illustrated in Figure A.12 to Figure A.17. The highest peak Von Mises stress observed was 24.11 MPa (see table A.1 and A.2), occurring in the 3mm element (secondary) models, identical for both force directions. The lowest peak stress was 23.68 MPa, again occurring identically in the secondary models (1mm element size in this case). The yield strength of 1050H14 sheet aluminium, as specified by manufacturers, is 103 MPa. The lowest safety factor for all models was 4.27. Note that this safety factor is lower than that predicted by the calculation in Section A.3.1, since this model accounts for factors such as stress concentration effects at the slots. Despite being lower, this safety factor is still acceptable.

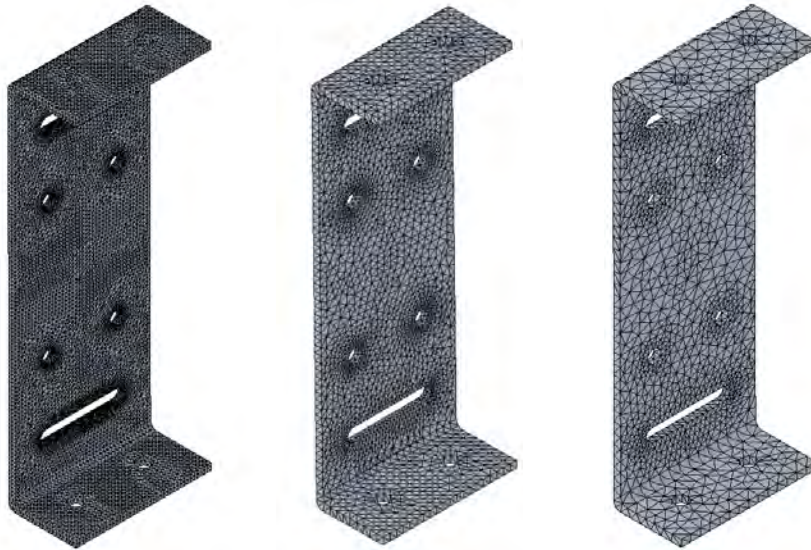


**Figure A.11** CAD models of the force sensing element illustrating the meshes used in the FEA models: 2mm mesh used as the primary model (centre), and the 1mm mesh (left) and 3mm mesh (right) used to confirm the results.

The safety factor was not the only design consideration for this component: the strain in the location of the strain gauges was also important. The “probe” feature in the FEA software was used to obtain an estimate of the strain that the strain gauges would experience. Only the strain in the vertical direction was probed, rather than principle or effective strains, since the strain gauges were only sensitive in that direction. The average strains probed in the region of the front and back gauges (as well as other relevant numerical data) are presented in table A.1 and table A.2.

**Table A.1** Numerical results from FEA model of force sensing element with positive forces applied. Note that the stresses are identical but the direction of the strains is reversed when compared with Table A.2.

Model type	Global element size [mm]	Mesh control element size [mm]	Peak Von Mises stress [MPa]	Change in Von Mises stress from primary model	Strain in outside sensor [ $\mu\epsilon$ ]	Strain in inside sensor [ $\mu\epsilon$ ]
Secondary	1	0.5	23.68	-1.1%	-107.0	93.9
Primary	2	1	23.94	-	-106.9	93.6
Secondary	3	1.5	24.11	0.7%	-106.2	92.8

**Table A.2** Numerical results from FEA model of force sensing element with negative forces applied. Note that the stresses are identical but the direction of the strains is reversed when compared with Table A.1.

Model type	Global element size [mm]	Mesh control element size [mm]	Peak Von Mises stress [MPa]	Change in Von Mises stress from primary model	Strain in outside sensor [ $\mu\epsilon$ ]	Strain in inside sensor [ $\mu\epsilon$ ]
Secondary	1	0.5	23.68	-1.1%	107.0	-93.9
Primary	2	1	23.94	-	106.9	-93.6
Secondary	3	1.5	24.11	0.7%	106.2	-92.8

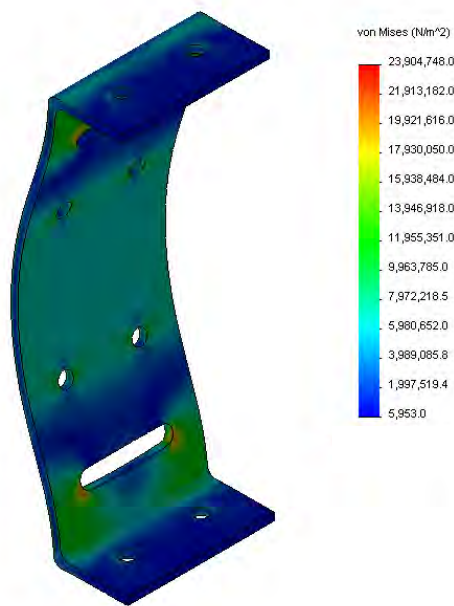


**Figure A.12** FEA model of the force sensing element with negative forces applied and with a mesh element size of 2mm. The image indicates the Von Mises stress distribution results of the FEA model (with exaggerated deformation). The legend provides Von Mises stress results measured in  $N.m^{-2}$  (i.e. pascals). This was the primary model, validated by the secondary models in Figure A.13 and Figure A.14.

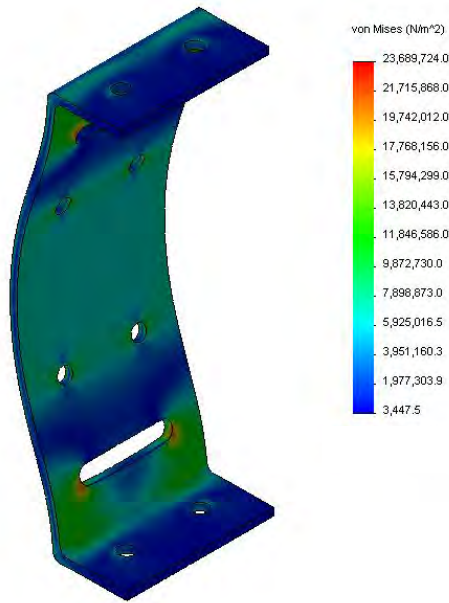


**Figure A.13** FEA model of the force sensing element with negative forces applied and with a mesh element size of 1mm. The image indicates the Von Mises stress distribution results of the FEA model (with exaggerated deformation). The legend provides Von Mises stress results measured in  $\text{N.m}^{-2}$  (i.e. pascals). This was a secondary model, used to validate the primary model in Figure A.12.

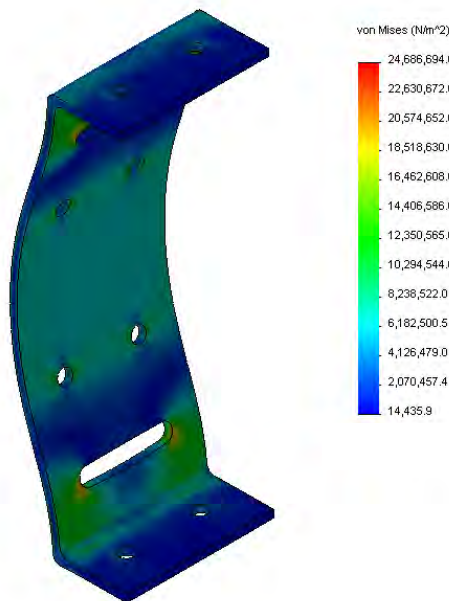


**Figure A.14** FEA model of the force sensing element with negative forces applied and with a mesh element size of 3mm. The image indicates the Von Mises stress distribution results of the FEA model (with exaggerated deformation). The legend provides Von Mises stress results measured in  $\text{N.m}^{-2}$  (i.e. pascals). This was a secondary model, used to validate the primary model in Figure A.12.

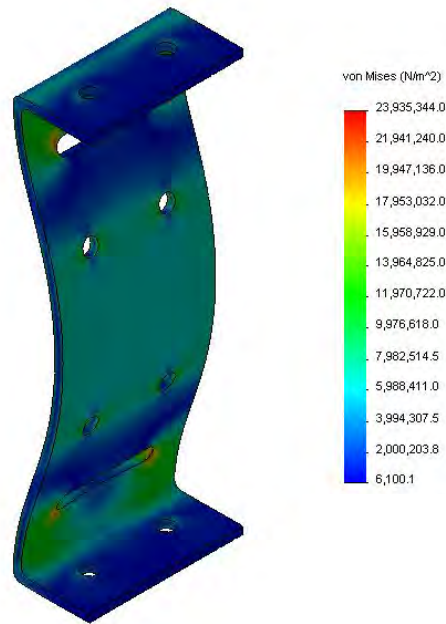


**Figure A.15** FEA model of a force sensing element with positive forces applied and with a mesh element size of 2mm. The image indicates the Von Mises stress distribution results of the FEA model (with exaggerated deformation). The legend provides Von Mises stress results measured in  $\text{N.m}^{-2}$  (i.e. pascals). This was the primary model, validated by the secondary models in Figure A.16 and Figure A.17.

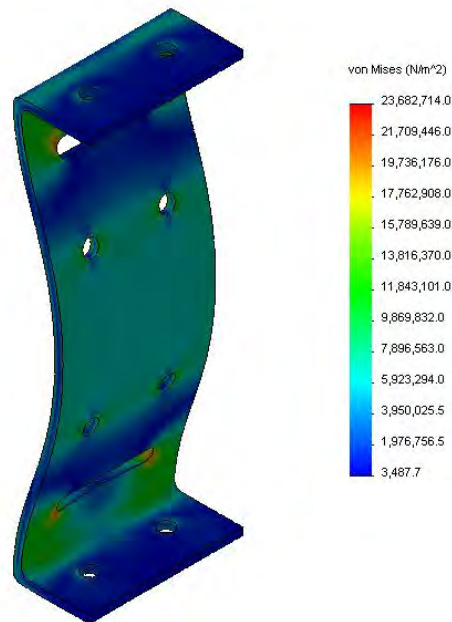


**Figure A.16** FEA model of the force sensing element with positive forces applied and with a mesh element size of 1mm. The image indicates the Von Mises stress distribution results of the FEA model (with exaggerated deformation). The legend provides Von Mises stress results measured in  $\text{N.m}^{-2}$  (i.e. pascals). This was a secondary model, used to validate the primary model in Figure A.15.

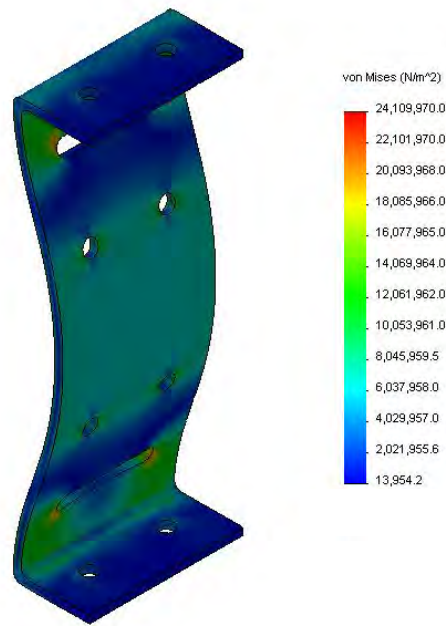


**Figure A.17** FEA model of the force sensing element with positive forces applied and with a mesh element size of 3mm. The image indicates the Von Mises stress distribution results of the FEA model (with exaggerated deformation). The legend provides Von Mises stress results measured in  $\text{N.m}^{-2}$  (i.e. pascals). This was a secondary model, used to validate the primary model in Figure A.15.

Note that the deviation of average stresses between the primary and secondary models was minor (see tables A.1 and A.2), indicating that the mesh had a negligible effect on the outcomes of the model. It could be assumed that the results were reliable, especially considering the large safety factor.

Also note that, as expected, the orientation of the applied force had little effect on the magnitude of the stresses and strain in the part. While there were differences between the outcomes of FEA model and those of the calculations in section A.3.1, they were probably due to simplifying assumptions made in each case. The FEA model was based on a geometrically accurate depiction of the final component, whereas the manual calculations did not take into account the effects of certain component design features. For example, in the manual calculations, stress concentration factors caused by the holes and slots were ignored. To a lesser extent, the restraint type may have been the cause of incongruence between the two analyses. The restraints used in the FEA model essentially locked the relevant design feature in space, disallowing any translation or rotation. Bending moments at the restraint sites were included in the models. In the calculations in section A.3.1, these were ignored.

The relative agreement between the strains predicted by the FEA model and the calculations was an indicator that the strains predicted in the later were reliable. The strain in the gauge section as observed in the FEA models were approximately  $100 \text{ } \mu\text{m}$ . Using Equation A.6 we can estimate that the corresponding output of the strain gauge circuitry would be 193 mV. In section A.3.1, an output voltage of 276.0 mV was predicted.

Based on these models, the parts were fabricated as described. Once construction had been completed, the calibration data (Figure A.7 and Figure A.8) indicated that the force measurement circuits were generally more sensitive than predicted. At 30N of loading, the calibration predicted that the output would be up to 1.275 V depending on the sensing element and the direction of loading. This could be due to many factors such as uncertainty in the amplification circuitry, inaccuracy in the modelling due to assumptions, etc. This was not a problem, however, since the output voltage varied linearly with applied load and the peak voltage would not saturate the recording instrumentation.

#### **A.4.2. Finite Element Analysis of Structural Elements**

The structural components involved in the mechanical stops were also modelled with FEA (see Figure 2.8). An approach was applied similar to that for the force sensing element (see Section A.4.1). It was decided to design the component conservatively and use FEA to confirm that the safety factor was sufficiently large.

The structural components of interest interfaced with other structural elements at the hinges, the mechanical stops, the force sensing elements and the gears (see Figure A.9). The mechanical stops that guard against hyperextension were likely to experience the highest stress. As such, the scenario under which full expected load would be applied to these features was modelled: simultaneous torque from the motor and that due to applied force from a participant in the negative direction (i.e. extension). While this was an unlikely event, the device was required to be modelled under worst-case scenarios.

In both the proximal and distal component models, restraints were selected to be at the hinge point around which the component rotated as well as the contact surface of the mechanical stop (see Figure A.18). Fixed hinge and sliding/roller type bearing restraints were applied at these features respectively. Fixed hinges allowed the inner surface of a hole to translate only tangentially, but nodes were restrained from moving axially or radially. Slider/roller restraints of a surface allowed translation of nodes parallel to the plane of the feature, but disallowed translation normal to it. As the names suggest, these simulated hinges and frictionless contact between two surfaces.

The analysis of the structural elements was performed first with the primary mesh, then with finer and coarser meshes for validation. Again, the primary mesh had a global element size of 2mm with site specific element size specified to be 1mm around the holes and along the surfaces near the mechanical stop. The secondary meshes had global elements of 1mm and 3mm, with site specific element sized of 0.5mm and 1.5mm in the same locations.

The distal and proximal structural components had different geometries and were modelled separately. As such, six models were created in total (see Figure A.19). The Von Mises stress distributions on the models' surfaces are shown in Figure A.20 to Figure A.25. Relevant numerical data are supplied in table A.3 and A.4.

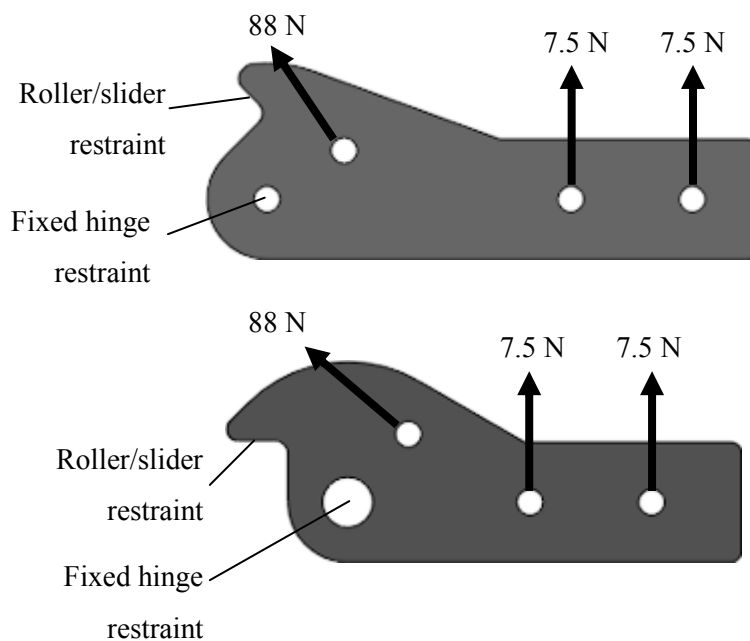


**Figure A.18** Front views of CAD models of the proximal (top) and distal (bottom) structural elements that were analysed, indicating how loading and restraints were applied in the FEA (see Figure A.9).



**Figure A.19** CAD models of the distal (left) and proximal (right) structural elements indicating the meshes used in the FEA models: 2mm mesh used as the primary model (centre), and the 1mm mesh (top) and 3mm mesh (bottom) used to confirm the results of the primary model (see Figure A.9).

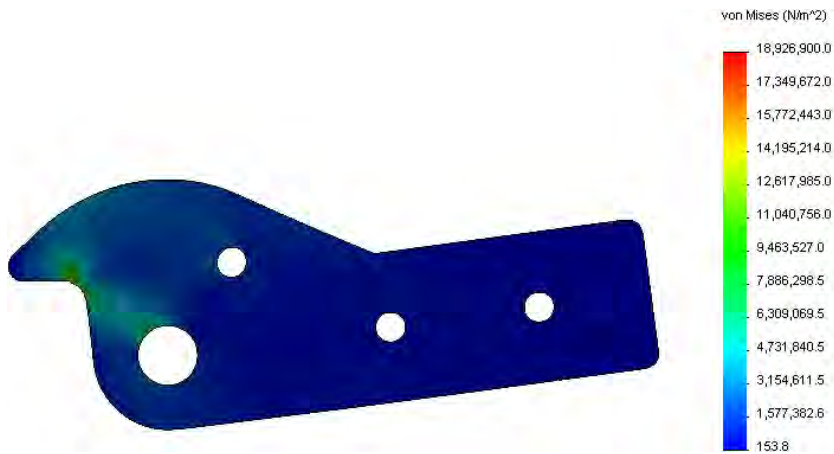


**Figure A.20** FEA model of the distal structural element and with a mesh element size of 2mm. The image indicates the Von Mises stress distribution results of the FEA model (with exaggerated deformation). The legend provides Von Mises stress results measured in  $\text{N}\cdot\text{m}^{-2}$  (i.e. pascals). This was a primary model, validated by the secondary models in Figure A.21 and Figure A.22.

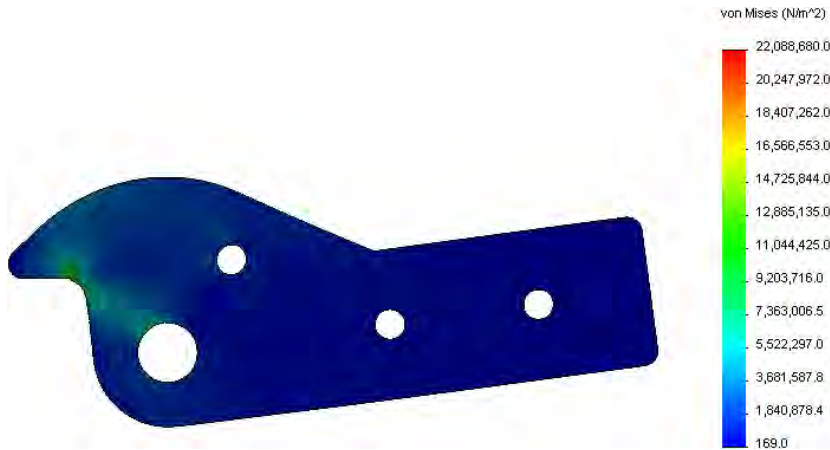


**Figure A.21** FEA model of the distal structural element and with a mesh element size of 1mm. The image indicates the Von Mises stress distribution results of the FEA model (with exaggerated deformation). The legend provides Von Mises stress results measured in  $\text{N}\cdot\text{m}^{-2}$  (i.e. pascals). This was a secondary model, used to validate the primary model in Figure A.20.

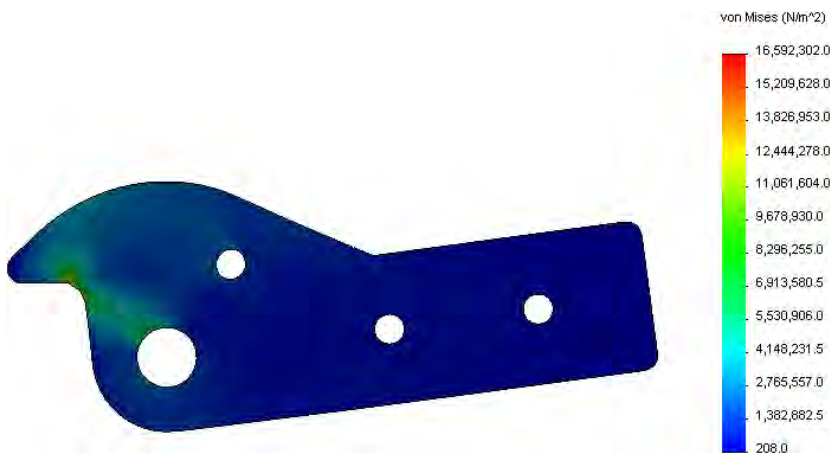


**Figure A.22** FEA model of the distal structural element and with a mesh element size of 3mm. The image indicates the Von Mises stress distribution results of the FEA model (with exaggerated deformation). The legend provides Von Mises stress results measured in  $\text{N}\cdot\text{m}^{-2}$  (i.e. pascals). This was a secondary model, used to validate the primary model in Figure A.20.

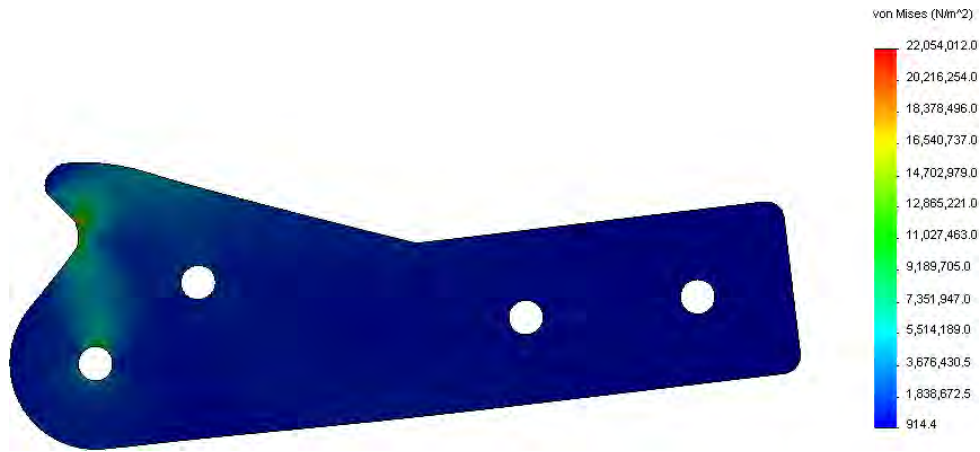


**Figure A.23** FEA model of the proximal structural element and with a mesh element size of 2mm. The image indicates the Von Mises stress distribution results of the FEA model (with exaggerated deformation). The legend provides Von Mises stress results measured in  $\text{N}\cdot\text{m}^{-2}$  (i.e. pascals). This was the primary model, validated by the secondary models in Figure A.24 and Figure A.25.

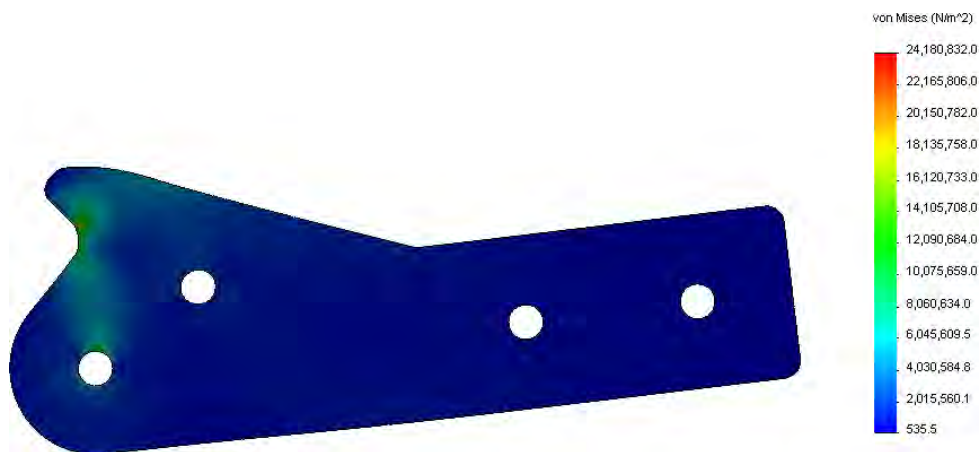


**Figure A.24** FEA model of the proximal structural element and with a mesh element size of 1mm. The image indicates the Von Mises stress distribution results of the FEA model (with exaggerated deformation). The legend provides Von Mises stress results measured in  $\text{N}\cdot\text{m}^{-2}$  (i.e. pascals). This was a secondary model, used to validate the primary model in Figure A.23.

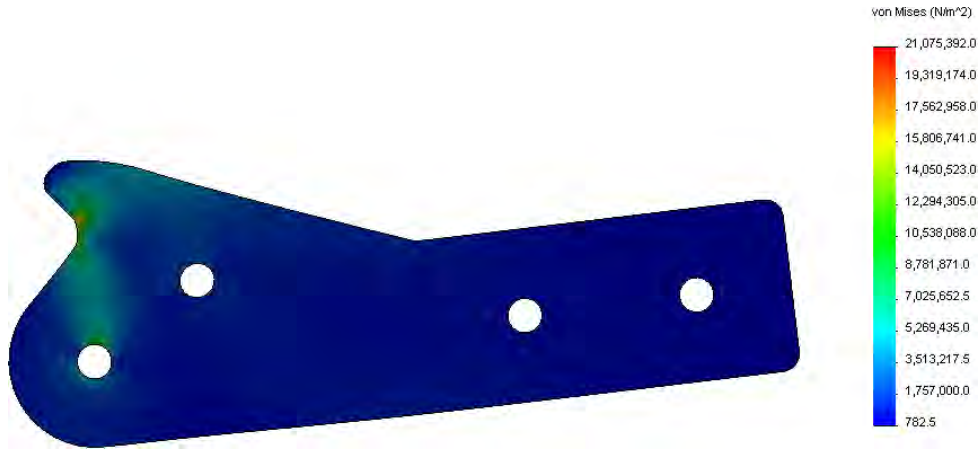


**Figure A.25** FEA model of the proximal structural element and with a mesh element size of 3mm. The image indicates the Von Mises stress distribution results of the FEA model (with exaggerated deformation). The legend provides Von Mises stress results measured in  $\text{N.m}^{-2}$  (i.e. pascals). This was a secondary model, used to validate the primary model in Figure A.23.

**Table A.3** Relevant numerical data from the FEA model of the proximal structural element under worst-case loading

Model type	Global element size [mm]	Mesh control element size [mm]	Peak Von Mises stress [MPa]	Change in peak Von Mises stress from primary model
Secondary	1	0.5	24.18	9.65%
Primary	2	1	22.05	-
Secondary	3	1.5	21.08	-4.40%

**Table A.4** Relevant numerical data from the FEA model of the distal structural element under worst-case loading

Model type	Global element size [mm]	Mesh control element size [mm]	Peak Von Mises stress [MPa]	Change in peak Von Mises stress from primary model
Secondary	1	0.5	22.09	16.75%
Primary	2	1	18.92	-
Secondary	3	1.5	16.59	-12.32%

It was not required of this model to know the stress at specific points. The use of sensors was not required. The overall safety factor of the whole part could be calculated from the peak stresses from the primary model for each. These were 18.92 MPa and 22.05 MPa (see Table A.3 and A.4).

The material in question, poly(methyl methacrylate), trade name “Perspex”, has an ultimate tensile stress of 75 MPa, as specified by the manufacturers. The overall safety factors in the models were 3.4 and 4.0 for the distal and proximal components respectively. Notice also that the peak stresses in the components occurred near the edges of restrained surfaces. These regions are susceptible to anomalous stress readings and the actual peak stresses were likely to be slightly lower than was predicted by the model. Regardless, a conservative design paradigm was confirmed by the large safety factors.

It can be seen in tables A.3 and A.4 that there was some difference in peak and average stress between the primary models and their corresponding secondary models. Thus, the mesh had an effect on the outcome of the model. In light of the large safety factors, it was again decided that the model was reliable, and that the uncertainty introduced by the mesh dependence was negligible.

[This page is intentionally left blank]

## **Appendix B – Electronics and Actuator Information**

### **B.1. Electric Motor and Motor Driver Specifications**

The actuators were brushed DC electric motors (see Figure B.1). The motors specified for the device had the following characteristics:

- Supply voltage: 12v
- Unloaded rotational speed: 10 RPM
- Rated torque: 0.59 N.m
- Gearbox ratio: 750:1

The motors were controlled by means of the L298 dual H-bridge IC, which was capable of supplying a total DC current of up to 4 A. The both motors were driven from a single IC.

The H-bridge allowed bidirectional motor control without the need for a negative voltage supply. The IC's enabling pins (required to be held high at 5 volts to enable output) were hardwired to the safety button system so that if either safety button was released, the motors were directly disabled. As a redundancy, the safety button also disabled the motors in software.

### **B.2. EMG Signal Acquisition**

OpenEEG circuit boards were used for acquisition of EMG ("The OpenEEG project," 2013). The circuit designs were intended for use with EEG, such as with EEG-biofeedback and brain-computer interface applications and to facilitate research into neurophysiology. Components were replaced so that the bandwidth of the amplifier circuits met the requirements of EMG signal acquisition (see Appendix C).

The OpenEEG system consists of separate amplifier and digital electronics (see Figure B.3 to Figure B.4). Each amplifier board had two signal acquisition channels. The digital boards received these signals and communicated them via serial connection, although this feature was not used in this study.

Up to three amplifier boards could interface with a digital board (creating six channels), although only two were used since four channels were required. The digital board was only used for optical isolation and power management of the amplifier boards only.

The amplifier board received its power from the digital board, which itself was required to be powered externally. The power supply was optically isolated from other electronics. The output of the amplifier board was an analogue signal between 0V and 4V, referenced to a virtual ground at 2 V.



**Figure B.1** A geared brushed DC electric motor as used in the device.

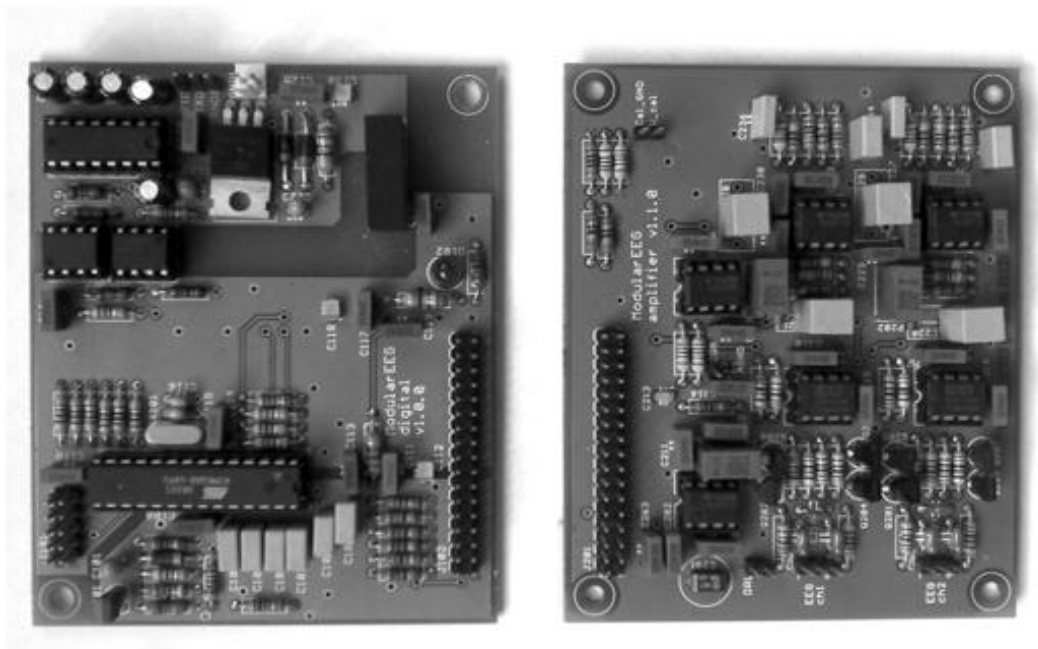
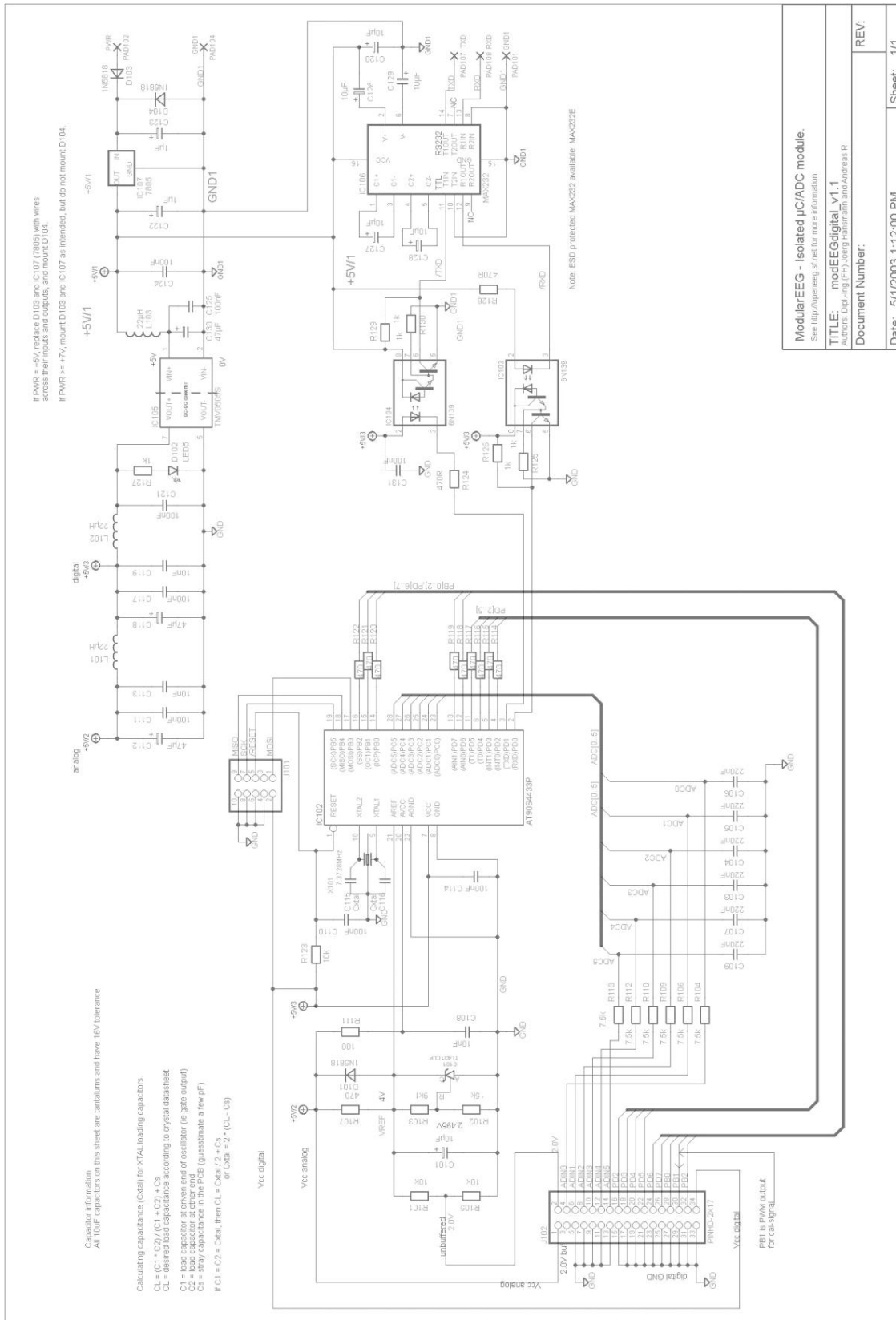


**Figure B.2** The OpenEEG digital board (left) and amplifier board (right) (See Figure B.3 and Figure B.4).





ModularEEG - Isolated $\mu$ C/ADC module. See <a href="http://openeeg.sf.net">http://openeeg.sf.net</a> for more information.	
TITLE: modEEGdigital_V1.1	
Author: Eepj-Eng (Engineering Department) and Andreas R	
Document Number:	REV:
Date: 5/1/2003 1:12:00 PM	Sheet: 1/1

**Figure B.4** Schematic of the unmodified OpenEEG digital board (“The OpenEEG project,” 2013). See figure B.2.

### B.3. EMG Signal Processing Circuit

EMG signal processing was partially performed in analogue electronics. The main functions required were filtering, rectifying, and enveloping (see Figure B.5 and Figure B.6). A fourth step – thresholding – was performed digitally by the microcontroller.

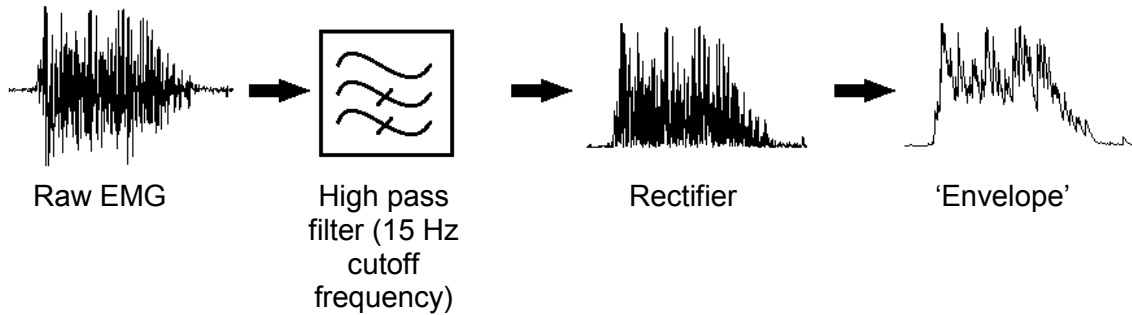


**Figure B.5** Functional requirements of the EMG signal processing circuit (reproduced from Figure 2.10).

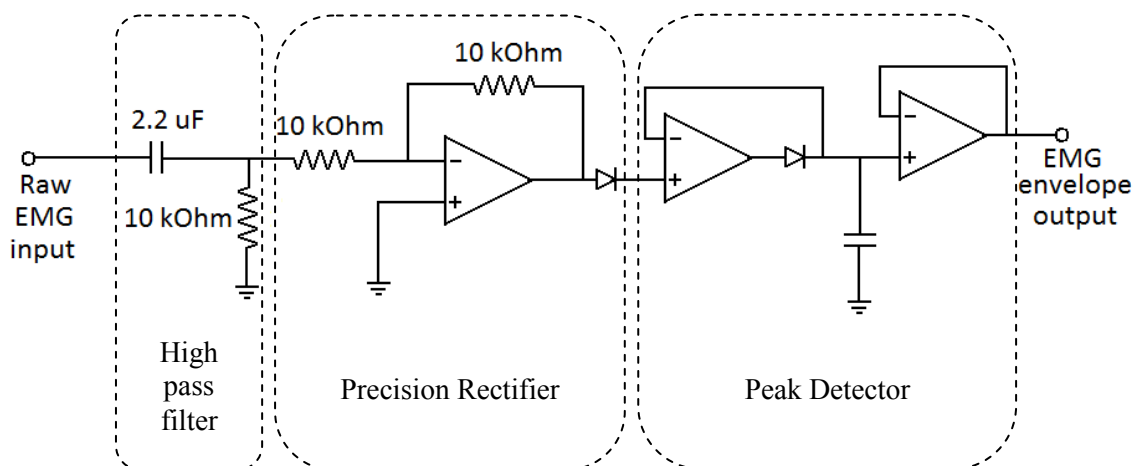


**Figure B.6** Schematic diagram of the EMG signal processing circuit for one channel (see Figure B.5).

#### B.3.1. Filtering

High pass filtering was performed to remove the DC offset due to the virtual ground as well as to reduce motion artefact. A simple RC filter was implemented, using a 2.2  $\mu\text{F}$  capacitor and a 10 kOhm resistor (cutoff frequency of 7.2 Hz).

### B.3.2. Rectification

A precision full-wave rectifier was implemented. The circuit (see Figure B.7) provided a fully rectified signal which was tested at frequencies up to 1000 Hz.

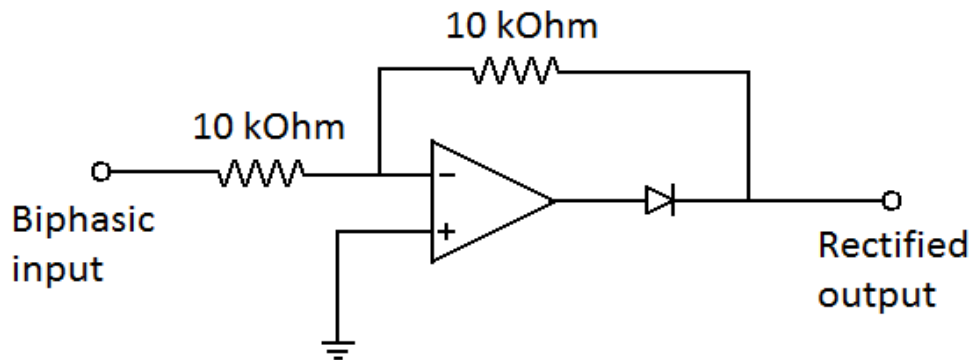


**Figure B.7** Schematic of the precision rectifier in the EMG signal processing board (see Figure B.10).

### B.3.3. Enveloping

An envelope of the rectified EMG signal was achieved by means of a peak detecting circuit (Horowitz and Hill, 1989). The circuit included two consecutive operational amplifier (op-amp) sub-circuits (see Figure B.8). The first op-amp drew its negative feedback after a diode, creating a precision diode (without the forward voltage drop). The capacitor would hold its charge due to the high input impedances of the second op-amp and due to the low leakage current of the diode.

The small input bias currents and leakage currents for the op-amps and diodes respectively resulted in a discharge (or “droop”) in output voltage over time. While normally seen as a circuit limitation, the droop was used to drop the circuit output to zero upon cessation of a muscle contraction. Through experimentation, it was found that a 1  $\mu\text{F}$  capacitor resulted in appropriate output signal decay – i.e. one such that the circuit output created an envelope of the EMG input, but returned to zero promptly once the muscle contraction had ceased.

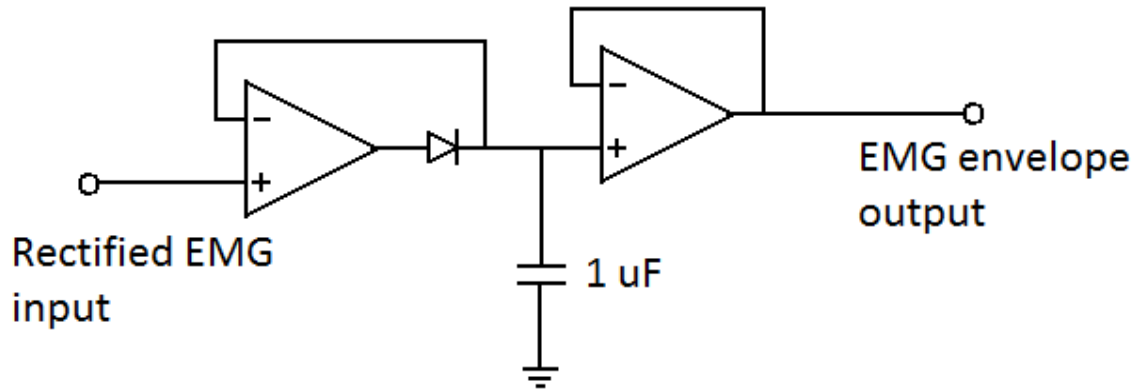


**Figure B.8** Schematic of the peak detector circuit used in the EMG signal processing board (Horowitz and Hill, 1989). See Figure B.10.

#### B.4. Strain Gauge Signal Processing Circuit

Two force transducers were present in the design – once measuring the force applied at the wrist joint and one at the finger joint. Each had identical hardware and software configurations.

The strain gauges were connected into a full bridge configuration to amplify bending loads (Juvinall and Marshek, 2011). Under expected loading each bridge produced output voltage „ $V_o$ “ such that:

$$V_o = -1 \times V_{ex} \times GF \times \varepsilon$$

(Equation B.1)

$V_{ex}$  was the excitation voltage (12 V). Strain gauge manufacturers specified a gauge (GF) of 2.1, and the expected strain ( $\varepsilon$ ) was calculated to be 142.7  $\mu\varepsilon$  (see Section A.3.1). As such, the maximum expected output was 36 mV.

An instrumentation amplifier (INA114AP) was used to amplify the signals from the strain gauge bridges (see Figure B.9). The amplifier gain was selected via an external resistor  $R_G$ :

$$Gain = 1 + \frac{50 \text{ k}\Omega}{R_G}$$

(Equation B.2)

$R_G$  was chosen to be 660  $\Omega$  such that the gain of the amplifier was 76.8. With the maximum bridge output voltage of 36 mV, the final output voltage was expected to be 276.0 mV. This was large

enough to be easily measured, but allowed a safety factor to prevent saturation of the data logger in the case of an unexpectedly large load.

Lastly, potentiometers were used with the reference adjustment pins to adjust DC offset to “zero” the output (see Figure B.9).

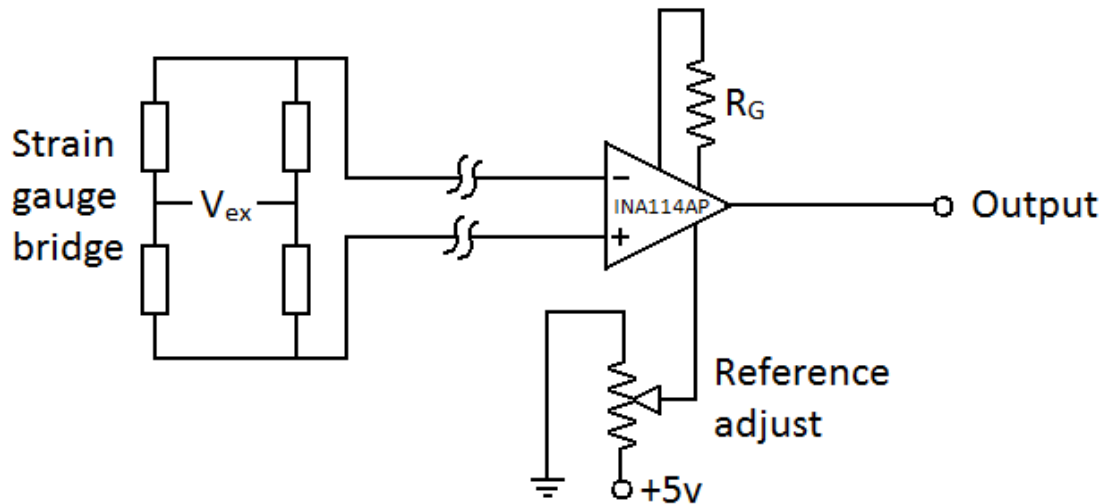


**Figure B.9** Schematic of the bridge and amplifier circuit used in the strain gauge force measurement system (see Figure B.10). Reproduced from Figure 2.11.

## B.5. Microprocessor and System Integration

A PIC16F917 microcontroller was used for system integration (see Figure B.10). Input from the various sub-systems was either analogue or digital. Outputs were digital control signals for the L298 H-bridge driver to control the motors (see section B.2), as well as for indicator lights and the LCD display.

Certain signals were monitored by the data logging system (see section 2.5) for the purposes of this study, such as raw EMG and amplified strain gauge voltage. Note that the PC only monitored signals from the system, and was not involved in control at all.

The microcontroller had the following basic specifications:

- PIC16F917, produced by Microchip Technologies
- 8-Bit CMOS Microcontrollers
- Internal oscillator operating at 8MHz clock speed (default), programmable up to 32MHz
- 14000 bytes flash memory

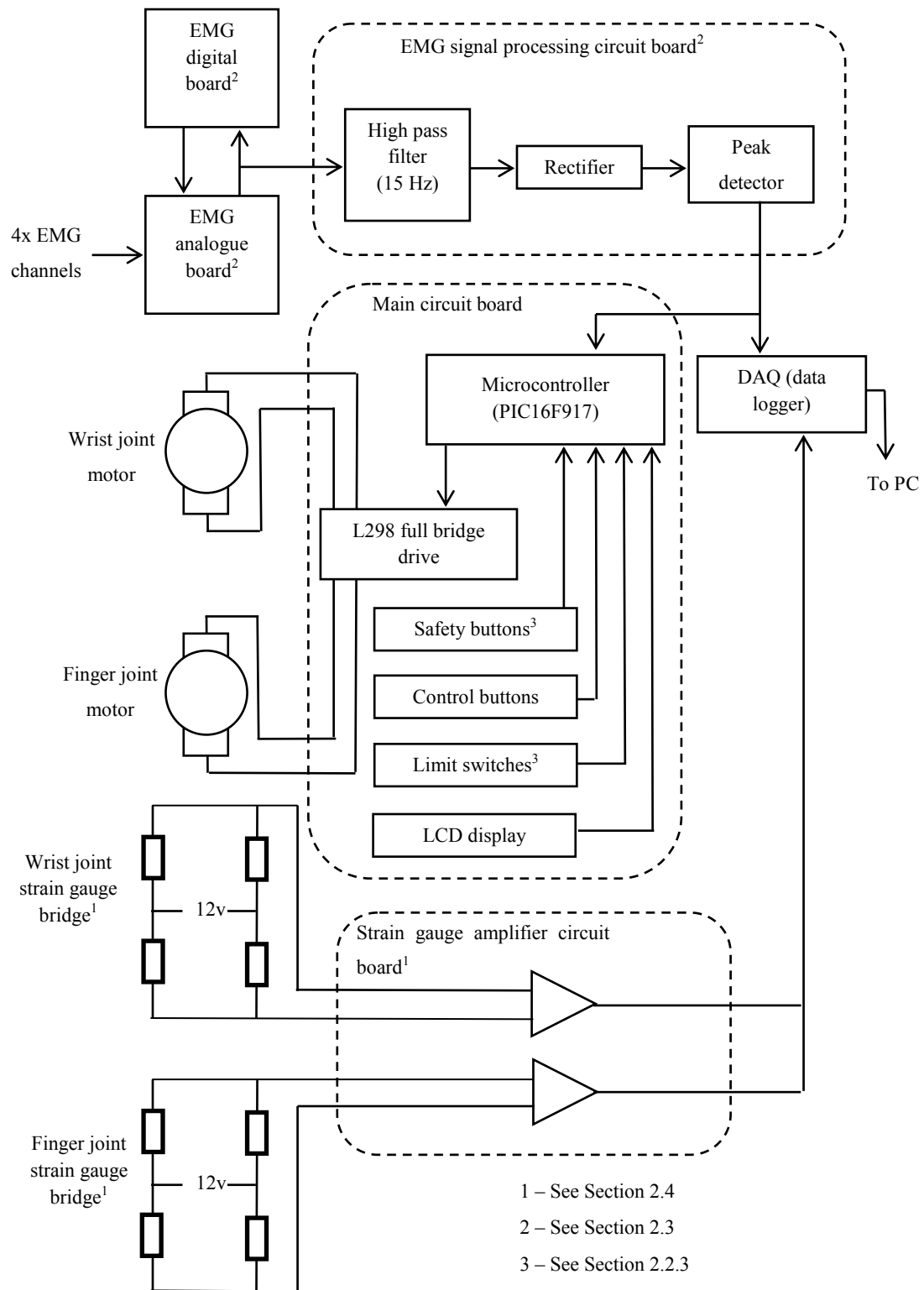


**Figure B.10** Functional overview of the components of the system (power management circuits not shown). Reproduced from Figure 2.5.

Aside from basic input and output (I/O), peripheral features included interrupts and analogue-to-digital (A2D) converters. The interrupt feature was used for the limit switches to ensure rapid response. The eight (A2D) converters were used to monitor EMG envelope signals and activation thresholds as control inputs for certain modes of operation. The amplified strain gauge signals had dedicated A2D pins, although these were not being used in this study.

## **B.6. User Interface Electronics**

All electronics (except the strain gauge amplifiers during the pilot clinical trial) were housed in the control box. The two control buttons provided a means to select modes of operation and other menu items. Potentiometers were used to adjust the EMG activation thresholds. Indicator lights and an LCD display were used to provide menu prompts and status information.

The primary method of information display was the LCD display module. The LMB162ABC module was used for this application. It connected with the microcontroller via an octal buffer IC (74HCT541). The display consisted of a 2x16 character output, and was used to prompt the user when input or actions were required.

[This page is intentionally left blank]

## Appendix C – Modifications to the OpenEEG System

The OpenEEG amplifiers were designed for use in electroencephalography (“The OpenEEG project,” 2013). Modifications were made such the amplifiers were suitable for EMG acquisition. The original bandwidth specifications were:

- Lower cutoff frequency: 280mHz
- Upper cutoff frequency: 58Hz

Useful EMG information can, however, be detected up to 500 Hz. Similarly, motion artefact usually occurs in the lower frequency range (<5 Hz). As such, the bandwidth of the amplifiers was changed to the desired range of between 5 Hz and 500 Hz.

The cut-off frequencies of an electronic circuit can be shifted by scaling all inductors and capacitor such that the impedance at the original and final frequency is unchanged (Horowitz and Hill, 1989):

$$X = \frac{1}{2\pi f_1 C_{old}} = \frac{1}{2\pi f_2 C_{new}}$$

X is the impedance of the filter, f is the frequency and C is the capacitance. Thus:

$$\frac{C_{new}}{C_{old}} = \frac{f_1}{f_2}$$

See Table C.1 for the changes made to the OpenEEG circuits. Despite these modifications, gain of the amplifiers was frequency dependent. Spectral scaling was implemented to process the recorded data (see Appendix E).

**Table C.1** Original and replacement capacitor values for bandwidth modification of the OpenEEG system (see Figure B.3 and Figure B.4).

Filter	Capacitor	Old value [nF]	New value (ideal) [nF]	E12 value [nF]
High Pass	C220 and C221	1000	56.2	57
	C228 and C229	1000	56.2	57
Low Pass	C321 and C235	220	25.67	22
	C232 and C233	10	1.17	1
	C234 and C236	33	3.85	3.3
	C103 and C109	220	25.67	22

[This page is intentionally left blank]

## Appendix D – Calibration of the EMG Amplification System

Four OpenEEG amplifier boards were used for amplification of EMG signals (“The OpenEEG project,” 2013). The output of each was an analogue signal with a peak-to-peak amplitude of 4 V (at a virtual ground of 2 V). These were recorded with a DAQ. It was found that the EMG amplifiers, modified using the method described in Appendix C, had inconsistent gains over the frequency range of interest (5 Hz to 500 Hz). In order to correct for frequency-dependent gains, spectral scaling was implemented. Transfer functions were determined empirically, and were used to determine the unamplified EMG amplitude using the method described in this appendix.

Since each EMG channel had a dedicated amplifier (no multiplexing was performed), each amplifier was analysed separately. Signal processing was performed offline in Matlab, version R2012a.

### D.1. Generation and Amplification of the Input Signal

In order to properly determine the transfer functions, a known signal needed to be generated and amplified by each channel. This unamplified input signal and the amplified output signals could be analysed against one another. Since EMG is of the order of microvolts to millivolts, the amplifier gain was expected to be large. An input signal of similarly small amplitude was required. For this purpose, a voltage divider was used in conjunction with a signal generator (Hewlett Packard 3314A function generator) to create a sine wave of sufficiently small amplitude (see Figure D.1).

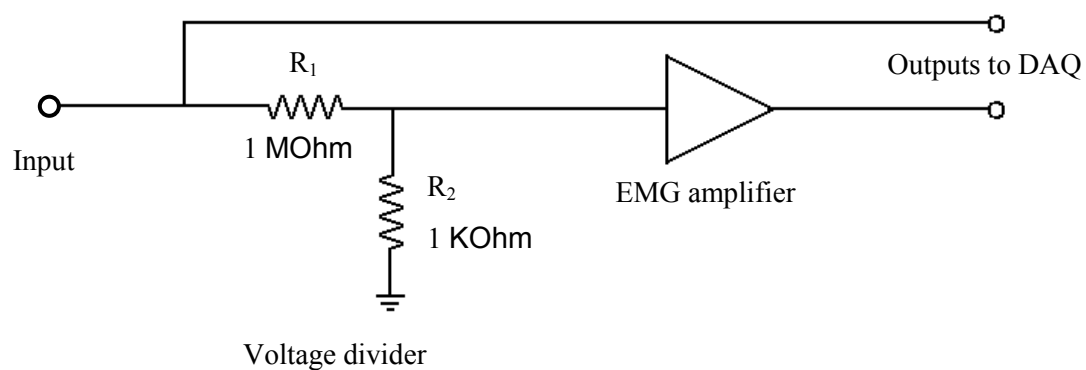


**Figure D.1** Schematic representation of the calibration setup for a single channel. The input signal (from a signal generator) was attenuated with a voltage divider by a factor of 1001, before being amplified by the EMG amplifier. Both the output from the amplifier being analysed and the input to the voltage divider were recorded simultaneously.

The sinusoidal input signal swept through from the minimum frequency capable with the signal generator through to the maximum frequency range of interest (i.e. 5 Hz to 500 Hz). The frequency range was chosen to be wide enough to encapsulate the majority of the EMG power. The sweep occurred over a time interval of roughly 14 second. The signals were recorded with a sampling frequency of 1000 Hz – the same as that of the actual EMG recordings made during testing - satisfying the Nyquist Sampling Theorem criterion; the measured signal was accurately resolved because the sampling rate is at least double the largest frequency of interest.

The amplitude of the input from the signal generator was varied until the output from the amplifiers was 2 V peak-to-peak. This was large enough to be accurately resolved by the DAQ, but would not saturate the amplifiers. Subsequently, the input signal amplitude was measured and found to be 418 mV peak-to-peak.

The equation governing the attenuation of a voltage divider circuit is as follows:

$$\frac{V_o}{V_i} = \frac{R_2}{(R_1 + R_2)}$$

(Equation E.1)

Where  $V_o$  is the output voltage,  $V_i$  is the input voltage, and  $R_1$  and  $R_2$  are the two resistors used in the voltage divider (see Figure D.1). These were 1 K $\Omega$  and 1 M $\Omega$  respectively (with 5% accuracy). Accounting for resistor uncertainty, the attenuation factor could be expected to lie between  $9.04 \times 10^{-4}$  and  $11.04 \times 10^{-4}$ . When an input sine wave of amplitude 20 V peak-to-peak was applied, it yielded an output signal of 19 mV peak-to-peak - an attenuation factor of  $9.50 \times 10^{-4}$ . This was in agreement with an estimate using Equation E.1.

Using this attenuation factor, the input sine wave (418 mV peak-to-peak) yielded an output to the EMG amplifier of 0.39 mV peak-to-peak that swept through the frequency range of 5 Hz to 500 Hz.

## **D.2. Inference of the Transfer Function**

The unattenuated input signal (from the signal generator) was multiplied by the attenuation factor ( $9.50 \times 10^{-4}$ ), to yield the attenuated sinusoid which swept through the range of frequencies. The unattenuated signal was recorded, since the attenuated version (the output of the voltage divider) was too small to be recorded. Using the attenuation factor, the attenuated signal was inferred in software. The first second of the recording of this inferred attenuated signal is shown in Figure D.2.

Simultaneously, a second recording of the output of the amplifier was made. A separate output recording was made for each amplifier channel. An example of such a recording is shown in Figure D.3. The waveforms for the other channels have the same basic appearance with small variations in amplitude.

Note that, in Figure D.3, the voltage spikes at 18s are due to the signal generator failing to transition smoothly from the 500 Hz signal to 0 V at the end of the sweep. This does not affect the calibration.

From the data in Figure D.2 and Figure D.3, there is enough information to determine the relationship between frequency and amplifier gain (i.e. transfer function). As can be seen from Figure D.3, the gain of the amplifier is dependent on the frequency of the input. This points to an error, either in the calculations for the modifications to the OpenEEG boards (see Appendix C), or the implementation thereof. Regardless, the transfer functions could be used to infer the unamplified EMG signals.

In Matlab, using the „tfestimate“ function, the transfer function, and also the phase shift characteristics, of the amplifier can be estimated based on the input and output vectors (such as those shown in Figure D.2 and Figure D.3). This process was repeated for all amplifier channels, and the gains and phase shifts for each are shown in Figure D.4. In Matlab, the gains over the frequency range were stored in a vector, referred to as the transfer function vector. The measured bandwidths of the amplifiers (i.e. the range in which the gain is within 3.01 dB of the peak) are shown in Table E.1.

**Table D.1** Bandwidths of amplifiers as calculated from transfer functions (see Figure D.4)

Channel	Peak gain frequency [Hz]	Bandwidth		dB drop at 150 Hz
		Lower Cutoff Frequency [Hz]	Upper Cutoff Frequency [Hz]	
1	23.7	5.6	100.8	6.66
2	19.3	5.6	100.8	6.50
3	19.3	6.1	100.5	5.35
4	25.9	5.6	104.7	6.02

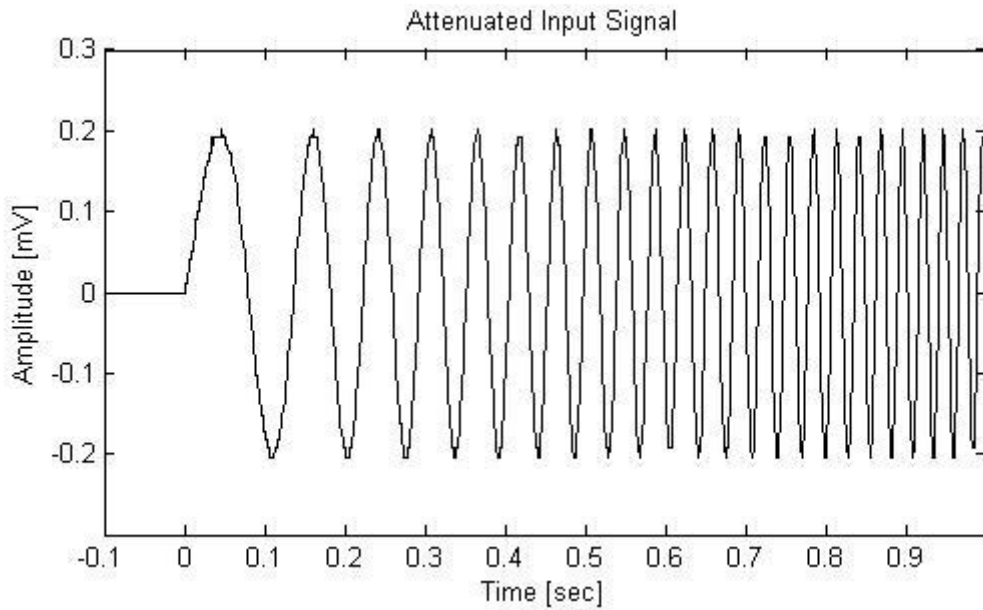


**Figure D.2** The first second of the recording of the attenuated input signal to the amplifier for calibration. The initial frequency was 5 Hz (shown at time 0 seconds here), and over roughly 14 seconds it swept through to 500 Hz. Using this data, and that shown in Figure D.3, the amplifier characteristics could be determined (see Figure D.4)

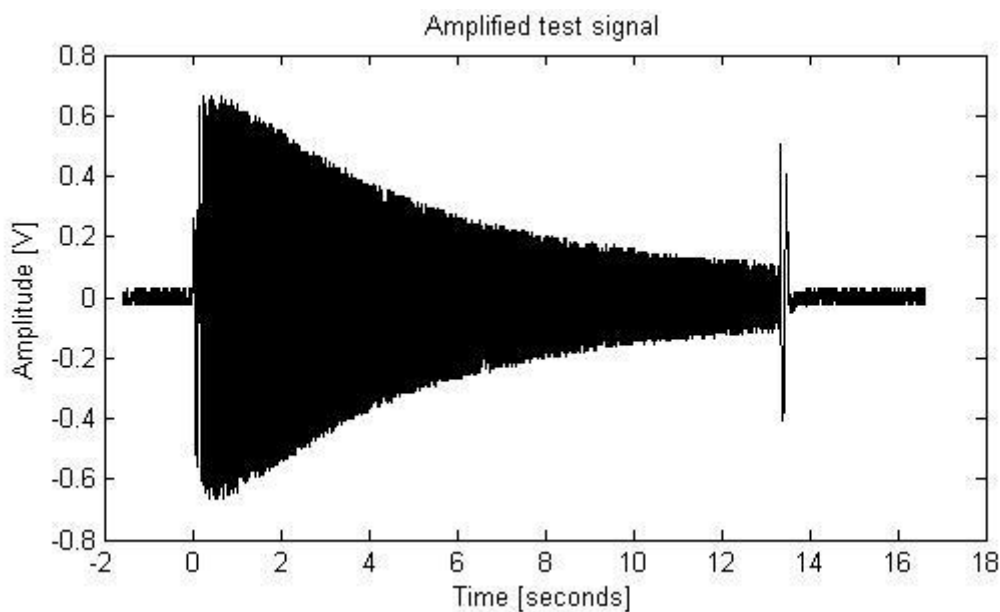


**Figure D.3** The recording of the amplified output signal from the amplifier for calibration. The input signal is shown in Figure D.2. The initial frequency was 5 Hz and over 15 seconds it swept through to 500 Hz. Using this data, and that shown in Figure D.2, the amplifier characteristics could be determined (see Figure D.4)

As can be seen from Table E.1, the bandwidths of the amplifiers are very narrow. The upper cutoff frequencies are roughly 100 Hz, and the lower cutoff frequencies were recorded as roughly 5 Hz. Note that the latter could be due to the fact that the function generator signal sweep only began at 5 Hz. Regardless, signals below this range are not of interest, as they are likely to be affected by disturbances such as baseline drift due to movement of the participant.

Despite the narrow bandwidth, inference of the unamplified EMG data from the recordings is still possible. The majority of EMG power lies below 150 Hz (see the Fourier transforms of the recorded signals in Figure D.6). Amplification is sufficient, however, that computation of unamplified data up to 500 Hz is still possible. The decibel drop at 150 Hz is shown in Table E.1.

### **D.3. Inference of Unamplified EMG signals**

To allow for comparison of EMG across participants, the unamplified EMG data must be inferred from the raw, amplified data that was recorded. This section illustrates the method used to infer the unamplified EMG by means of an example.

The following method was used to correct the recorded EMG signals:

- Since the transfer functions were dependent of frequency, the recorded EMG needed to be analysed in the frequency domain. A discrete Fourier transform was applied to determine the EMG spectral density.
- Once the vector containing the spectral density distribution of the EMG recording had been established, it was divided by the amplifier gain vector (also in the frequency domain). In this way, the components of the EMG across the frequency spectrum would be corrected using the appropriate gain for that frequency.
- The corrected EMG spectral density was then converted back into the time domain to yield the corrected EMG.

A discrete Fourier transform was used to determine the spectral density of the recorded EMG data. This was performed using the „fft“ function in Matlab (see Figures E.5 and E.6).

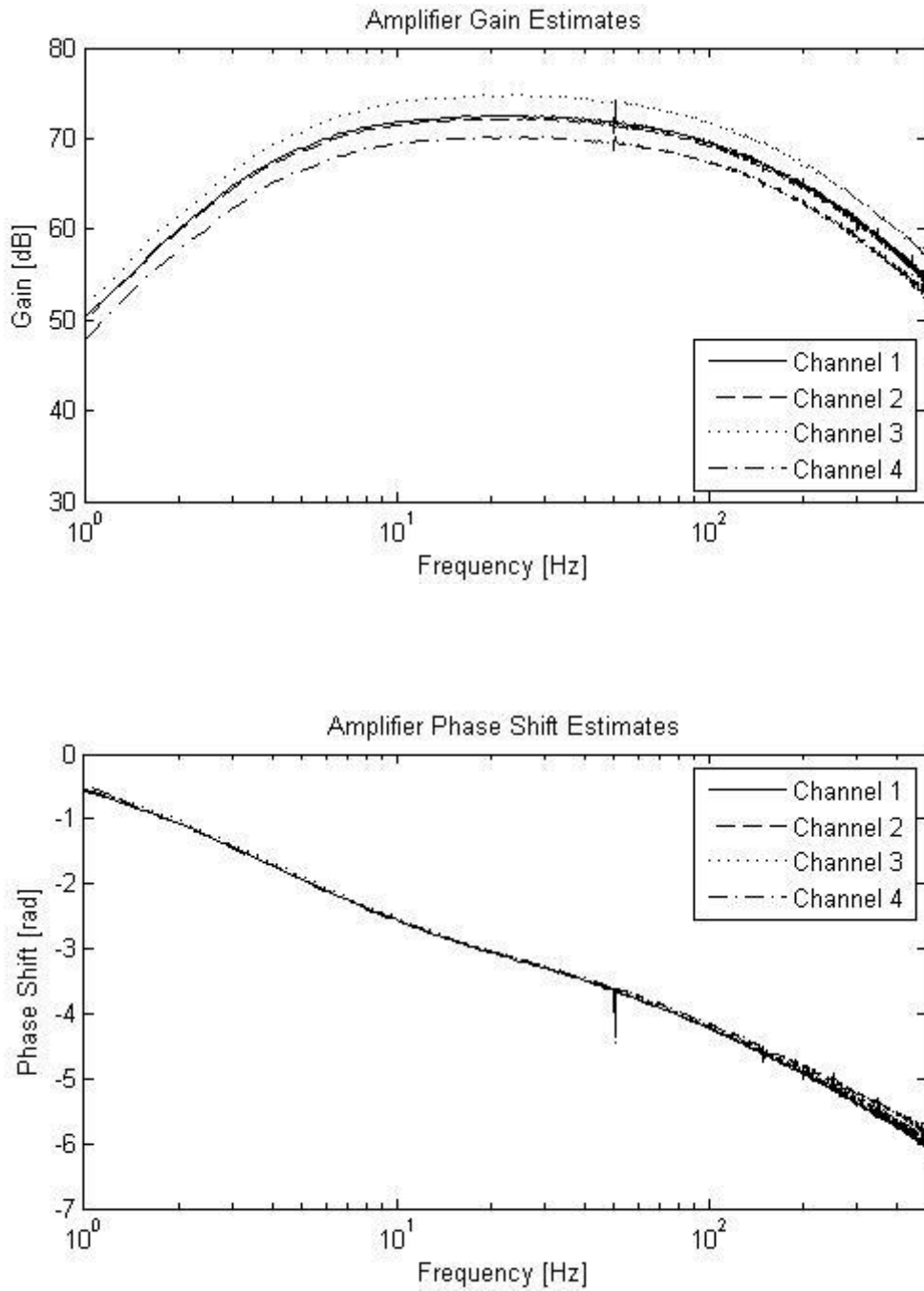


**Figure D.4** Estimates of the transfer functions (top) and phase shifts (bottom) for each amplifier channel. Amplifier characteristics are based on the input and output recordings such as those shown in Figure D.2 and Figure D.3. The estimates were made using the “tfeestimate” function in Matlab. Notice that the functions are not constant over the frequency. The disruptions observed at 50 Hz are due to electrical noise.

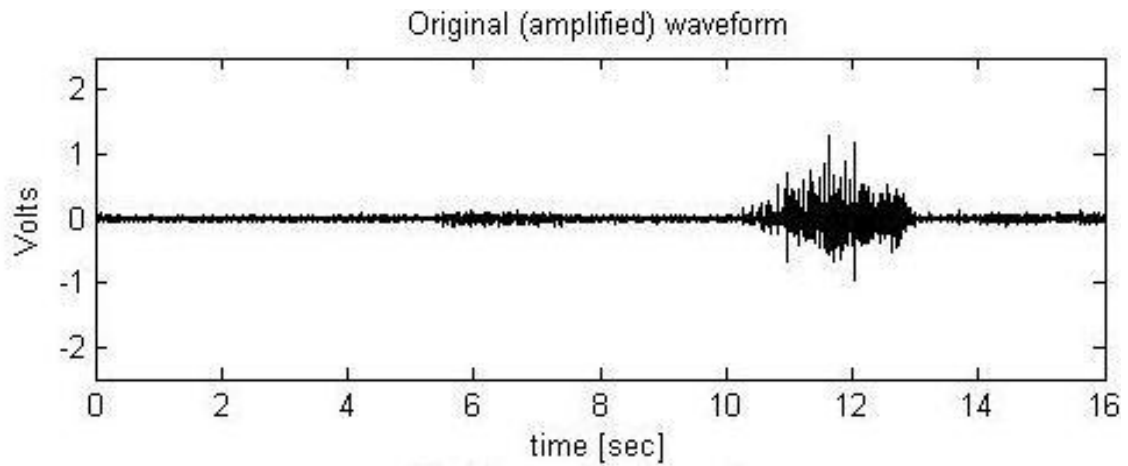


**Figure D.5** Example of an amplified EMG waveform. Data was collected from the flexor carpi radialis muscle, amplified and recorded using channel 4. (See Figure D.4 for amplifier characteristics).

The spectral density vector was divided by the transfer function vector (see Figure D.4), such that the amplitude of the EMG was corrected on the basis of its frequency components (see Figure D.6).

Once the corrected spectral density had been obtained, the inverse Fourier transform could be invoked to determine the unamplified EMG signal in the time domain. To implement this, the „ifft“ function in Matlab was used (see Figure D.7) for the final, unamplified EMG data.

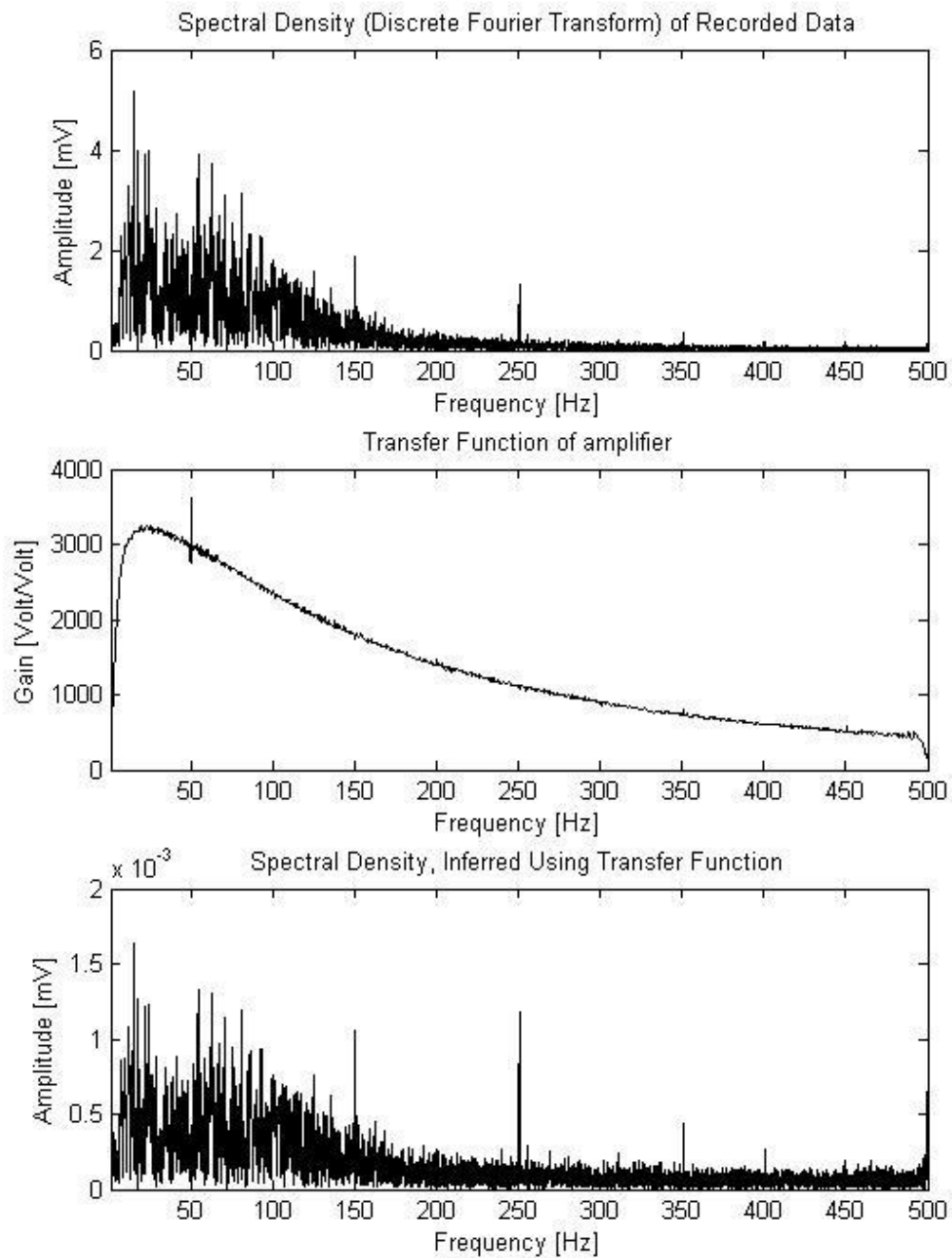


**Figure D.6** Top: The spectral density of the EMG recording shown in Figure D.5. Middle: The transfer function for channel 4 (see Figure D.4). Bottom: The final, unamplified spectral density, inferred by dividing the EMG spectral density vector by the transfer function vector (see Figure D.7) for the unamplified EMG in the time-domain.

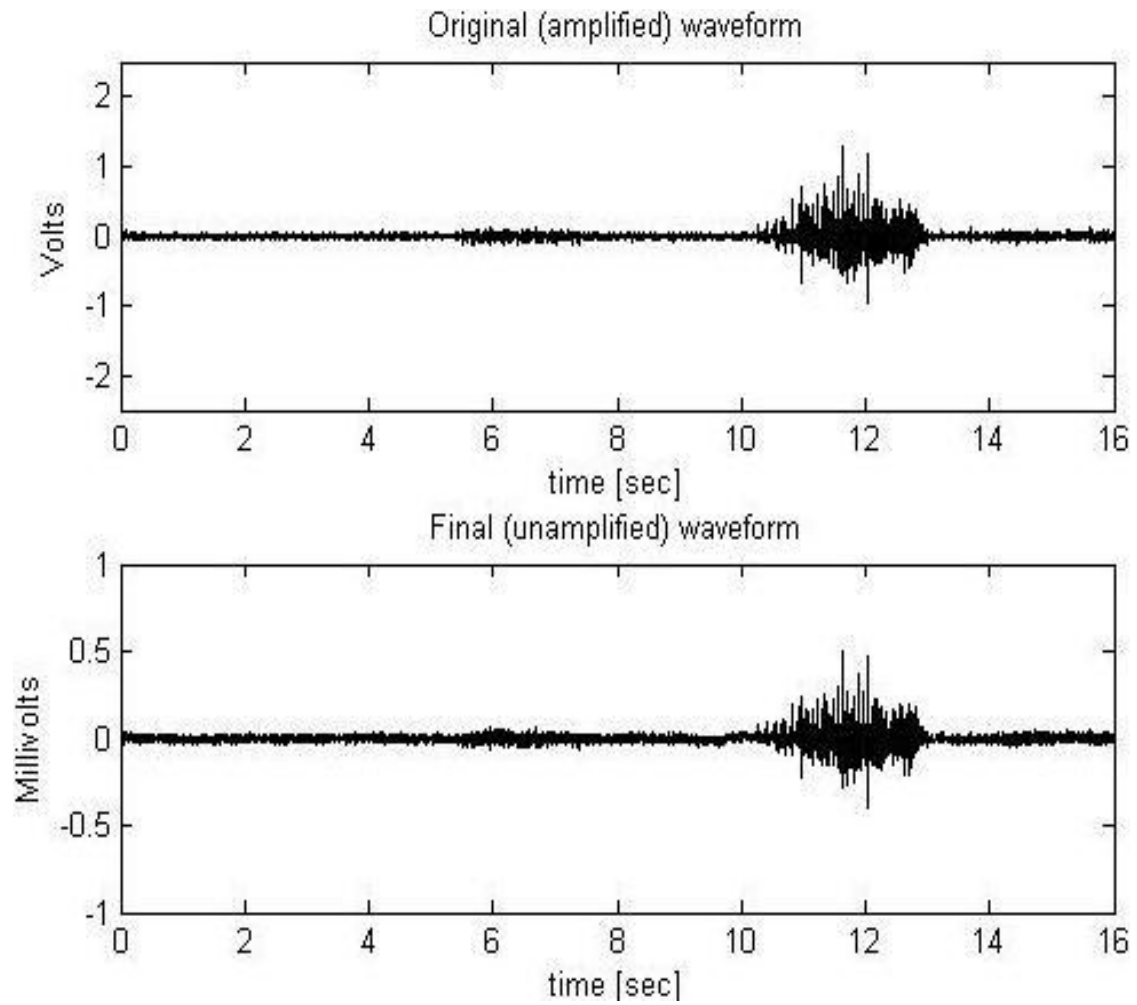


**Figure D.7** Original (amplified) and final (unamplified) EMG data, as inferred from the recorded EMG data (see Figure D.5), and using the transfer function (see Figure D.4).

[This page is intentionally left blank]

## Appendix E – Microcontroller Code

The following code was used in the microcontroller (PIC16F917) to integrate the various sub-systems. These were namely:

- Four analogue input to capture the processed EMG envelope
- Two analogue input to capture the EMG threshold adjustments (these also served the dual purpose of allowing manual control of the device if position adjustments needed to be made)
- Functionality for the four limit switches on the device
- Pushbuttons on the control box
- The LCD display module
- The safety buttons (using an interrupt algorithm)
- Bidirectional control of each motor

The code was developed in MPLab v8.50 Development Environment, and required the use of the HITECH C compiler plug-in. The compiled algorithm was uploaded to the microcontroller using a PICKit 2 uploader, distributed by Microchip Technology Inc. The code was as follows.

```
/*This version includes functionality for:
two modes of operation: EMG driven and evaluation mode. The following is functional in the code below:
    4x EMG channel input (with "hysteresis thresholds" and further smoothing)
    2x manual control using threshold pots
    Threshold adjustment input (analog x2)
    Limit switches (x4)
    Safety buttons (with interrupt, x1)
    Bi-directional motor drive (controlled by the above features, x2)
*/

#include <htc.h>
#include "LCD library.C"

//variables and arrays:
unsigned int SAFE=0; //status of safety buttons
unsigned int FLAG[4]; //for thresholding
float EMG_IN[4]; //read in EMG
float EMG_MA[4]; //EMG after smoothing
float THRESHOLD[2]; //read in from pots
unsigned int EMG_BINARY[4]; //binary "on or off", product of EMG thresholding
int speed;
int speed_min=50;
int speed_max=150;
int pause_time=30000;
int run_time=30000; //used to move motors to neutral position during initialization. Value depends on
motor type - set higher if slower motors

//index variables:
unsigned int i=0;
unsigned int j=0;
unsigned int k=0;

//function prototypes:
```

```

void interrupt isr(); //immediately kill motors and change SAFE
to false if push buttons released
short analog_read_in (int channel); //read in analog signals (EMG, thresholds, strain
gauges)
int bool_EMG(float EMG, float THRESH, int FLAG); //change analog EMG signal into binary value depending on threshold
values
void manual_control(void); //allow manual control of motors using
threshold pots
void EMG_control(void);
void Eval_control(void);
void EvalW_control(void);
void checksafe(void);
void Eval_rep(void);
void EvalW_rep(void);
void FFM(void);
void FWM(void);
void EFM(void);
void EWM(void);
void FF45(void);
void FWS(void);

//main function:
void main (void)
{
//setup and initialize:
TRISA=0b11111111; //PORTA (EMG, strain gauge, threshold
inputs) as input
TRISB=0b11111111; //PORTB (limit switches) as input
TRISE=0b11111111; //PORTE (EMG, strain gauge, threshold
inputs) as input
TRISC=0; //PORTC (motor control) as output
TRISD=0; //PORTD (LCD and LED's) as output
PORTC=0;
PORTD=0;

CMCON0=0; //turn off comparators
ANSEL=0b11111111; //RA0,RA1,RA2,... = analog input (all AN
inputs set to analog)
ADCON1=0b01100000; //Timing for analog input
SSPCON=0;
TICON=0;
RCSTA=0; //disable serial port (free up RC6 and RC7)
LCDCON=0; //disable PIC LCD driver module

lcd_init(); //initialize LCD module - function in include
file "LCD library.C"

//interrupt config:
//RBPU=0; //disable weak pullups on PortB
INTCON=0b10010000; //enable external interrupts only.
INTEDG=0; //killswitches (RB0) set to falling edge -
trigger killswitch if buttons are released

//display welcome screen
lcd_string("Welcome"); //display text

for (i=0;i<60000;i++); //wait

lcd_command(0x01); //clear screen
lcd_string("A: EMG mode"); //display text
lcd_command(0xc0); //next line
lcd_string("B: Eval mode"); //display text

while(1)

```

```

{
if (RB2)
    //Confirmation of mode selection:
    {lcd_command(0x01); //clear screen
    lcd_string("EMG mode?"); //display text
    for (i=0;i<60000;i++); //short pause
    lcd_command(0xc0); //next line
    lcd_string("A: Confirm"); //display text
    while(!RB2); //wait and poll pushbutton 1
    //envoke EMG control
    EMG_control();
    }
if (RB3)
    //Confirmation of mode selection:
    {lcd_command(0x01); //clear screen
    lcd_string("Eval mode?"); //display text
    for (i=0;i<60000;i++); //short pause
    lcd_command(0xc0); //next line
    lcd_string("A: Confirm"); //display text
    while(!RB2); //wait and poll pushbutton 1

    //choose eval mode (wrist or wrist + fingers)
    {lcd_command(0x01); //clear screen
    lcd_string("Which Eval mode?"); //display text
    for (i=0;i<60000;i++); //short pause
    lcd_command(0xc0); //next line
    lcd_string("A: W+F B: W"); //display text
    while(1) //wait and poll pushbutton 1
        {if(RB2) //envoke Eval control
            Eval_control();
        if(RB3) //wait and poll pushbutton 2
            //envoke EvalW control
            EvalW_control();
        }
    }
}
}

}

}

//=====
=====

//function definitions:
void interrupt isr()
{
    for (i=0;i<100;i++) //when the external interrupt pin is
    deactivated //change SAFE to false to disable future
        if (!RB0) //and deactivate all motors before returning
            {
                SAFE=0;
                RC0=0;
                RC1=0;
                RC2=0;
                RC3=0;
            }
INTF=0;
return;
}

//=====
=====short analog_read_in (int channel)

```

```

{
switch (channel)
{
case 0:
ADCON0=0b10000001; //AN0 - Strain gauge input channel 1 (not in
use yet)
break;
case 1:
ADCON0=0b10000101; //AN1 - Strain gauge input channel 2 (not in
use yet)
break;
case 2:
ADCON0=0b10001001; //AN2 - EMG channel 1
break;
case 3:
ADCON0=0b10001101; //AN3 - EMG channel 2
break;
case 4:
ADCON0=0b10010001; //AN4 - EMG channel 3
break;
case 5:
ADCON0=0b10010101; //AN5 - EMG channel 4
break;
case 6:
ADCON0=0b10011001; //AN6 - threshold 1
break;
case 7:
ADCON0=0b10011101; //AN7 - threshold 2
break;
default:
break;
}
for (j=0;j<10;j++); //wait to charge capacitor
unsigned int ADCON_old=ADCON0+2; //save value of ADCON0 for later
comparison to determine flag bit status
ADCON0=ADCON0+2; //begin conversion (set second bit of
ADCON0 high)
while (ADCON0==ADCON_old); //wait for conversion (flag bit will
automatically go low when complete)
ADCON0=0; //reset ADCON0 (not strictly necessary)
return ADRESH*256+ADRESL; //return results
}

//=====
int bool_EMG(float EMG, float THRESH, int FLAG)
{
if (EMG>THRESH) //if EMG above threshold,
{
FLAG=1; //FLAG used to determine hysteresis
between thresholds
return 1; //if High threshold > EMG > low threshold,
then function will return 1 if FLAG== 1 and 0 if FLAG==0.
}
else
if (EMG>(0.1*THRESH)) //low threshold is 30% of high threshold
{
if (FLAG==1)
return 1;
else
return 0;
}
else
{
FLAG=0;
return 0;
}
}

```

```

}

//=====
void manual_control(void)
{
    RD0=1; //change LEDs to show manual mode is
active    RD1=0;

    while (RB3) //loop as long as manual button is pressed
    {
        THRESHOLD[0] = analog_read_in(6); //read-in of threshold values
        THRESHOLD[1] = analog_read_in(7);

        if (THRESHOLD[1]>200 && THRESHOLD[1]<800 && THRESHOLD[0]>200 && THRESHOLD[0]<800)
inactive range //wait till both thresholds are in
            break; //continue to rest of function
        else //kill motors and continue to wait
        {
            RC0=0;
            RC1=0;
            RC2=0;
            RC3=0;
        }
    }
    while (RB3)
    {
        THRESHOLD[0] = analog_read_in(6); //read-in of threshold values for motor control
        THRESHOLD[1] = analog_read_in(7);

        //Same actions as for EMG mode, but with different conditions for activation.
        if (!RB0) //if killswitch released, change SAFE to false
and kill motors //Note: this action is repeated in the interrupt
        {
            RC0=0;
            RC1=0;
            RC2=0;
            RC3=0;
            SAFE=0;
        }
        else //else set SAFE to true
        {
            SAFE=1;
        }

        //Motor 1 - finger
        if (THRESHOLD[1]>200 && THRESHOLD[1]<800)
        {
            RC2=0; //kill motor
            RC3=0;
        }
        if (THRESHOLD[1]>800 && SAFE) //finger flexion limit switch
        {
            if (RB4) //flex fingers
            {
                RC2=0; //flex fingers
                RC3=1;
            }
            else
            {
                RC3=0;
                RC2=0;
            }
        }
        if (THRESHOLD[1]<200 && SAFE) //finger extension limit switch
        {
            if (RB5) //extend fingers
            {
                RC3=0; //extend fingers
                RC2=1; //extend fingers
            }
        }
    }
}

```

```

        }
        else
            {RC3=0;
             RC2=0;
            }
    }
    //Motor 2 - wrist
    if (THRESHOLD[0]>200 && THRESHOLD[0]<800)
        {
            RC1=0; //kill motor if no EMG activity
            RC0=0;
        }
    if (THRESHOLD[0]>800 && SAFE)
        {if (RB6) //wrist flexion limit switch
            {RC1=0; //flex wrist
             RC0=1; //flex wrist
            }
        else
            {RC0=0;
             RC1=0;
            }
        }
    if (THRESHOLD[0]<200 && SAFE)
        {if (RB7) //wrist extension limit switch
            {RC0=0; //extend wrist
             RC1=1; //extend wrist
            }
        else
            {RC0=0;
             RC1=0;
            }
        }
    }
    RD0=0;
    RD1=1;
    return;
}

=====
void EMG_control(void)
{
    lcd_command(0x01); //clear screen
    lcd_string("EMG mode. Hold"); //display text
    lcd_command(0xc0); //next line
    lcd_string("'B' for manual"); //display text
    while (1)
    {
        if (RB3)
            manual_control();
        RD0=0; //change LEDs to show normal mode is
        active
        RD1=1;
        //reading in of EMG:
        EMG_IN[0]=analog_read_in(2);
        EMG_IN[1]=analog_read_in(3);
        EMG_IN[2]=analog_read_in(4);
        EMG_IN[3]=analog_read_in(5);

        //further smoothing (application of 'moving average'):
        EMG_MA[0]=EMG_MA[0]*0.8+EMG_IN[0]*0.2;
        EMG_MA[1]=EMG_MA[1]*0.8+EMG_IN[1]*0.2;
        EMG_MA[2]=EMG_MA[2]*0.8+EMG_IN[2]*0.2;
        EMG_MA[3]=EMG_MA[3]*0.8+EMG_IN[3]*0.2;

        //reading in of threshold:

```

```

THRESHOLD[0] = analog_read_in(6);
THRESHOLD[1] = analog_read_in(7);
THRESHOLD[0] = THRESHOLD[0]*0.3;           //decrease sensitivity of threshold pots
THRESHOLD[1] = THRESHOLD[1]*0.3;

//Schmidt trigger:
EMG_BINARY[0]=bool_EMG(EMG_MA[0],THRESHOLD[1],FLAG[0]); //finger flexor muscles
EMG_BINARY[1]=bool_EMG(EMG_MA[1],THRESHOLD[1],FLAG[1]); //finger extensor muscles
EMG_BINARY[2]=bool_EMG(EMG_MA[2],THRESHOLD[0],FLAG[2]); //wrist flexor muscles
EMG_BINARY[3]=bool_EMG(EMG_MA[3],THRESHOLD[0],FLAG[3]); //wrist extensor muscles

//
//***** Action: *****
//
// the pins RC<0:3> control the motor direction. RC0 and RC1 should not be high together, neither should RC2 and
RC3.
//
// Each pin has the following function:
//
// RC0 - wrist motor flexion
//
// RC1 - Wrist motor extension
//
// RC2 - finger motor extension
//
// RC3 - finger motor flexion.
//
//
// The following is the convention for the limit switches (High is unengaged):
//
// !RB4 - finger flexion limit switch - !RB4
//
// !RB5 - finger extention limit switch - !RB5
//
// !RB6 - wrist flexion limit switch - !RB6
//
// !RB7 - wrist extention limit switch - !RB7
//*****

checksafe();           //check safety button

if (!EMG_BINARY[0] && !EMG_BINARY[1])
    {
        RC2=0;           //kill motor if no EMG activity
        RC3=0;
    }
if (EMG_BINARY[0] && EMG_BINARY[1])
    {
        RC2=0;           //kill motor if dual antagonistic EMG
        RC3=0;
    }
activity

if (EMG_BINARY[0] && !EMG_BINARY[1] && SAFE)
    {if (RB4)           //finger flexion limit switch
        {RC2=0;       //flex fingers
        RC3=1;       //flex fingers
        }
    else
        {RC3=0;
        RC2=0;
        }
    }
if (!EMG_BINARY[0] && EMG_BINARY[1] && SAFE)
    {if (RB5)           //finger extention limit switch
        {RC3=0;       //extend fingers
        RC2=1;       //extend fingers
        }
    else
        {RC3=0;
        RC2=0;
        }
    }

if (!EMG_BINARY[2] && !EMG_BINARY[3])
    {
        RC1=0;           //kill motor if no EMG activity
    }

```

```

        RC0=0;
        }
    if (EMG_BINARY[2] && EMG_BINARY[3])
        {
            RC1=0;
            activity //kill motor if dual antagonistic EMG
            RC0=0;
        }
    if (EMG_BINARY[2] && !EMG_BINARY[3] && SAFE)
        {if (RB6 && !RC2) //wrist flexion limit switch and check to
            {RC1=0; //flex wrist
             RC0=1; //flex wrist
             }
            else
            {RC0=0;
             RC1=0;
             }
        }
    if (!EMG_BINARY[2] && EMG_BINARY[3] && SAFE)
        {if (RB7 && !RC3) //wrist extension limit switch and check to
            {RC0=0; //extend wrist
             RC1=1; //extend wrist
             }
            else
            {RC0=0;
             RC1=0;
             }
        }
    }
}

//=====
====void Eval_control(void)
{
    lcd_command(0x01); //clear screen
    lcd_string("Eval mode."); //display text
    lcd_command(0xc0); //next line
    lcd_string("Initializing..."); //display text
    for (i=0;i<60000;i++); //short pause
    if (!RB0)
    {
        lcd_command(0x01); //clear screen
        lcd_string("Please hold"); //display text
        lcd_command(0xc0); //next line
        lcd_string("safety button."); //display text
        while(!RB0); //wait for safety buttons
        lcd_command(0x01); //clear screen
        lcd_string("Eval mode."); //display text
        lcd_command(0xc0); //next line
        lcd_string("Initializing..."); //display text
    }

    EFM(); //Extend fingers to max, short pause
    EWM(); //Extend wrist to max, short pause
    FWS(); //flex wrist to straight, short pause
    FF45(); //flex fingers to 45'

    lcd_command(0x01); //clear screen
    lcd_string("Please secure"); //display text
    lcd_command(0xc0); //next line
    lcd_string("patient."); //display text

    for (i=0;i<60000;i++);
}

```

```

lcd_command(0x01); //clear screen
lcd_string("Press 'A' when"); //display text
lcd_command(0xc0); //next line
lcd_string("ready"); //display text

while(!RB2); //wait and poll RB2

while(1)
{Eval_rep();
lcd_command(0x01); //clear screen
lcd_string("Repeat?"); //display text
lcd_command(0xc0); //next line
lcd_string("A: Yes, B: No"); //display text

while(!RB2 && !RB3); //RB2 is button A

if (RB3)
break;
}

lcd_command(0x01); //clear screen
lcd_string("Test complete"); //display text
lcd_command(0xc0); //next line
lcd_string("Thank you."); //display text

while(1);
}

//=====
====void EvalW_control(void)
{
lcd_command(0x01); //clear screen
lcd_string("Eval(W) mode."); //display text
lcd_command(0xc0); //next line
lcd_string("Initializing..."); //display text
for (i=0;i<60000;i++); //short pause
if (!RB0)
{
lcd_command(0x01); //clear screen
lcd_string("Please hold"); //display text
lcd_command(0xc0); //next line
lcd_string("safety button."); //display text
while(!RB0); //wait for safety buttons
lcd_command(0x01); //clear screen
lcd_string("Eval mode."); //display text
lcd_command(0xc0); //next line
lcd_string("Initializing..."); //display text
}
}

EFM(); //Extend fingers to max, short pause
EWM(); //Extend wrist to max, short pause
FWS(); //flex wrist to straight, short pause
FF45(); //flex fingers to 45'

lcd_command(0x01); //clear screen
lcd_string("Please secure"); //display text
lcd_command(0xc0); //next line
lcd_string("patient."); //display text

for (i=0;i<60000;i++);

lcd_command(0x01); //clear screen
lcd_string("Press 'A' when"); //display text

```

```

lcd_command(0xc0); //next line
lcd_string("ready"); //display text

while(!RB2); //wait and poll RB2

while(1)
{EvalW_rep();
lcd_command(0x01); //clear screen
lcd_string("Repeat?"); //display text
lcd_command(0xc0); //next line
lcd_string("A: Yes, B: No"); //display text

while(!RB2 && !RB3); //RB2 is button A

if (RB3)
break;
}

lcd_command(0x01); //clear screen
lcd_string("Test complete"); //display text
lcd_command(0xc0); //next line
lcd_string("Thank you."); //display text

while(1);
}

=====
====void checksafe(void)
{
if (!RB0) //if killswitch released, change SAFE to false
and kill motors //Note: this action is repeated in the interrupt
{
isr() function for redundancy
RC0=0;
RC1=0;
RC2=0;
RC3=0;
SAFE=0;
}
else //else set SAFE to true
{SAFE=1;
}
}

=====
====
void Eval_rep(void)
{
lcd_command(0x01); //clear screen
for (i=0;i<60000;i++);
lcd_string("Test in"); //display text
lcd_command(0xc0); //next line
lcd_string("progress"); //display text

for (i=0;i<30000;i++); //short pause

//program sequence:
=====
EFM(); //extend fingers to max then pause for 60000 cycles
for (i=0;i<60000;i++); //long pause
for (i=0;i<60000;i++); //long pause
for (i=0;i<60000;i++); //long pause
FFM(); //flex fingers to max then pause for 60000 cycles.
EFM(); //extend fingers to max then pause for 60000 cycles

```

```

FF45); //flex fingers to roughly 45 degrees then pause for 60000 cycles
FWM()); //flex wrist to max then pause for 60000 cycles
EWM()); //extend wrist to max then pause for 6000 cycles
FWS()); //flex wrist to straight then pause for 60000 cycles
EFM()); //extend fingers to max then pause for 60000 cycles
}

=====
void EvalW_rep(void)
{
  lcd_command(0x01); //clear screen
  for (i=0;i<60000;i++);
  lcd_string("Test in"); //display text
  lcd_command(0xc0); //next line
  lcd_string("progress"); //display text

  for (i=0;i<30000;i++); //short pause

//program sequence:
=====
EWM()); //extend wrist to max then pause for 6000 cycles
FWM()); //flex wrist to max then pause for 60000 cycles
EWM()); //extend wrist to max then pause for 6000 cycles
FWS()); //flex wrist to straight then pause for 60000 cycles
}

=====
// Action:
//*****
// the pins RC<0:3> control the motor direction. RC0 and RC1 should not be high together, neither should RC2 and
RC3.
// Each pin has the following function:
// RC0 - wrist motor flexion
// RC1 - Wrist motor extension
// RC2 - finger motor extension
// RC3 - finger motor flexion.
//
// The following is the convention for the limit switches (High is unengaged):
// !RB4 - finger flexion limit switch
// !RB5 - finger extension limit switch
// !RB6 - wrist flexion limit switch
// !RB7 - wrist extension limit switch
//*****

=====
void FFM(void) //Flex fingers to maximum
{
  speed=speed_min;
  i=0;
  while(i<pause_time)
  {
    if (!RB4) //flex fingers to max, wait at limit for 60000
    cycles
      {
        RC2=0;
        RC3=0;
        i++;
      }
    else
    {
      checksafe(); //check safe to move
      if (SAFE && RB4)
      {

```

```

RC2=0;
RC3=1; //flex fingers
if (speed<speed_max)
    {speed++;
    for (j=0; j<speed; j++); //soft start using PWM
    RC3=0;
    for (j=0; j<(speed_max-speed); j++);
    }
else
    {
    RC3=0;
    RC2=0;
    }
}
}

=====
====void EFM(void) //Extend fingers to maximum
{speed=speed_min;
i=0;
while(i<pause_time)
    {
    if (!RB5) //extend fingers to max, wait at limit for
60000 cycles
        {
        RC2=0;
        RC3=0;
        i++;
        }
    else
    {
    checksafe(); //check safe to move
    if (SAFE && RB5)
        {
        RC3=0;
        RC2=1; //flex fingers
        if (speed<speed_max)
            {speed++;
            for (j=0; j<speed; j++); //soft start using PWM
            RC2=0;
            for (j=0; j<(speed_max-speed); j++);
            }
        }
    else
        {
        RC2=0;
        RC3=0;
        }
    }
}

=====
====void FWM(void) //Flex wrist to maximum
{speed=speed_min;
i=0;
while(i<pause_time)
    {
    if (!RB6) //extend wrist to max, wait at limit for 60000
cycles
        {
        RC1=0;
        RC0=0;
        i++;

```

```

    }
    else
    {
        checksafe(); //check safe to move
        if (SAFE && RB6)
        {
            RC1=0;
            RC0=1; //flex fingers
            if (speed<speed_max)
            {
                speed++;
                for (j=0; j<speed; j++); //soft start using PWM
                RC0=0;
                for (j=0; j<(speed_max-speed); j++);
            }
        }
    }
    else
    {
        RC0=0;
        RC1=0;
    }
}

}

//=====
====void EWM(void) //Extend wrist to maximum
{
    speed=speed_min;
    i=0;
    while(i<pause_time)
    {
        if (!RB7) //extend wrist to max, wait at limit for 60000
        cycles
        {
            RC0=0;
            RC1=0;
            i++;
        }
        else
        {
            checksafe(); //check safe to move
            if (SAFE && RB7)
            {
                RC0=0;
                RC1=1; //flex fingers
                if (speed<speed_max)
                {
                    speed++;
                    for (j=0; j<speed; j++); //soft start using PWM
                    RC1=0;
                    for (j=0; j<(speed_max-speed); j++);
                }
            }
        }
        else
        {
            RC0=0;
            RC1=0;
        }
    }
}

}

//=====
====void FWS(void) //Flex wrist straight
{
    speed=speed_min;

```

```

for (i=0;i<run_time;) //flex fingers to roughly 45 degrees - Adjust
terminating value for i in "for" loop till correct
{checksafe();
if (SAFE && RB6)
    {
    RC1=0;
    RC0=1; //flex fingers
    if (speed<speed_max)
        {speed++;
        for (j=0; j<speed; j++); //soft start using PWM
        RC0=0;
        for (j=0; j<(speed_max-speed); j++);
        }
    i++;
    }
else
    {
    RC0=0;
    RC1=0;
    }
}
RC0=0;
RC1=0;

for(i=0;i<pause_time;i++); //pause after finger flex
}

//=====
====void FF45(void) //Flex fingers to 45 degrees
{speed=speed_min;
for (i=0;i<run_time;) //flex fingers to roughly 45 degrees - Adjust
terminating value for i in "for" loop till correct
{checksafe();
if (SAFE && RB4)
    {
    RC2=0;
    RC3=1; //flex fingers
    if (speed<speed_max)
        {speed++;
        for (j=0; j<speed; j++); //soft start using PWM
        RC3=0;
        for (j=0; j<(speed_max-speed); j++);
        }
    i++;
    }
else
    {
    RC2=0;
    RC3=0;
    }
}
RC2=0;
RC3=0;

for(i=0;i<pause_time;i++); //pause after finger flex
}

```

[This page is intentionally left blank]

## Appendix F – Matlab Code

The following section contains the Matlab code used to process the raw force data collected during the pilot clinical trial (see Section 3.2). The code was executed, and the resulting data plots are presented in Section 4.2. The code was developed in Matlab version R2012a. The code was as follows:

```
%This program reads in data from text files and processes it in the
following ways:
% - Filterring to remove electrical noise from motors
% - Removes baseline drift
% - EMG 50Hz notch filter (electrical noise)

%List of variables and their purposes:
%RAW - raw data, read in directly from file
%BASELINE - average of first second of recorded data

clear all;
clc;

%READ IN DATA:
%=====
%read in baseline drift values (BLDRIFT and NOISE vectors)
%UPDATE FOR TYPE OF TEST PERFORMED (Wrist + fingers or Wrist only)
DRIFT=dlmread('Hand out W+F.txt');
S_noise=size(DRIFT);

%read in participant data
%UPDATE FOR EACH PARTIIPANT
RAW=dlmread('Participant A.txt');
S_data=size(RAW);

%BASELINE ZEROING:
%=====
BASELINE=mean(RAW(1:1000,2)); %average of first second of reading.
RAW(:,2)= RAW(:,2)-BASELINE; %Zero data
BASELINE_drift=mean(DRIFT(1:1000,2));

%DETERMINE TIME MARKERS:
%=====
%Determine drift markers
j=1;
ilim=0;
for i=1:S_noise(1,1)
    if(DRIFT(i,2)-BASELINE_drift<-0.3 && i>ilim)
        MARKERS_drift(j)=i;
        ilim=i+1000;
        j=j+1;
    end
end

%determine data markers
Fc=200;
[b,a] = butter(1,Fc/500);
```

```

DATA_noise=zeros(S_data(1,1),2);
DATA_noise(:,1)=RAW(:,1);

DATA_noise(:,2)=filter(b,a,RAW(:,2));
DATA_noise(:,2)=RAW(:,2)-DATA_noise(:,2);

j=1;
ilim=0;
for i=1:S_data(1,1)
    if(DATA_noise(i,2)<-0.15 && i>ilim)
        MARKERS_data(j)=i;
        ilim=i+1000;
        j=j+1;
    end
end

%CROP DATA FOR TIME WINDOW:
%=====
%start/end at same time
START_TIME_data=MARKERS_data(1)-2000; %identify start and end times
END_TIME_data=MARKERS_data(numel(MARKERS_data))+2000;

START_TIME_noise=MARKERS_drift(1)-2000; %identify start and end times
END_TIME_noise=MARKERS_drift(numel(MARKERS_drift))+2000;

DATA=zeros(END_TIME_data-START_TIME_data,2); %create matrix of appropriate
time window
for i=START_TIME_data:END_TIME_data
    DATA(i+1-START_TIME_data,1)=i-START_TIME_data;
    DATA(i+1-START_TIME_data,2)=RAW(i,2);
end

DRIFT_adjusted=zeros(END_TIME_noise,2); %create matrix of appropriate time
window
for i=START_TIME_noise:END_TIME_noise
    DRIFT_adjusted(i+1-START_TIME_noise,1)=i-START_TIME_noise;
    DRIFT_adjusted(i+1-START_TIME_noise,2)=DRIFT(i,2)-BASELINE_drift;
end

MARKERS_drift(numel(MARKERS_drift)+1)=END_TIME_noise;
MARKERS_data(numel(MARKERS_data)+1)=END_TIME_data;
MARKERS_drift=MARKERS_drift-START_TIME_noise;
MARKERS_data=MARKERS_data-START_TIME_data;

%SEGMENT, RESIZE AND CONCATENATE DRIFT DATA
%=====
%segment drift data
pause_big = 781;
pause_small = 459;
SEGMENT_1_DRIFT=DRIFT_adjusted(1:MARKERS_drift(1),2);
SEGMENT_2_DRIFT=DRIFT_adjusted(MARKERS_drift(1)+1:MARKERS_drift(2)-
pause_big,2);
SEGMENT_3_DRIFT=DRIFT_adjusted(MARKERS_drift(2)+1:MARKERS_drift(3)-
pause_big,2);
SEGMENT_4_DRIFT=DRIFT_adjusted(MARKERS_drift(3)+1:MARKERS_drift(4)-
pause_small,2);

```

```

SEGMENT_5_DRIFT=DRIFT_adjusted(MARKERS_drift(4)+1:MARKERS_drift(5)-
pause_big,2);
SEGMENT_6_DRIFT=DRIFT_adjusted(MARKERS_drift(5)+1:MARKERS_drift(6)-
pause_big,2);
SEGMENT_7_DRIFT=DRIFT_adjusted(MARKERS_drift(6)+1:MARKERS_drift(7)-
pause_big,2);
SEGMENT_8_DRIFT=DRIFT_adjusted(MARKERS_drift(7)+1:MARKERS_drift(8)-
pause_big,2);

PAUSE1drift=DRIFT_adjusted(MARKERS_drift(2)-pause_big:MARKERS_drift(2),2);
PAUSE2drift=DRIFT_adjusted(MARKERS_drift(3)-pause_big:MARKERS_drift(3),2);
PAUSE3drift=DRIFT_adjusted(MARKERS_drift(4)-
pause_small:MARKERS_drift(4),2);
PAUSE4drift=DRIFT_adjusted(MARKERS_drift(5)-pause_big:MARKERS_drift(5),2);
PAUSE5drift=DRIFT_adjusted(MARKERS_drift(6)-pause_big:MARKERS_drift(6),2);
PAUSE6drift=DRIFT_adjusted(MARKERS_drift(7)-pause_big:MARKERS_drift(7),2);
PAUSE7drift=DRIFT_adjusted(MARKERS_drift(8)-pause_big:MARKERS_drift(8),2);

SEGMENT_DATA1=DATA(1:MARKERS_data(1),2);
SEGMENT_DATA2=DATA(MARKERS_data(1)+1:MARKERS_data(2)-pause_big,2);
SEGMENT_DATA3=DATA(MARKERS_data(2)+1:MARKERS_data(3)-pause_big,2);
SEGMENT_DATA4=DATA(MARKERS_data(3)+1:MARKERS_data(4)-pause_small,2);
SEGMENT_DATA5=DATA(MARKERS_data(4)+1:MARKERS_data(5)-pause_big,2);
SEGMENT_DATA6=DATA(MARKERS_data(5)+1:MARKERS_data(6)-pause_big,2);
SEGMENT_DATA7=DATA(MARKERS_data(6)+1:MARKERS_data(7)-pause_big,2);
SEGMENT_DATA8=DATA(MARKERS_data(7)+1:MARKERS_data(8)-pause_big,2);

% %Resize drift segments to match data segments
Sseg1_drift=size(SEGMENT_1_DRIFT);
Sseg1_data=size(SEGMENT_DATA1);

Sseg2_drift=size(SEGMENT_2_DRIFT);
Sseg2_data=size(SEGMENT_DATA2);

Sseg3_drift=size(SEGMENT_3_DRIFT);
Sseg3_data=size(SEGMENT_DATA3);

Sseg4_drift=size(SEGMENT_4_DRIFT);
Sseg4_data=size(SEGMENT_DATA4);

Sseg5_drift=size(SEGMENT_5_DRIFT);
Sseg5_data=size(SEGMENT_DATA5);

Sseg6_drift=size(SEGMENT_6_DRIFT);
Sseg6_data=size(SEGMENT_DATA6);

Sseg7_drift=size(SEGMENT_7_DRIFT);
Sseg7_data=size(SEGMENT_DATA7);

Sseg8_drift=size(SEGMENT_8_DRIFT);
Sseg8_data=size(SEGMENT_DATA8);

ratio1=Sseg1_data(1,1)/Sseg1_drift(1,1);
ratio2=Sseg2_data(1,1)/Sseg2_drift(1,1);
ratio3=Sseg3_data(1,1)/Sseg3_drift(1,1);
ratio4=Sseg4_data(1,1)/Sseg4_drift(1,1);
ratio5=Sseg5_data(1,1)/Sseg5_drift(1,1);
ratio6=Sseg6_data(1,1)/Sseg6_drift(1,1);

```

```

ratio7=Sseg7_data(1,1)/Sseg7_drift(1,1);
ratio8=Sseg8_data(1,1)/Sseg8_drift(1,1);

for i=1:Sseg2_data
    if (round(i/ratio2)>0.5)
        SEG_2_DRIFT_RESIZED(i)=SEGMENT_2_DRIFT(round(i/ratio2));
    else
        SEG_2_DRIFT_RESIZED(i)=SEGMENT_2_DRIFT(round(i/ratio2+1));
    end
end
for i=1:Sseg3_data
    if (round(i/ratio3)>0.5)
        SEG_3_DRIFT_RESIZED(i)=SEGMENT_3_DRIFT(round(i/ratio3));
    else
        SEG_3_DRIFT_RESIZED(i)=SEGMENT_3_DRIFT(round(i/ratio3+1));
    end
end
for i=1:Sseg4_data
    if (round(i/ratio4)>0.5)
        SEG_4_DRIFT_RESIZED(i)=SEGMENT_4_DRIFT(round(i/ratio4));
    else
        SEG_4_DRIFT_RESIZED(i)=SEGMENT_4_DRIFT(round(i/ratio4+1));
    end
end
for i=1:Sseg5_data
    if (round(i/ratio5)>0.5)
        SEG_5_DRIFT_RESIZED(i)=SEGMENT_5_DRIFT(round(i/ratio5));
    else
        SEG_5_DRIFT_RESIZED(i)=SEGMENT_5_DRIFT(round(i/ratio5+1));
    end
end
for i=1:Sseg6_data
    if (round(i/ratio6)>0.5)
        SEG_6_DRIFT_RESIZED(i)=SEGMENT_6_DRIFT(round(i/ratio6));
    else
        SEG_6_DRIFT_RESIZED(i)=SEGMENT_6_DRIFT(round(i/ratio6+1));
    end
end
for i=1:Sseg7_data
    if (round(i/ratio7)>0.5)
        SEG_7_DRIFT_RESIZED(i)=SEGMENT_7_DRIFT(round(i/ratio7));
    else
        SEG_7_DRIFT_RESIZED(i)=SEGMENT_7_DRIFT(round(i/ratio7+1));
    end
end
%concatenate drift segments
RESIZED(:,2)=[SEGMENT_1_DRIFT; SEG_2_DRIFT_RESIZED'; PAUSE1drift ;
SEG_3_DRIFT_RESIZED'; PAUSE2drift ; SEG_4_DRIFT_RESIZED'; PAUSE3drift ;
SEG_5_DRIFT_RESIZED'; PAUSE4drift ; SEG_6_DRIFT_RESIZED'; PAUSE5drift ;
SEG_7_DRIFT_RESIZED' ; PAUSE6drift ; SEGMENT_8_DRIFT ; PAUSE7drift ];

S_resized_drift=size(RESIZED);
RESIZED(:,1)=1:S_resized_drift(1,1);

%smooth drift segments
Fc=50;
[b,a] = butter(1,Fc/500);
RESIZED(:,2)=filter(b,a,RESIZED(:,2));

```

```

%SUBTRACT DRIFT FROM TEST DATA:
%=====
%subtract drift from data and smooth
if S_resized_drift(1,1) < END_TIME_data-START_TIME_data
    S_final=S_resized_drift(1,1);
else
    S_final=END_TIME_data-START_TIME_data;
end

CORRECTED=zeros(S_final,2);
for i=1:S_final
    CORRECTED(i,1)=i;
    CORRECTED(i,2)=DATA(i,2)-RESIZED(i,2);
end

CORRECTED_s(:,1)=CORRECTED(:,1);

Fc=10;
[b,a] = butter(1,Fc/500);
CORRECTED_s(:,2)=filter(b,a,CORRECTED(:,2));

CORRECTED_s_HP(:,1)=CORRECTED(:,1);
Fc=1.2;
[b,a] = butter(1,Fc/500);
CORRECTED_s_HP(:,2)=CORRECTED_s(:,2)-filter(b,a,CORRECTED_s(:,2))+0.5;

%IDENTIFY PEAK STRESS IN EXTENSION PHASE
%=====
%Marker identifying beginning of extension phase:
MARKER_start = 5;
T_start = MARKERS_data(MARKER_start);
T_end = MARKERS_data(MARKER_start+1);

PEAK_volts = min(CORRECTED_s(T_start:T_end,2));
if PEAK_volts < 0
    PEAK_force = PEAK_volts/-0.0425
else
    PEAK_force = PEAK_volts/-0.0216
end

T = find(CORRECTED_s(T_start:T_end,2)==min(CORRECTED_s(T_start:T_end,2))) +
T_start

MAX=[T/1000, PEAK_volts];

file = fopen('Awrist.txt','w+');
for i= 1:length(CORRECTED_s)
    fprintf(file,'%6.2f\n',CORRECTED_s(i,2));
end
fclose all;

%convert force data to newtons:
%=====
for i=1:length(CORRECTED_s)
    if CORRECTED_s(i,2)<0
        CORRECTED_s(i,2)=CORRECTED_s(i,2)/-0.0425;
    else
        CORRECTED_s(i,2)=CORRECTED_s(i,2)/-0.0216;
    end
end

```

```

    end
end

%DATA PRESENTATION:
%=====
hold off
figure(1)
hFig = figure(1);
set(hFig, 'Position', [100 400 1000 500])
set(gca, 'FontSize', 15)
plot(CORRECTED_s(:,1)/1000, CORRECTED_s(:,2), 'b', DATA_noise(:,1)-
START_TIME_data/1000, DATA_noise(:,2)*10+50, 'r');
%plot(CORRECTED_s(:,1)/1000, CORRECTED_s(:,2), MAX(:,1), MAX(:,2), MAX(:,1), MAX
(:,2));
ylim([-40 60]);
lim=(END_TIME_data-START_TIME_data)+2000)/1000;
xlim([0 lim])
xlabel('Time [seconds]');
ylabel('Force [N]');
legend('Wrist', 'Fingers', 'Location', 'SouthEast');
grid ON;

```

[This page is intentionally left blank]

## **Appendix G – Facility Approval Documentation and Participant Consent Forms**